UC Irvine

UC Irvine Electronic Theses and Dissertations

Title

Primary Cilia as Spatiotemporal Regulators of Brain Functions and behaviors

Permalink

https://escholarship.org/uc/item/5fb1872c

ISBN

9798173738288

Author

Vakilmonfared, Roudabeh

Publication Date

2026-11-04

Peer reviewed|Thesis/dissertation

eScholarship.org Powered by the California Digital Library
University of California

UNIVERSITY OF CALIFORNIA,
IRVINE

Primary Cilia as Spatiotemporal Regulators of Brain Functions and behaviors

DISSERTATION

submitted in partial satisfaction of the requirements
for the degree of

DOCTOR OF PHILOSOPHY

in Pharmacological Sciences

by

Roudabeh Vakilmonfared

Dissertation Committee:
Professor Amal Alachkar, Chair
Professor Olivier Civelli
Professor Qun-Yong Zhou

2026

Chapter 2 © 2025 Plos Biology.
All other materials © 2026 Roudabeh Vakilmonfared

DEDICATION

To my father, whose battle with Alzheimer's disease inspired my passion for science and set me on this path.

To my husband, whose love, patience, and support sustained me throughout this journey.

To my mother, whose encouragement and belief in me never wavered.

Table of Content **Page**

List of Figures v
Acknowledgements vii
Vita viii
Abstract of the Dissertation x

Chapter 1: Introduction **1**
1. Primary Cilia 2
1.1 History of Primary Cilia 2
1.2 Ciliogenesis 3
1.3 Structural Organization and Intraflagellar Transport 4
1.4 Dynamic Regulation of Primary Cilia 7
1.5 Primary Cilia as Signaling Hubs 8
1.6 Primary Cilia in Neurological and Psychiatric Disorders 11
1.7 Primary Cilia and Physiology 12
1.8 Primary Cilia and Circadian Rhythm 15
2. Nucleus Accumbens Core 19
2.1 Anatomical and Circuit Organization of the NAcC 19
2.2 NAcC in Circadian and Sleep-Wake Regulation 20
2.3 NAcC in Social Behavior and Reward 22
3. Primary Cilia in the Nucleus Accumbens Core 23

Chapter 2: Cilia in the Brain Display Region-Dependent Oscillations of Length and Orientation **25**
Abstract 26
Introduction 27
Methods 29
Results 41
Discussion 57

Chapter 3: Loss of Primary Cilia in the Nucleus Accumbens Increases Wakefulness and Reduces Locomotor Activity and NREM Sleep **65**
Abstract 66
Introduction 67
Materials and Methods 70

Results 74
Discussion 82

Chapter 4: Cilia Loss in the Nucleus Accumbens Impairs Social Behavior and Disrupts Cortical Oscillatory Coordination 87
Abstract 88
Introduction 89
Materials and Methods 91
Results 96
Discussion 108

Chapter 5: Primary Cilia on Nucleus Accumbens D1 Neurons Are Required for Social Behavior but Not Circadian Regulation 114
Abstract 115
Introduction 116
Materials and Methods 119
Results 130
Discussion 142

Chapter 6: Conclusion and Perspectives 147
6.1 Revisiting the Question 148
6.2 The Atlas: Cilia Are Not Static 148
6.3 A Circuit Cut Broadly: Two Phenotypes Emerge 149
6.4 Narrowing the Cell Type: A Dissociation 150
6.5 An Integrated Model 151
6.6 Limitations 152
6.7 Future Directions 153
6.8 Closing Statement 155

References 156
Chapter 1 References 156
Chapter 2 References 166
Chapter 3 References 178
Chapter 4 References 181
Chapter 5 References 189

List of Figures **Page**

Figure 1.1. Schematic structure of a primary cilium. 5
Figure 2.1. Experimental design and data analysis. 42
Figure 2.2. Cilia length analysis in different brain regions. 45
Figure 2.3. Cilia circular angle analysis, based on individual cilia measurements. 46
Figure 2.4. Cilia circular angle analysis based on section-averaged circular means. 48
Figure 2.5. Fluctuation of cilia length and cilia circular angle across 24-hours' time. 50
Figure 2.6. Circadian rhythms of cilia length. 52
Figure 2.7. Correlation of cilia length and circular angle among various brain regions and relationship between cilia length/angle and network connectivity. 55
Figure 3.1. Stereotaxic AAV-mediated Cre delivery ablates primary cilia from CaMKII-expressing neurons in the NAcC. 75
Figure 3.2. Wheel-running activity in control and NAcC IFT88 KO mice under a 12:12h light-dark cycle. 77
Figure 3.3. Food intake in control and NAcC IFT88 KO mice under a 12:12 h light dark cycle. 79
Figure 3.4. Sleep-wake architecture in control and NAcC IFT88 KO mice assessed by EEG/EMG. 81
Figure 3.5. Cosinor analysis of sleep-wake states in control and NAcC IFT88 KO mice. 82
Figure 4.1. Selective ablation of primary cilia in CaMKII-expressing neurons of the nucleus accumbens core. 96
Figure 4.2. NAcC cilia KO mice exhibit deficits in social motivation and social memory. 98
Figure 4.3. Preserved spectral organization in frontal and parietal cortex across social behavior epochs. 100
Figure 4.4. Absolute LFP band power across behavioral epochs. 102
Figure 4.5. Elevated frontal–parietal coherence in IFT88 KO mice during social behavior epochs. 104
Figure 4.6. Phase–amplitude coupling across behavioral epochs and band pairs. 106
Figure 5.1. Validation of cell-type-specific cilia ablation in NAcC D1-MSNs. 131
Figure 5.2. Wheel-running activity and food intake in control and D1-cKO mice under

a 12:12 h light-dark cycle. 133
Figure 5.3. Sleep-wake architecture in control (WT) and D1-cKO mice assessed by EEG/EMG. 135
Figure 5.4. Social interaction and social novelty behavior in control and D1-cKO mice. 137
Figure 5.5. Cortical local field potential dynamics during social behavior in control and D1-cKO mice. 138
Figure 5.6. Frontal cortex (EEG1) spectral dynamics in control and D1-cKO mice across acclimatization (ACC), social interaction (SI), and social novelty (SN) epochs. 140
Figure 5.7. Frontal-parietal EEG asymmetry and EMG activity in control and D1-cKO mice. 141

Acknowledgements

First and foremost, I would like to express my deepest gratitude to Dr. Alachkar. Her trust in me, belief in my abilities, and unwavering support throughout my graduate training helped me grow into the scientist I am today. She consistently encouraged me to pursue ambitious goals, provided guidance through challenges, and fostered an environment that allowed me to develop both professionally and personally. Beyond her role as a mentor, she showed remarkable compassion during some of the most difficult periods of my life. Her kindness, understanding, and support helped me navigate those challenging times, for which I will always be deeply grateful.

I would also like to extend my sincere gratitude to Dr. Civelli. His thought-provoking questions challenged me to think more critically and broaden my scientific perspective. In addition, he played an important role in creating a welcoming, collaborative, and supportive laboratory environment that truly felt like a second home. I am deeply grateful for his guidance, wisdom, and encouragement.

I am also sincerely thankful to Dr. Qun-Yong Zhu for his continuous support, valuable advice, and insightful feedback throughout my research journey. His expertise and thoughtful suggestions greatly strengthened my work and contributed significantly to my development as a researcher.

I am deeply grateful to my lab mates, past and present, for their friendship and support throughout my graduate studies. Their willingness to share knowledge, provide assistance, and celebrate successes made the laboratory a collaborative and enjoyable place to work. The scientific discussions, shared challenges, and memorable moments we experienced together made this journey far more meaningful.

I would like to express my heartfelt gratitude to my family and friends for their unwavering love, encouragement, and support throughout this journey. Their belief in me sustained me through moments of doubt and celebrated me through moments of success. I am especially grateful for their patience, understanding, and constant encouragement during the many challenges that accompanied graduate school. This achievement would not have been possible without the strength and support they provided along the way.

Vita

Roudabeh Vakil monfared

2026 Doctor of Philosophy in Pharmacological Sciences, University of California, Irvine

2022 Master of Science in Pharmaceutical Sciences, University of California, Irvine

2015 Master of Science in Cellular and Molecular Biology, University of Guilan, Iran

2013 Bachelor of Science in Biology, University of Guilan, Iran

Awards

Takeda Pharmaceuticals DMPK Internship *– Drug Metabolism and Pharmacokinetics Intern at Takeda Pharmaceuticals, Boston MA, June-September 2024*

Henry Wood Elliot Award *– Outstanding Research Achievement,* Department of Pharmaceutical Sciences, University of California, Irvine, 2025

Vertex Pharmaceuticals Fellowship Award *– Recognized for excellence in translational neuroscience research bridging primary cilia biology and psychiatric disorders,* Vertex Pharmaceuticals, 2025–2026

Publications

1. **Monfared RV**, Abdelkarim S, Derdeyn P, Chen K, Wu H, et al. (2025) Cilia in the brain display region-dependent oscillations of length and orientation. PLOS Biology 23(7): e3003197
2. Chen, K., Ashtiani, K.C., **Monfared, R.V**. *et al.* Circadian cilia transcriptome in mouse brain across physiological and pathological states. *Mol Brain* **17**, 67 (2024).
3. Alhassen, W., Alhassen, S., Chen, J., **Monfared, R. V.,** & Alachkar, A. (2023). Cilia in the striatum mediate timing-dependent functions. Molecular Neurobiology, 60(2), 545-565.
4. Lee, J., Chen, S., **Monfared, R. V.**, Derdeyn, P., Leong, K., Chang, T., ... & Alachkar, A. (2023). Reanalysis of primate brain circadian transcriptomics reveals connectivity-related oscillations. Iscience, 26(10).
5. Alachkar, A., Lee, J., Asthana, K., **Vakil Monfared, R**., Chen, J., Alhassen, S., ... & Baldi, P. (2022). The hidden link between circadian entropy and mental health disorders. Translational psychiatry, 12(1), 281.
6. **Monfared, R. V**., Alhassen, W., Truong, T. M., Gonzales, M. A. M., Vachirakorntong, V., Chen, S., ... & Alachkar, A. (2021). Transcriptome profiling of dysregulated GPCRs reveals overlapping patterns across psychiatric disorders and age-disease interactions. Cells, 10(11), 2967.
7. Chen, S., Alhassen, W., **Vakil Monfared, R**., Vachirakorntong, B., Nauli, S. M., Baldi, P., & Alachkar, A. (2021). Dynamic changes of brain cilia transcriptomes across the human lifespan. International journal of molecular sciences, 22(19), 10387.
8. **Vakil Monfared, R**., & Mashayekhi, F. (2018). OX40L gene polymorphism and breast cancer in Iranian population. Experimental Oncology.

In Preparation:

9. **Vakil Monfared, R**., Popa, A., Dabbour, T., Shevachman, D., Alzaim, A., Zhou, Q.-Y., Civelli, O., & Alachkar, A. Cilia loss in the nucleus accumbens impairs social behavior and disrupts cortical oscillatory coordination. Brain Communications (under revision).

Abstract of the Dissertation

Primary Cilia as Spatiotemporal Regulators of Brain Functions and behaviors
by
Roudabeh Vakilmonfared
Doctor of Philosophy in Pharmacological Sciences
University of California, Irvine, 2026
Professor Amal Alachkar, Chair

Primary cilia are microtubule-based, non-motile organelles that extend from the surface of nearly all mammalian neurons and concentrate G protein-coupled receptors, including dopamine D1 and D2 receptors, melanin-concentrating hormone receptor 1, and adenosine A2A receptor, within a physically restricted signaling compartment. Although these receptors are established regulators of circadian behavior, motivation, and social engagement, whether the ciliary organelle itself contributes functionally to these behaviors, and whether it does so uniformly or through specific neuronal populations, was unknown. This dissertation addresses this question in the mouse nucleus accumbens core (NAcC), a ventral striatal region that integrates dopaminergic input from the ventral tegmental area with glutamatergic input from prefrontal, hippocampal, and amygdala circuits to drive goal-directed, social, and circadian behavior.

The first study established the structural foundation for this work by generating a high-throughput, brain-wide atlas of primary cilia across 22 mouse brain regions. Using automated image analysis applied to coronal sections collected at twelve time points across a 24-hour period, over 10 million individual cilia were measured for length and

orientation, yielding the largest spatiotemporal atlas of ciliary structure assembled to date. Cilia length and orientation varied substantially by brain region and were not static: length fluctuated significantly across the light-dark cycle in the majority of regions examined, and the NAcC was among five regions, alongside the arcuate nucleus, dorsomedial and ventromedial hypothalamus, and somatosensory cortex, showing statistically significant circadian rhythmicity in cilia length, with peak length occurring in the hours preceding the onset of the active phase.

Building on this structural rationale, primary cilia were selectively ablated from CaMKII-expressing NAcC neurons in adult mice via stereotaxic AAV-Cre delivery to Ift88-floxed animals, removing the intraflagellar transport protein required for ciliary maintenance. This manipulation was assessed across two independent behavioral domains. In the circadian domain, cilia-ablated mice showed a selective reduction in dark-phase wheel running, decreased total NREM sleep, and increased wakefulness measured by 48-hour EEG/EMG recording, while the timing, phase, and day-to-day stability of the light-dark-entrained rhythm, along with food intake, remained statistically indistinguishable from controls, indicating a deficit in the amplitude, or gain, of circadian behavioral output rather than in the clock mechanism itself. In the social domain, the same ablation abolished normal social approach preference and social novelty recognition, and altered corticolimbic network dynamics recorded via local field potential during social interaction, including a selective reduction in parietal theta power, changes in delta-centered phase-amplitude coupling, elevated frontal-parietal coherence, and elevated baseline motor output prior to social exposure.

Because the CaMKII-driven manipulation targets a heterogeneous neuronal population encompassing D1- and D2-expressing medium spiny neurons and interneurons, a third study tested whether either phenotype could be attributed to a single, genetically defined cell type: D1 receptor-expressing medium spiny neurons (D1-MSNs). Using D1-Cre-dependent AAV deletion of IFT88 to ablate cilia specifically from NAcC D1-MSNs, this study found a complete loss of social approach preference and social novelty recognition, with discrimination indices indistinguishable from zero in both assays, alongside a distinct frontal cortical EEG signature, a steeper aperiodic spectral slope, reduced spectral entropy, and increased signal regularity, that was present even before social stimulus exposure, suggesting an altered baseline motivational or arousal state rather than a stimulus-locked encoding deficit. In marked contrast to the broader CaMKII manipulation, circadian locomotor rhythms and feeding rhythms were fully preserved in D1-MSN-specific knockouts, and sleep architecture was largely intact, with only a modest redistribution of wakefulness across the light phase and no change in total sleep amount or spectral power.

Together, these findings demonstrate that primary cilia in the NAcC are structurally dynamic across the circadian cycle and functionally necessary for both circadian behavioral gain and social behavior, but that these two functions are mediated by dissociable neuronal populations: D1-MSN cilia are selectively required for social approach and recognition memory, while the circadian gain phenotype produced by broader ciliary ablation depends on a distinct, non-D1 population within the NAcC. This dissertation establishes primary cilia as a cell-type-specific subcellular mechanism through which a single neural circuit achieves functionally distinct behavioral outputs,

offering a new framework for understanding how compartmentalized organelle signaling contributes to the flexibility and specificity of adult neural circuit function.

Chapter 1: Introduction

1. Primary Cilia

Primary cilia are solitary, microtubule-based organelles present on nearly every mammalian cell type. Unlike motile cilia, which generate fluid movement through a 9+2 microtubule arrangement, primary cilia generally possess a 9+0 axoneme and function primarily as sensory and signaling organelles, although structural exceptions exist for both classes of cilia[1, 2].

1.1 History of Primary Cilia

The first observations of cilia date back to the seventeenth century, when Antoni van Leeuwenhoek described hair-like projections on protozoa. Although primary cilia were later identified in vertebrate tissues [3], they were largely regarded as vestigial cellular appendages throughout much of the twentieth century [4]. Interest in these organelles increased following advances in electron microscopy, which enabled detailed characterization of ciliary ultrastructure [5].

A major turning point came with the discovery of intraflagellar transport (IFT), a bidirectional transport system required for cilium assembly and maintenance [6]. Subsequent studies linking defects in IFT proteins to human diseases, including polycystic kidney disease, established primary cilia as essential signaling organelles rather than evolutionary remnants [7]. Since then, primary cilia have emerged as critical regulators of diverse developmental and physiological processes, serving as specialized compartments that coordinate extracellular signaling pathways, including Hedgehog, Wnt, GPCR, calcium, and cAMP signaling [8].

1.2 Ciliogenesis

Primary cilia are highly dynamic organelles whose assembly and disassembly are tightly coordinated with the cell cycle. In most mammalian cells, ciliogenesis occurs as cells exit the cell cycle and enter the quiescent G0/G1 phase, whereas cilia are resorbed before mitosis to allow the centrosome to resume its role in spindle formation [9].

Ciliogenesis begins when the mother centriole of the centrosome matures into the basal body and docks at the plasma membrane. Following membrane docking, microtubules extend from the basal body to form the axoneme, the structural backbone of the cilium, which remains enclosed by a specialized ciliary membrane [10, 11]. At the junction between the basal body and axoneme lies the transition zone, a highly organized structure that functions as a selective diffusion barrier regulating the entry and exit of proteins and lipids from the ciliary compartment [12]. This compartmentalization enables the primary cilium to maintain a molecular composition that is distinct from the surrounding plasma membrane and is essential for its signaling functions.

Because mature cilia lack the machinery required for local protein synthesis, their assembly and maintenance depend on continuous trafficking of structural proteins and signaling molecules between the cell body and the ciliary compartment. This transport is mediated primarily by the intraflagellar transport (IFT) system, which is discussed in the following sections.

1.3 Structural Organization and Intraflagellar Transport

1.3.1 Structural Organization of the Primary Cilium

Although the primary cilium is continuous with the plasma membrane, it is a highly specialized signaling compartment with a distinct molecular composition. Its architecture consists of four major structural domains: the basal body, transition zone, axoneme, and ciliary membrane. Together, these compartments establish the structural framework required for selective protein trafficking and signal transduction.

The basal body, derived from the mother centriole, anchors the cilium to the cell surface and serves as the site where proteins destined for the cilium are assembled and sorted before entering the organelle. Extending from the basal body is the axoneme, a microtubule scaffold that provides structural support and serves as the track for intracellular transport [10].

Between the basal body and the axoneme lies the transition zone, a specialized gating structure composed of protein complexes that connect the axoneme to the surrounding membrane. Rather than functioning simply as a structural junction, the transition zone acts as a selective diffusion barrier that regulates the movement of proteins and lipids into and out of the ciliary compartment, thereby maintaining the unique molecular identity of the primary cilium [12].

Surrounding the axoneme is the ciliary membrane, which differs from the plasma membrane in both protein and lipid composition. The membrane is enriched in signaling receptors, ion channels, and G protein-coupled receptors (GPCRs), while its distinctive lipid environment—including cholesterol, sphingolipids, and phosphoinositides—contributes to receptor localization, membrane organization, and ciliary signaling [13-16]. The establishment and maintenance of this specialized membrane are essential for the cilium's role as a signaling organelle.

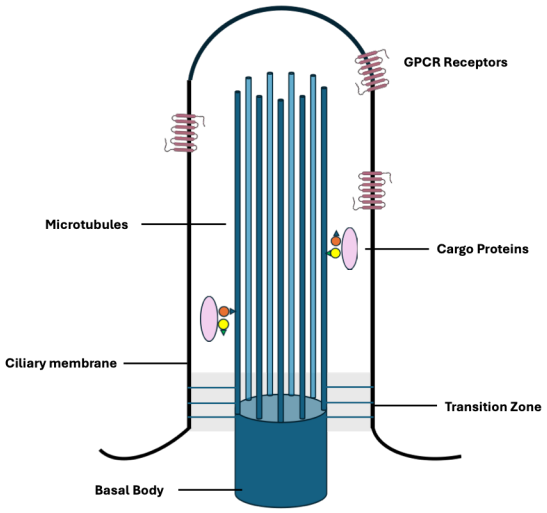


Figure 1.1. Schematic structure of a primary cilium.

A simplified illustration of the primary cilium highlighting major structural and trafficking components. The axoneme extends from the basal body and contains nine microtubule doublets arranged in a 9+0 configuration. Intraflagellar transport (IFT) machinery operates along the axoneme, while the transition zone forms a selective barrier

regulating the entry of ciliary proteins. Additionally, GPCRs are localized on the ciliary membrane.

1.3.2 Intraflagellar Transport

Because primary cilia lack ribosomes and therefore cannot synthesize proteins locally, all structural components and signaling molecules must be transported from the cell body into the ciliary compartment. This process is mediated by intraflagellar transport (IFT), a highly conserved bidirectional trafficking system that is essential for both cilium assembly and signaling [6, 17].

IFT particles are organized into two multiprotein complexes, IFT-A and IFT-B, which associate with molecular motors to move cargo along axonemal microtubules. Anterograde transport, from the basal body toward the ciliary tip, is driven primarily by kinesin-2 in association with IFT-B, whereas retrograde transport back to the cell body is mediated by cytoplasmic dynein-2 together with IFT-A [18]. At the ciliary tip, IFT particles undergo remodeling before initiating retrograde transport, allowing continuous recycling of transport machinery and maintenance of ciliary structure.

Beyond delivering structural proteins required for ciliogenesis, IFT also regulates the localization of signaling molecules within the cilium. Numerous ciliary GPCRs rely on IFT-dependent trafficking for proper localization, often through interactions with adaptor proteins such as TULP3 and the BBSome [19, 20]. Disruption of these trafficking pathways impairs receptor localization, alters downstream signaling, and ultimately compromises ciliary function.

Together, the specialized architecture of the primary cilium and the continuous activity of the IFT machinery enable the cilium to function as a dynamic signaling compartment capable of integrating extracellular stimuli with intracellular signaling pathways.

1.4 Dynamic Regulation of Primary Cilia

Unlike static cellular organelles, primary cilia are highly dynamic structures whose assembly, maintenance, and morphology continuously respond to developmental, physiological, and environmental cues. Rather than serving solely as passive sensory attachments, primary cilia undergo structural remodeling that directly influences their signaling capacity.

Maintenance of ciliary structure depends on a balance between axonemal assembly and disassembly. Continuous turnover of axonemal microtubules requires the delivery of structural proteins through intraflagellar transport (IFT), while disassembly occurs through coordinated microtubule depolymerization. Experimental disruption of anterograde IFT causes progressive ciliary shortening, demonstrating that sustained protein trafficking is required to maintain mature cilia [21]. These findings suggest that ciliary length reflects the dynamic equilibrium between assembly and disassembly rather than a fixed structural property.

In addition to IFT, membrane composition contributes to ciliary stability and morphology. Phosphoinositides regulate membrane organization, protein trafficking, and Hedgehog signaling within the cilium, and mutations affecting phosphoinositide metabolism disrupt both cilia length and function [13, 22-24]. These observations further illustrate that ciliary morphology is closely linked to signaling competence.

Neuronal primary cilia are similarly regulated by extracellular signaling. Several ciliary GPCR pathways alter cilia length, indicating that neuromodulators can remodel ciliary structure. Dopamine signaling through D5 receptors promotes ciliary elongation, whereas loss of D2 receptor signaling results in elongated striatal cilia [25, 26]. Likewise, activation of melanin-concentrating hormone receptor 1 (MCHR1) shortens cilia in the nucleus accumbens and other striatal regions, while inhibition of the serotonin receptor 5-HT6 reduces ciliary length [27, 28]. Together, these findings demonstrate that ciliary morphology is regulated by multiple neurotransmitter systems and is responsive to ongoing neuronal activity.

The dynamic regulation of cilia length has important functional implications. Because many signaling receptors are concentrated within the ciliary membrane, alterations in ciliary structure are likely to influence receptor localization, second-messenger signaling, and cellular responsiveness to extracellular stimuli. These observations raise the possibility that changes in cilia morphology are not merely structural adaptations but represent an additional mechanism for regulating neuronal signaling under different physiological conditions.

1.5 Primary Cilia as Signaling Hubs

Primary cilia are highly specialized signaling organelles that compartmentalize receptors, ion channels, and intracellular signaling molecules within a restricted membrane domain. Rather than serving as passive cellular appendages, they organize diverse signaling pathways that regulate cellular development, homeostasis, and communication with the extracellular environment. By concentrating receptors and their

downstream effectors within a confined compartment, primary cilia enhance both the spatial and temporal precision of signal transduction.

During development, primary cilia are essential for several highly conserved signaling pathways, including Hedgehog (Hh), Wnt, Notch, and transforming growth factor-β (TGFβ) signaling. Together, these pathways regulate cell proliferation, differentiation, tissue patterning, and organogenesis. Consequently, disruption of ciliary signaling results in a broad spectrum of developmental abnormalities and underlies numerous human ciliopathies [29-34]. Although these developmental pathways established the biological importance of primary cilia, increasing evidence indicates that neuronal primary cilia remain active signaling compartments throughout adulthood, where they regulate neuronal physiology rather than developmental fate.

Unlike primary cilia in developing tissues, neuronal primary cilia are enriched with G protein-coupled receptors (GPCRs), making them important centers for neuromodulatory signaling. Numerous neuronal GPCRs—including somatostatin receptor 3 (SSTR3), serotonin receptor 6 (5-HT6), melanin-concentrating hormone receptor 1 (MCHR1), melanocortin 4 receptor (MC4R), dopamine receptors, and other neuromodulatory receptors—localize preferentially to the ciliary membrane, where their spatial organization enables highly regulated signaling responses [35-40] . Proper localization of these receptors depends on intraflagellar transport (IFT) machinery and trafficking adaptors such as TULP3 and the BBSome, highlighting the importance of ciliary protein trafficking for maintaining neuronal signaling competence[19, 20].

Among the signaling pathways concentrated within neuronal primary cilia, calcium and cyclic adenosine monophosphate (cAMP) signaling are particularly important. The restricted volume of the ciliary compartment permits localized changes in intracellular calcium concentration that can occur independently of the surrounding cytoplasm. Calcium-permeable channels, including polycystins and members of the transient receptor potential (TRP) channel family, contribute to the regulation of intraciliary calcium signaling, allowing primary cilia to function as specialized calcium signaling domains [41-43].

Calcium signaling is closely integrated with cAMP signaling through adenylyl cyclase 3 (ADCY3), one of the most abundant signaling proteins localized to neuronal primary cilia. ADCY3 generates cAMP within the ciliary compartment and serves as a major regulator of downstream GPCR signaling. Because ADCY3 activity is itself modulated by calcium and calmodulin, these second messenger systems are tightly interconnected, allowing extracellular stimuli to produce coordinated intracellular responses [44-49]. Compartmentalization of calcium and cAMP signaling within the primary cilium therefore provides an additional level of signaling specificity that cannot be achieved through cytoplasmic signaling alone.

Emerging evidence suggests that ciliary signaling extends beyond regulation of individual receptors to influence neuronal excitability and network activity. Localized second messenger signaling within primary cilia has been proposed to regulate membrane excitability through potassium channels positioned at the ciliary base and ciliary pocket, providing a potential mechanism through which ciliary GPCR activation influences cellular physiology [14, 50-54]. Although the mechanisms by which ciliary

signals are integrated into whole-cell electrical activity remain incompletely understood, these observations support the concept that primary cilia function as signaling centers capable of coordinating cellular responses beyond the ciliary compartment itself.

Collectively, these findings establish primary cilia as highly specialized signaling organelles that integrate extracellular signals with intracellular responses. Rather than functioning through a single signaling pathway, neuronal primary cilia coordinate multiple GPCR- and second messenger-mediated signaling networks that regulate neuronal physiology. This signaling complexity positions primary cilia to influence higher-order brain functions, including metabolism, sleep, circadian rhythms, motivation, and social behavior, providing the biological framework for the studies presented in this dissertation.

1.6 Primary Cilia in Neurological and Psychiatric Disorders

The importance of primary cilia in the nervous system extends beyond normal physiology and is increasingly recognized in neurological and psychiatric disease. Although ciliopathies were initially characterized by developmental abnormalities affecting multiple organ systems, accumulating evidence indicates that disruption of ciliary signaling also contributes to disorders of higher brain function. Altered ciliary structure, impaired protein trafficking, and dysregulated ciliary signaling have been associated with cognitive dysfunction, mood disorders, and neurodevelopmental disease, highlighting primary cilia as important regulators of neuronal homeostasis.

Transcriptomic analyses have identified widespread dysregulation of cilia-associated genes across major psychiatric disorders, including schizophrenia (SCZ), autism

spectrum disorder (ASD), bipolar disorder (BP), and major depressive disorder (MDD), with schizophrenia exhibiting the highest proportion of differentially expressed ciliary genes [55]. Notably, many of these dysregulated genes are shared among disorders, suggesting that impaired ciliary signaling may represent a common molecular mechanism contributing to diverse neuropsychiatric phenotypes. Consistent with this concept, molecular pathways governing ciliogenesis and ciliary maintenance are disrupted in both schizophrenia and bipolar disorder [56], further supporting the hypothesis that primary cilia represent a point of convergence for neuronal dysfunction across psychiatric disease.

While the precise contribution of primary cilia to psychiatric disorders remains incompletely understood, these observations suggest that disruption of ciliary signaling may alter neuronal communication, circuit function, and behavior. Understanding how primary cilia regulate neural circuits under physiological conditions is therefore likely to provide important insight into mechanisms underlying neuropsychiatric disease.

1.7 Primary Cilia and Physiology

Primary cilia and metabolic regulation

The localization of numerous G protein-coupled receptors (GPCRs) to neuronal primary cilia has established these organelles as important regulators of whole-body physiology, particularly energy homeostasis. Ciliary GPCRs, including somatostatin receptors, serotonin receptors, melanin-concentrating hormone receptor 1 (MCHR1), leptin receptor, and insulin receptor, coordinate signaling pathways that regulate feeding behavior, metabolism, and body weight [35, 38, 40, 57].

Genetic studies have demonstrated that disruption of ciliary signaling produces profound metabolic phenotypes. Deletion of the ciliary protein Kif3a from hypothalamic proopiomelanocortin neurons causes obesity and glucose intolerance, closely resembling metabolic abnormalities observed in Bardet–Biedl and Alström syndromes [58, 59]. Similarly, adenylyl cyclase III (ADCY3), a major ciliary signaling protein, is essential for body weight regulation. Loss of ADCY3 in the ventromedial hypothalamus promotes obesity, whereas mice expressing a humanized ADCY3 allele exhibit elongated primary cilia and increased resistance to diet-induced obesity [60, 61].

Melanocortin 4 receptor (MC4R), another ciliary GPCR, regulates energy balance through cAMP-dependent signaling within primary cilia. Disruption of MC4R localization or signaling impairs appetite regulation and energy homeostasis, while melanocortin receptor accessory protein 2 (MRAP2) controls MC4R localization within the ciliary membrane, providing an additional level of regulation [62, 63]. Likewise, disruption of ciliary dopamine D1 receptor localization, either through loss of primary cilia or defects in Bardet–Biedl syndrome proteins, results in obesity that is driven primarily by reduced locomotor activity rather than increased food intake [64].

Beyond metabolism, primary cilia also contribute to cognitive function. Selective removal of neuronal cilia from the hippocampus and cortex impairs learning, memory, and aversive conditioning, demonstrating that ciliary signaling regulates multiple behavioral domains beyond metabolic control [65].

Primary cilia and sleep.

Compared with other physiological functions, relatively little is known about the contribution of primary cilia to sleep regulation. Nevertheless, several lines of evidence suggest that ciliary signaling participates in the neural circuits controlling sleep architecture.

Melanin-concentrating hormone (MCH) is a well-established regulator of REM sleep, and its receptor, MCHR1, localizes specifically to neuronal primary cilia. Microinjection of MCH into either the median raphe or dorsal raphe nucleus increases REM sleep, suggesting that ciliary MCHR1 signaling may contribute to REM sleep regulation [66, 67].

Additional evidence comes from studies of adenylyl cyclase III (ADCY3), one of the most abundant signaling proteins within neuronal primary cilia. Mice lacking ADCY3 exhibit altered sleep architecture, increased REM sleep, and reduced neuronal activity, indicating that intact ciliary cAMP signaling is required for normal sleep regulation [68].

More recently, inducible deletion of IFT88 throughout the adult nervous system was shown to alter sleep architecture, reduce EEG power, and impair phase-amplitude coupling, demonstrating that primary cilia influence both sleep behavior and large-scale neural dynamics [69]. Similarly, deletion of Ift88 from adult striatal medium spiny neurons reduces long-range excitatory connectivity and weakens glutamatergic transmission, highlighting an essential role for primary cilia in maintaining striatal circuit function [70]. Together, these findings suggest that primary cilia regulate sleep not only through individual signaling pathways but also through broader modulation of neuronal network activity.

Primary cilia and locomotor behavior.

Primary cilia also contribute to the regulation of locomotor behavior. Altered localization of dopamine D1 receptors within primary cilia produces obesity accompanied by reduced spontaneous physical activity, indicating that ciliary dopamine signaling influences movement independently of food intake [64].

The behavioral effects of cilia disruption, however, depend on both neuronal subtype and behavioral context. While removal of primary cilia has little effect on baseline locomotor activity, it significantly reduces amphetamine-induced locomotor responses in dopaminergic neurons of both sexes. In contrast, deletion of cilia from GAD2-positive GABAergic neurons selectively decreases locomotor activity in males, suggesting that primary cilia regulate motor behavior through distinct neuronal populations and behavioral states [71].

Collectively, these studies demonstrate that neuronal primary cilia regulate diverse physiological processes, including metabolism, sleep, cognition, and locomotor behavior. Rather than functioning as isolated signaling structures, primary cilia integrate extracellular signals to coordinate complex behavioral outputs across multiple neural circuits. These findings raise the possibility that ciliary signaling similarly contributes to higher-order functions, including circadian regulation and social behavior, which form the central focus of this dissertation.

1.8 Primary Cilia and Circadian Rhythm

Circadian rhythms are endogenous, approximately 24-hour oscillations that coordinate physiology and behavior with the external light-dark cycle. These rhythms regulate diverse biological processes, including sleep-wake behavior, locomotor activity, metabolism, hormone secretion, body temperature, and cognitive performance. Although the suprachiasmatic nucleus (SCN) functions as the master circadian pacemaker, rhythmic behavior emerges through coordinated interactions between the SCN and distributed neural circuits throughout the brain. Increasing evidence suggests that primary cilia are integrated into these circadian networks and may contribute to the temporal regulation of neuronal signaling.

Primary cilia are particularly well suited to participate in circadian regulation because they are dynamic sensory organelles whose structure and signaling capacity respond to both extracellular and intracellular cues. Mechanical stimulation, cerebrospinal fluid flow, and intracellular second messenger systems such as calcium and cyclic AMP (cAMP) regulate ciliary morphology, while neuromodulators including dopamine, serotonin, melanin-concentrating hormone (MCH), and adenosine alter ciliary length and receptor signaling. Because changes in ciliary morphology influence receptor localization and signaling efficiency, primary cilia provide a mechanism through which neuronal responsiveness can be modulated over time.

Many physiological processes regulated by primary cilia exhibit pronounced daily rhythmicity. Feeding behavior, sleep-wake cycles, energy expenditure, body temperature, and locomotor activity all follow circadian patterns and are controlled, in part, by signaling pathways enriched within the ciliary compartment. Consistent with

these functions, numerous ciliary GPCRs—including melanocortin-4 receptor (MC4R), melanin-concentrating hormone receptor 1 (MCHR1), neuropeptide Y receptors, somatostatin receptor 3 (SSTR3), serotonin receptor 6 (5-HT6), dopamine D1 and D2 receptors, and adenosine A2A receptors—participate in behaviors that display strong circadian modulation. These observations suggest that primary cilia are strategically positioned to integrate environmental and physiological signals that vary across the day.

Support for this hypothesis has emerged from transcriptomic analyses of the mammalian brain. Genome-wide studies across multiple primate brain regions revealed that a large proportion of cilia-associated genes exhibit circadian oscillations, with particularly strong rhythmicity observed in striatal regions [72]. Similar analyses in the mouse brain demonstrated rhythmic expression of ciliary genes within the nucleus accumbens core (NAcC) and further showed that deletion of dopamine D2 receptors markedly reduced the number of rhythmically expressed ciliary genes, identifying dopaminergic signaling as an important regulator of ciliary rhythmicity [73]. Together, these findings indicate that primary cilia are not static cellular structures but are themselves subject to circadian regulation.

Our recent work extends these observations from gene expression to ciliary structure. Using high-resolution quantitative imaging, we demonstrated that primary cilia within the NAcC undergo robust circadian oscillations in length, reaching maximal length near Zeitgeber Time 11 (ZT11), immediately preceding the onset of the active phase [74]. Because ciliary length influences receptor localization and signaling capacity, these structural oscillations suggest that neuronal responsiveness may also fluctuate across

the circadian cycle. This finding provides direct evidence that primary cilia are dynamic components of the circadian system and raises the possibility that temporal regulation of ciliary signaling contributes to daily changes in behavior.

The relationship between dopamine signaling and primary cilia further supports this concept. Neuronal primary cilia are enriched with dopamine D1 and D2 receptors, together with several other neuromodulatory GPCRs that regulate motivation, arousal, and reward. Dopamine signaling bidirectionally regulates ciliary morphology, with D1 receptor activation promoting ciliary elongation and D2 receptor activation inducing ciliary shortening [26, 75]. Likewise, activation of MCHR1 alters ciliary length within the NAcC and other striatal regions [27]. These observations suggest that ciliary structure and signaling are continuously modified by neuromodulatory systems that themselves exhibit strong circadian variation.

Functional studies provide additional evidence linking primary cilia to circadian and sleep-related behaviors. Selective ablation of primary cilia from striatal medium spiny neurons impairs motor learning, executive function, working memory, attention, and interval timing without disrupting baseline locomotion [76]. Broad neuronal deletion of IFT88 alters sleep architecture, reduces electroencephalographic (EEG) power, and disrupts phase-amplitude and cross-frequency coupling [69], while deletion of Ift88 from adult striatal medium spiny neurons weakens glutamatergic transmission and reduces long-range excitatory connectivity [70]. Collectively, these studies demonstrate that intact ciliary signaling is required not only for normal neuronal function but also for coordinated network activity underlying complex behaviors.

Taken together, accumulating evidence supports a model in which primary cilia function as dynamic regulators of circadian neuronal signaling rather than passive sensory organelles. Their molecular composition, structural organization, and signaling capacity vary across time, and these changes are closely linked to dopaminergic signaling, neuronal excitability, and network dynamics. Despite these advances, whether primary cilia directly regulate circadian behavior and sleep-wake function within specific neural circuits remains largely unknown. Addressing this question requires examination of cilia within brain regions that integrate circadian information with motivated behavior, among which the nucleus accumbens core has emerged as a particularly compelling candidate.

2. Nucleus Accumbens Core

2.1 Anatomical and Circuit Organization of the NAcC

The nucleus accumbens core (NAcC), a principal subdivision of the ventral striatum, serves as a central hub for motivated behavior by integrating dopaminergic input from the ventral tegmental area (VTA) with glutamatergic projections from the prefrontal cortex, hippocampus, and basolateral amygdala to guide goal-directed actions [77-80]. Approximately 95% of neurons within the NAcC are GABAergic medium spiny neurons (MSNs), which are broadly classified according to their expression of dopamine D1- or D2-type receptors, while the remaining neuronal population consists primarily of GABAergic and cholinergic interneurons [81]. Although D1- and D2-MSNs are classically associated with the direct and indirect basal ganglia pathways, respectively, this distinction is less pronounced within the ventral striatum, where both

neuronal populations cooperate to regulate motivated behaviors rather than functioning as strictly opposing pathways [81].

The NAcC is anatomically and functionally distinct from the adjacent nucleus accumbens shell (NAcSh). These subregions differ in their cytoarchitecture, afferent and efferent connectivity, and behavioral functions. Whereas the NAcC projects predominantly to ventral pallidal structures involved in action selection, the NAcSh additionally communicates with limbic regions, including the lateral hypothalamus, supporting roles in emotional processing and homeostatic regulation [82]. Consequently, the NAcC has been more strongly associated with instrumental learning, cue-guided behavior, and goal-directed action, whereas the shell is preferentially involved in affective processing and reward valuation [82].

Beyond reward processing, the NAcC has emerged as an important regulator of behaviors that exhibit pronounced temporal organization, including sleep-wake regulation, circadian locomotor activity, and social behavior. While the circuit architecture of the NAcC has been extensively characterized, the subcellular mechanisms that coordinate these diverse behavioral functions remain poorly understood. Identifying these mechanisms is therefore critical for understanding how the NAcC integrates motivational and physiological signals to generate adaptive behavior.

2.2 NAcC in Circadian and Sleep-Wake Regulation

Although the suprachiasmatic nucleus (SCN) functions as the master circadian pacemaker, the expression of circadian behavior depends on distributed neural circuits that translate clock signals into physiological and behavioral outputs. Among these, the

nucleus accumbens core has emerged as an important downstream node linking dopaminergic signaling with sleep-wake regulation, locomotor activity, and circadian behavior.

Functional studies demonstrate that the NAcC actively regulates vigilance states. Selective lesions of the NAcC increase wakefulness while reducing non-rapid eye movement (NREM) sleep, particularly when damage is confined to the core subregion [83]. Conversely, activation of adenosine A2A receptor-expressing neurons promotes sleep, whereas inhibition of these neurons suppresses sleep [84].

Dopaminergic signaling further modulates arousal within the NAcC, as activation of D1 receptors promotes wakefulness and motivated feeding through downstream hypothalamic and midbrain circuits [85, 86], while D2 receptors mediate both arousal and sleep rebound following fentanyl administration [87]. Together, these findings identify the NAcC as an active regulator of sleep-wake state rather than simply a recipient of circadian information.

The NAcC also contributes to circadian locomotor behavior. Deletion of melanin-concentrating hormone receptor (MCHR1) signaling within the NAc increases spontaneous locomotor activity [88], while epigenetic regulation within the ventral striatum influences daily locomotor rhythms [89]. At the molecular level, disruption of striatal clock genes alters circadian rest-activity rhythms, and dopamine D1 receptor signaling reciprocally regulates clock gene expression through CREB-dependent pathways [90, 91]. These findings demonstrate that the NAcC participates in both the molecular and circuit-level regulation of circadian behavior.

Despite growing evidence linking the NAcC to circadian and sleep-wake regulation, the cellular mechanisms through which these functions are coordinated remain incompletely understood. Given the enrichment of neuromodulatory GPCRs and circadian signaling molecules within neuronal primary cilia, ciliary signaling represents a compelling candidate mechanism through which the NAcC may integrate circadian information.

2.3 NAcC in Social Behavior and Reward

The nucleus accumbens is a central component of the neural circuitry underlying social reward and affiliative behavior. Social interaction engages distributed networks spanning cortical, limbic, and midbrain regions, with the NAcC integrating motivational, sensory, and contextual information to promote appropriate social responses [77, 78]. Disruption of these circuits contributes to social deficits observed in autism spectrum disorder, schizophrenia, and major depressive disorder [77].

Effective social behavior requires not only activation of specific neuronal populations but also precise temporal coordination of neural activity across local and distributed circuits. Oscillatory synchronization and coordinated population dynamics are increasingly recognized as fundamental mechanisms supporting cognition, learning, and social behavior [92-94]. However, the cellular mechanisms that organize this temporal coordination remain largely unknown.

Within the NAcC, D1 receptor-expressing medium spiny neurons (D1-MSNs) play a particularly prominent role in motivated and social behaviors. Activation of D1-MSNs

promotes effort-based responding, voluntary exercise, and conditioned preference for social stimuli while reducing food consumption [95]. Social experience enhances excitatory synaptic input onto D1-MSNs, and disruption of oxytocin receptor signaling within this population impairs both social reward and social memory [77, 79, 96]. These findings identify D1-MSNs as a critical neuronal population linking dopaminergic signaling to social motivation and affiliative behavior.

Interestingly, the same D1-MSN population has also been implicated in circadian regulation and motivated locomotor behavior, suggesting that common cellular mechanisms may contribute to multiple NAcC-dependent behavioral outputs. Whether these shared functions are coordinated by neuronal primary cilia remains unknown.

3. Primary Cilia in the Nucleus Accumbens Core

Primary cilia are uniquely positioned to regulate the diverse behavioral functions of the NAcC. As discussed in Chapter 1, neuronal primary cilia compartmentalize GPCR signaling, second messenger pathways, and circadian regulators that influence neuronal excitability and network function. Within the NAcC, cilia-associated genes exhibit circadian oscillations, and dopamine signaling contributes to the temporal regulation of these molecular programs. Moreover, D1-MSNs combine ciliary D1 receptor signaling with established roles in both circadian behavior and social reward, making them particularly compelling candidates through which cilia may influence NAcC function.

Despite these observations, the functional contribution of primary cilia within the NAcC remains largely unexplored. It is unknown whether primary cilia broadly regulate

circadian and sleep-wake behaviors across the NAcC or whether specific neuronal populations, such as D1-MSNs, mediate distinct behavioral functions. Addressing this question is essential for understanding how ciliary signaling contributes to neural circuit function.

This dissertation directly tests these hypotheses by examining the consequences of disrupting primary cilia both broadly throughout the NAcC and selectively within D1-MSNs. By comparing these complementary approaches, the studies presented here distinguish circuit-wide functions of neuronal primary cilia from cell type-specific mechanisms regulating circadian behavior, sleep-wake architecture, and social behavior.

Chapter 2 Cilia in the Brain Display Region-Dependent Oscillations of Length and Orientation

Roudabeh Vakil monfared, Sherif Abdelkarim, Pieter Derdeyn, Kiki Chen, Hanting Wu, Kenneth Leong, Tiffany Chang, Justine Lee, Sara Versales, Surya M. Nauli, Kevin Beier, Pierre Baldi, Amal Alachkar ***Cilia in the brain display region-dependent oscillations of length and orientation****. PLoS Biology, 2025. 23(7): p. e3003197.*

Abstract

In this study, we conducted high-throughput spatiotemporal analysis of primary cilia length and orientation across 22 mouse brain regions. We developed automated image analysis algorithms, which enabled us to examine over 10 million individual cilia, generating the largest spatiotemporal atlas of cilia. We found that cilia length and orientation display substantial variations across different brain regions and exhibit fluctuations over a 24-h period, with region-specific peaks during light-dark phases. Our analysis revealed unique orientation patterns of cilia, suggesting that cilia orientation within the brain is not random but follows specific patterns. Using BioCycle, we identified rhythmic fluctuations in cilia length across five brain regions: the nucleus accumbens core, somatosensory cortex, and the dorsomedial, ventromedial, and arcuate hypothalamic nuclei. Our findings present novel insights into the brain cilia dynamics, and highlight the need for further investigation into cilia's role in the brain's response to environmental changes and regulation of oscillatory physiological processes.

Introduction

Cilia are evolutionarily conserved, microtubule-based organelles that extend from the surface of eukaryotic cells, including neurons in the mammalian brain. Their presence in diverse organisms from single-celled organisms to complex multicellular animals emphasizes their fundamental importance in a wide range of biological processes. Primary cilia, in particular, serve as essential sensory and signaling hubs, playing critical roles in cellular homeostasis, development, and signal transduction [1-9].

A striking feature of cilia is their dynamic nature, which is manifested in the continuous modulation of their structure and function in response to various environmental cues and cellular signaling events [5,6,10-16]. Mechanical forces or cerebrospinal fluid (CSF) flow can induce elongation or shortening of cilia, while intracellular signaling pathways mediated by cyclic AMP (cAMP) or calcium can reversibly modulate their morphology [17-20]. We and others have shown that neurotransmitters such as dopamine, serotonin, melanin-concentrating hormone (MCH), and adenosine can modulate primary cilia length, affecting their signaling capacity [21-24]. Although primary cilia are non-motile, their orientation can be dynamic due to the underlying cellular structures and signaling pathways regulating their relative positions. This dynamic orientation allows primary cilia to adapt to environmental changes and respond to different extracellular cues more effectively. Cilia orientation may adjust in response to numerous and varied cellular events, such as during cell migration [25,26], tissue repair [25], or in response to extracellular stimuli [27] such as mechanical stress or chemical gradients.

Many environmental stimuli and cellular signaling events sensed by cilia often follow rhythmic temporal patterns, such as light-dark cycles and fluctuations in temperature or

nutrient availability [28-34]. These patterns also extend to a broad range of functions influenced by cilia signaling, such as daily sleep-wake cycles, feeding behaviors, sexual/reproductive behaviors, energy balance, metabolism, and regulation of body temperature [35-42]. Furthermore, G-protein coupled receptors (GPCRs) located on primary cilia, including melanocortin 4 receptor (MC4R), melanin-concentrating hormone receptor 1 (MCHR1), neuropeptide Y receptors 2 and 5 (NPY2R, NPY5R), somatostatin receptor 3 (SSTR3), serotonin receptor 6 (5HT6), and dopamine receptor 1 (DRD1), DRD2, and galanin receptor are involved in various rhythmic functions such as food intake, body temperature regulation, and sleep [37,43-47]. We have previously uncovered a high degree of circadian rhythmicity and spatiotemporal oscillations in cilia-associated gene expression across mouse and primate brain areas, together with dynamic shifts in the expression of genes associated with primary cilia throughout the human life span [48,49]. This was further supported by our research into cilia gene dysregulation in major psychiatric disorders, hinting at shared pathophysiological processes [50]. This implies that cilia-signaling dysfunctions may underlie common neurological deficits across these disorders.

Despite significant advancements in our understanding of primary cilia structural dynamics, evidence linking cilia dynamics to biological rhythms remains limited. This study aims to characterize the dynamic nature of primary cilia in the mouse brain by analyzing spatiotemporal variations in cilia length and orientation and assessing their time-of-day-dependent fluctuations. Through a comprehensive analysis of cilia properties and their temporal changes, we hope to provide a foundation for future studies to

investigate the functional roles of cilia across brain regions and their potential contributions to time-dependent physiological processes.

Methods

Animals

All experimental procedures were approved by the Institutional Animal Care and Use Committee (IACUC) of the University of California, Irvine (Protocol #AUP-23-017), and were conducted in accordance with national and institutional guidelines for the care and use of laboratory animals. Eight-week-old Swiss Webster male mice were obtained from Charles River (North Carolina, USA). The mice were maintained on a 12-h light/dark cycle and provided with food and water ad libitum.

Brain tissue collection

Mice were deeply anesthetized using isoflurane and subsequently transcardially perfused with a combination of 0.9% saline and 4% paraformaldehyde (PFA). We used a total of 56 mice, perfusing 4–5 mice at every 2-h interval over a 24-h period, resulting in 12 time points. This sample size was chosen to provide sufficient statistical power to detect significant cilia morphological differences, as validated for accuracy and reproducibility in our earlier publications. Following perfusion, we harvested the brains, preserved them in PFA overnight, and then transferred them to a 30% sucrose solution. The brains were then coronally sectioned at a thickness of 30 μm using a microtome.

Immunohistochemistry and imaging

For immunohistochemistry preparation, 3−4 sections were selected from various levels across the brain. The sections were then blocked using goat serum in PBS containing 0.3% Triton X-100 for 1h. Following this step, the brain sections were incubated in blocking buffer solution containing the rabbit primary anti-adenylate cyclase 3 (ADCY3) antibody (LSBIO-C204505), at a dilution of 1:500. Post-primary antibody incubation, the sections were rinsed with PBS and incubated with the secondary antibody, Invitrogen AlexaFluor546 goat anti-rabbit, at a dilution of 1:500, along with DAPI at a dilution of 1:10,000 (Thermo Fisher Scientific). The sections were then washed with PBS and mounted onto slides. The cilia were imaged using the Keyence BZ-9000 fluorescence microscope with a 20× objective lens. Brain regions analyzed include: Anterior hypothalamic area (AHC), Arcuate nucleus (ARC), Dorsomedial hypothalamus (DMH), Lateral hypothalamus (LH), Median preoptic area (MPO), Hypothalamic paraventricular nucleus (PVN), Suprachiasmatic nucleus (SCN), Supraoptic nucleus (SON), Ventromedial hypothalamus (VMH), Caudal striatum (CS), Nucleus accumbens core (NAc), Nucleus accumbens shell (NAs), Rostral striatum (RS), Olfactory tubercle (TU), Cornu Ammonis 1 (CA1), Cornu Ammonis 3 (CA3), Dentate Gyrus (DG), Motor cortex (MC), Prefrontal cortex (PFC), Piriform cortex (Pir), Somatosensory cortex (SSC), Medial amygdala (MA). Dual-staining immunohistochemistry was performed to verify the base and tip of primary cilia. The basal body was detected using a rabbit anti-Centrin 1 polyclonal antibody (Proteintech, 12794-1-AP) at a 1:200 dilution, while the cilia were stained with a chicken anti-ADCY3 antibody (EnCor Bio, CPCA-ACIII) at a 1:500 dilution. Secondary antibodies included Alexa Fluor 488 goat anti-rabbit (Invitrogen, A-11008) and Alexa Fluor 564 goat anti-chicken (Invitrogen, A-11040), both at a 1:200 dilution. Images were captured using fluorescence microscopy at 40x magnification.

Cilia length and angle measurement

Our first step involved pre-processing the images by converting them to grayscale, to make them conducive for analysis and to mitigate color-related complications. We then applied Gaussian blur to the images to minimize noise or minor details that might compromise the accuracy of our measurements. Next, we used canny edge detection to find all the edges in the images. This allowed us to identify the cilia more easily and accurately. We applied a threshold value to the canny edge detection output to obtain a binary image where the edges were represented by white pixels and the background is represented by black pixels. After obtaining the binary image, we used the findContours() function in OpenCV to detect all the cilia in the image. This function identifies and segments all the distinct objects in the image, in this case, the cilia, and returns a list of their contours. However, some of these contours may be noise or not relevant to our analysis. Therefore, we filtered them based on their size, aspect ratio, and other factors to only capture the ones that are likely to be cilia. For instance, we filter the contours based on their length, as cilia are typically longer than they are wide. We set a minimum and maximum length threshold for the contours to keep only the ones that fall within this range. In our implementation, we use a minimum length of 1 μm and a maximum length of 15 μm. Furthermore, we filter the contours based on their aspect ratio, as cilia are generally slender structures with a length-to-width ratio greater than 3:2. We set a minimum aspect ratio threshold for the contours to remove any that do not meet this criterion. In our implementation, we used a minimum aspect ratio of 1.5. For each contour, we fit a bounding box around it using the cv2.boundingRect() function. This gave us the length and angle of the cilia. The length was calculated as the distance between the top

and bottom points of the bounding box, and the angle was calculated as the angle between the major axis of the box and the horizontal axis. However, we also needed to determine the base of the cilia accurately. To achieve this, we used the cv2.minMaxLoc() function to find the brightest pixel in the grayscale image within the bounding box of the cilia. The cilia's base is typically the most illuminated section, and this method enables us to pinpoint it with precision. To further improve the accuracy of our angle measurements, we combine the location of the base of the cilia with the center point of the bounding box. By comparing the relative positions of these points, we were able to determine which quartile the cilia were facing and adjust the angle measurement accordingly. Finally, we saved all the information about the cilia, including their lengths, angles, and positions, in a CSV file. This allowed us to analyze the data more easily and systematically. The two programs we developed and used are provided as supplementary materials (S1 Code), referred to as Program 1 and Program 2. A detailed, step-by-step description of the analysis pipeline is outlined below, and a visual walkthrough demonstrating each step is available in supplementary materials (S1 Video).

Analysis pipeline

The cilia detection pipeline consists of three main phases: contours extraction, contours filtering, length, and angle measurement. The specific OpenCV functions used for each step are included.

Phase 1: Contours extraction.

1. Canny Edge Detection: Purpose — Detect edges in the image, highlighting regions of rapid intensity change, which often correspond to object boundaries. Method — The

grayscale image is processed using cv2.Canny edge detection. The Canny function takes two thresholds to detect strong and weak edges. The lower threshold is calculated as 0.67 × median intensity, and the upper threshold is slightly increased to detect a broader range of edges.

2. Close holes: Purpose — Fill small holes in the binary image to create more complete and connected foreground regions. Method — Morphological closing is applied using cv2.morphologyEx with the cv2.MORPH_CLOSE operation and a rectangular kernel of size (2, 2).

3. Erode edges: Purpose — Refine the detected edges by removing small noise and shrinking the boundaries of detected regions slightly. Method — Erosion is applied using cv2.erode with a rectangular kernel of size (1, 1) for one iteration, which helps clean up the edges of the detected contours.

4. Find contours: Purpose — Identify the boundaries of the foreground regions, which represent the cilia structures. Method — Contours are extracted from the processed binary image using cv2.findContours with cv2.RETR_EXTERNAL and cv2.CHAIN_APPROX_SIMPLE.

Phase 2: Contours filtering.

1. Minimum and maximum length: Purpose — Ensure that only contours of appropriate length are considered, excluding those that are too short or too long. Method — The length of each contour is calculated using the dimensions from cv2.minAreaRect, and contours with a length greater than 1 μm and less than 15 μm are retained.

2. Minimum length-to-width ratio: Purpose — Filter out contours that do not meet a minimum aspect ratio, ensuring that only elongated structures, which are characteristic of cilia, are included. Method — For each contour, the ratio of its length to width is calculated. Contours with a ratio greater than or equal to 1.5 are kept, while those below this threshold are discarded.

Phase 3: Length and angle measurement.

1. Getting length and angle for each contour: Purpose — Measure the initial length and angle of each cilium to provide quantitative data on their orientation and size. Method — For each filtered contour, the length and width are extracted using cv2.minAreaRect. The cv2.contourArea function calculates the area, and the cv2.minAreaRect function provides the minimum bounding rectangle, from which the dimensions and initial angle are derived.

2. Adjusting the angle based on base and tip prediction: Purpose — Refine the initial angle measurement by determining the base and tip of the cilium for more accurate orientation data. Method — To refine the angle measurement, each cilium is drawn separately on a mask, and the location of the maximum intensity within the mask is found using cv2.minMaxLoc. The purpose is to find the brightest spot within the cilium, which usually indicates the base. The relative position between the base to the center is used to adjust the angle appropriately, ensuring the measured angle reflects the true orientation of the cilium.

Circular angles' mean calculation

Due to the circular nature of angles, the traditional arithmetic mean method is not applicable for calculating angle means. Therefore, we computed the circular mean, also

known as the angular mean, to calculate meaningful statistics for our angle dataset. The circular mean of our angle dataset was calculated as follows: First, the angle values were converted to radians, and all the data were subsequently transformed into sines and cosines. The means of the sines and cosines were calculated by summing the values and dividing them by the total count of each value. The circular mean was determined using the atan2 function, a variant of the arctangent function that accepts two arguments and yields results within the appropriate quadrant. The obtained results were then converted back to degrees using the equation: Degrees = radians × (180/π). If negative outputs were obtained from the atan2 function and the data ranged from 0 to 360, 360 was added to those values to align them within the correct range.

Quantification of cilia density across mouse brain

To determine the cilia density in each of the 22 brain regions, we calculated the percentage of ADCY3-stained cilia relative to the number of DAPI-stained cells within the same region.

In order to detect cells in DAPI-staining images, the pipeline processes images to detect and analyze contours, focusing on the identification of significant structures within the image. The methodology consists of three main phases: contours extraction, contours clustering, and contours filtering.

Phase 1: Contours extraction.

1. Image equalization: Purpose — Enhance the contrast of the grayscale image to improve the visibility of features. Method — Apply Contrast Limited Adaptive Histogram Equalization (CLAHE) using OpenCV's cv2.createCLAHE function with clipLimit=2.0 and

tileGridSize=(8, 8). This method adjusts the image contrast in localized regions, enhancing the structural details.

2. Adaptive thresholding: Purpose — Convert the grayscale image into a binary image to segment the foreground from the background. Method — Use OpenCV's cv2.adaptiveThreshold function with parameters maxValue=255, adaptiveMethod=cv2.ADAPTIVE_THRESH_MEAN_C, thresholdType=cv2.THRESH_BINARY, blockSize=41, and C=-10. This technique applies a threshold based on the local mean intensity, effectively segmenting the image.

3. Distance transform: Purpose — Compute the distance to the nearest zero pixel for each pixel in the binary image to prepare for isolating the foreground objects. Method — Implement OpenCV's cv2.distanceTransform function with distanceType=cv2.DIST_L2 and maskSize=3. This transformation aids in distinguishing foreground components.

4. Thresholding: Purpose — Refine the binary image to emphasize significant foreground regions. Method — Apply OpenCV's cv2.threshold function with thresh=0.2, maxval=1.0, and type=cv2.THRESH_BINARY. This step applies a fixed threshold to the distance-transformed image to highlight the foreground areas.

5. Dilation: Purpose — Expand the foreground regions to ensure connectivity of close components. Method — Use OpenCV's cv2.dilate function with a kernel of np.ones((3, 3), np.uint8) and iterations=1. This morphological operation enlarges the foreground regions, making them more pronounced and connected.

6. Isolate foreground and background: Purpose — Separate the sure foreground, sure background, and unknown regions for better segmentation. Method — Identify the sure

foreground by dilating the thresholded image, and the sure background by inverting and dilating the foreground mask using cv2.bitwise_not and cv2.dilate with kernel=np.ones((3, 3), np.uint8) and iterations=1. The unknown region is derived by subtracting the sure foreground from the sure background using cv2.subtract.

7. Extract contours from foreground: Purpose — Identify the boundaries of the foreground objects. Method — Extract contours from the sure foreground mask using OpenCV's cv2.findContours function with mode=cv2.RETR_EXTERNAL and method=cv2.CHAIN_APPROX_SIMPLE. This step identifies the boundaries of the foreground objects for further analysis.

Phase 2: Contours clustering.

1. Cluster contours with DBScan: Purpose — Group closely situated contours to manage fragmented contours representing a single object. Method — Use the DBSCAN (Density-Based Spatial Clustering of Applications with Noise) algorithm from scikit-learn with parameters eps=30 and min_samples=1 to cluster the contours based on their centroid positions. This clustering helps in grouping related contours.

2. Merge contours within each cluster: Purpose — Combine contours within each cluster to form a single, cohesive contour for each detected object. Method — Merge contours by calculating the convex hull of all points within each cluster using OpenCV's cv2.convexHull. This step ensures that all points in a cluster are enclosed in a single contour.

Phase 3: Contours filtering.

1. Minimum and maximum area: Purpose — Ensure that only contours of relevant size are considered for analysis. Method — Filter contours based on area (in pixels) using OpenCV's cv2.contourArea function with minimum area = 20 pixels and maximum area = 1000 pixels. This step excludes contours that are too small or too large to be relevant.

2. Minimum circularity: Purpose — Eliminate contours that do not meet the minimum shape criteria, focusing on more circular objects. Method — Calculate the circularity of each contour and retain only those with a circularity above the specified threshold using OpenCV's cv2.arcLength function and a minimum circularity of 0.01. Circularity is calculated as: circularity = $4\pi \cdot \text{Area} / \text{Perimeter}^2$

Verification of the automated measurements of cilia lengths and angles

To validate the automated measurements of cilia lengths and angles, and to verify the accuracy of our pipeline in identifying and measuring cilia structures, we conducted manual checks on random samples, selecting at least 10 cilia from each of the 22 brain regions. The measurements were performed blindly using both manual and automated methods. We then compared the results by calculating the recall and mean absolute error (MAE) for both length and angle measurements.

Since cilia length and orientation were measured from 2D images, projecting 3D structures like cilia onto a 2D plane can introduce measurement errors. To address this, we estimated the potential errors introduced by this approach using basic geometric principles, including the Pythagorean theorem. Detailed calculations are provided in the supplementary material (Figs A–C in S1 Text).

Comparative and correlational analysis of cilia lengths and angles

We analyzed the data using two different approaches: first, by assessing the lengths and angles of individual cilia to provide a detailed frequency distribution across all examined brain regions; and second, by calculating the mean length and angle of cilia in each section of the left and right hemispheres, treating these averages as single values for further analysis.

To analyze differences in cilia lengths and angles across various brain regions at different times of the day, we performed one-way ANOVA. Multiple comparisons were adjusted by controlling the False Discovery Rate (FDR) using the two-stage linear step-up procedure of Benjamini, Krieger, and Yekutieli. Additionally, we computed the Pearson correlation coefficient (r) for each pair of region-specific cilia lengths and angles across 24-h time points, generating a correlation matrix to examine the relationships among all brain regions. Data were analyzed using GraphPad Prism 9.4, with statistical significance set at $p<0.05$, and expressed as mean ± standard error of the mean (SEM).

Network analysis

Using the Allen Mouse Brain Connectivity Atlas data, we built a structural network of the regions used in our study. We normalized projections from source regions to other regions of interest by dividing the projection density by the injection volume. The normalized projection density was averaged across all experiments for each pair of source and target regions to generate a connectivity matrix. These values were log normalized to produce a more effective distribution for use as edge weights in a network. Community detection was carried out using the Louvain algorithm implemented in scikit-network with a resolution parameter of 1. We identified three main clusters of brain regions: purple (NAc, NAs, and others), green (PFC, MC, and others), and red (CA1, CA3, and DG). We

examined the correlation between cilia length and angle with various network features. We examined all pairs of regions within and across different clusters, identifying varying fractions of region pairs correlated by either cilia length or angle. We also analyzed whether these fractions would likely occur if regions were correlated randomly, shuffling all correlations across region pairs for this purpose. We constructed cilia correlation networks using a log-scaled R value to achieve a desirable distribution for edge weights. Network analysis was performed in Python using NetworkX, with network visualizations created using Plotly.

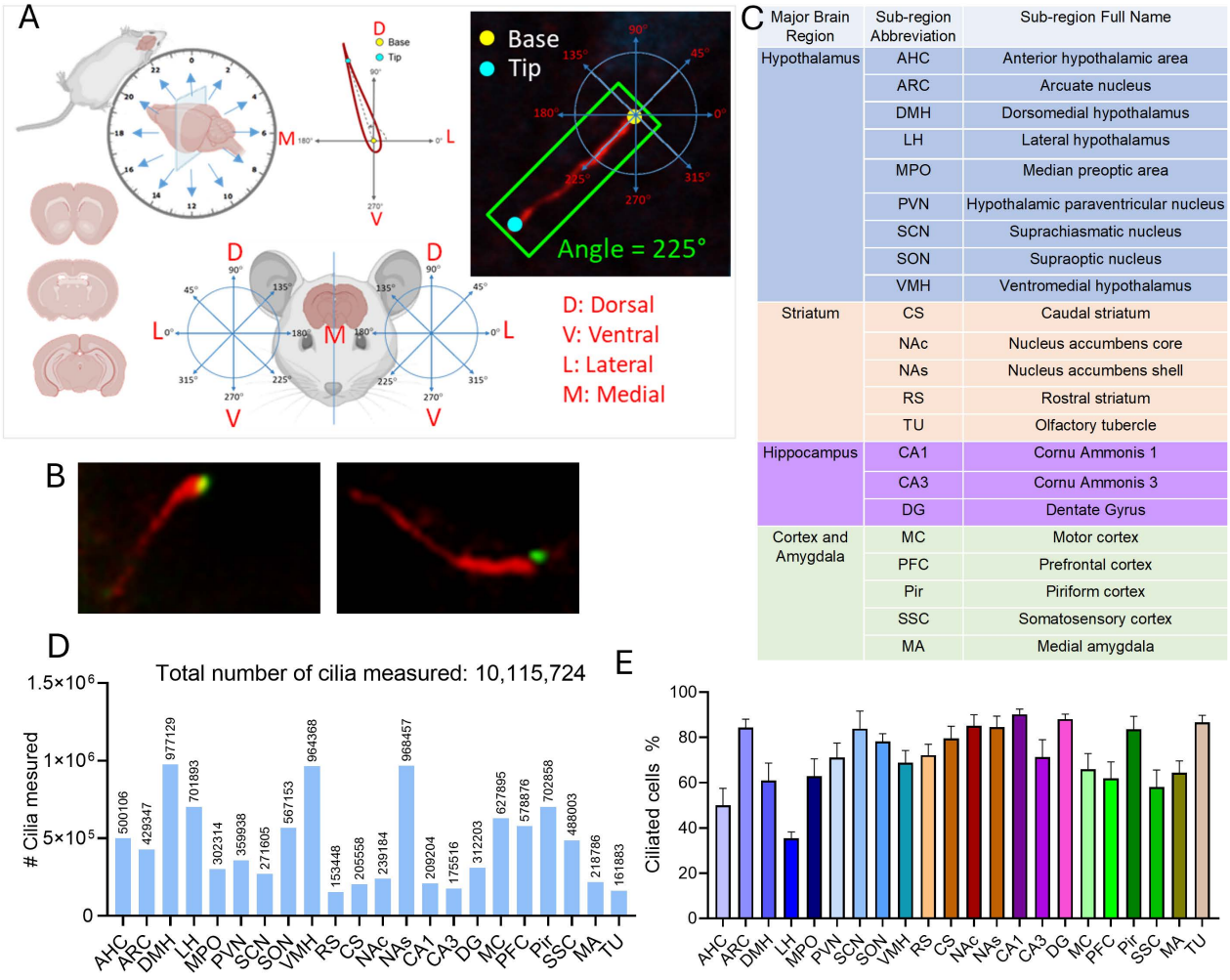
Circadian rhythmicity analysis

BIO_CYCLE, a deep-learning model designed for assessing periodicity of signals, was utilized to determine significant circadian patterns in cilia length and angle, as well as their oscillation's amplitude and phase. BIO_CYCLE is trained using synthetic and real biological time series datasets with labeled periodic and aperiodic signals. This tool comprises a deep neural network (DNN) for classification, which distinguishes periodic from non-periodic signals, and another DNN for regression estimating the signal's period, phase, and amplitude. The oscillation status of a parameter is defined based on a p-value (with a cutoff of 0.05) computed by BIO_CYCLE as follows: N aperiodic signals are first generated from the synthetic time series datasets, and the N output values V(i) (i=1, …, N) of the classification DNN on these aperiodic signals are calculated. The output value V of the new signal s is then compared to V(i) (i=1, …, N), producing the estimate for the probability of obtaining an output of size V or greater (p-value), assuming that the signal is part of the null distribution (aperiodic signals). A smaller p-value suggests a higher likelihood of the signal being periodic. The related q-values are calculated via the

Benjamini and Hochberg procedure. BIO_CYCLE is freely accessible from the CircadiOmics web portal: http://circadiomics.igb.uci.edu.

Results

We mapped the spatiotemporal patterns of cilia length and orientation across various brain regions in mice. We developed and used a special program to analyze cilia in brain sections from a large cohort of over 50 mice, with a minimum of four mice at each of the twelve 2-h intervals within a 24-h cycle (Fig 1A and Fig D in S1 Text). We verified the cilia base through dual immunostaining of Centrin 1, a well-established marker for the ciliary basal body, and ADCY3 (Fig 1B). We examined 3–4 brain sections per region at each time interval across 22 cilia-rich brain regions (Fig 1C). Our automated method allowed us to analyze 10 million cilia and more than 20 million data points, with counts of cilia assessed in specific regions ranging from 153,448 in the RS to 977,129 in the DMH (Fig 1D). The original raw data for these analyses are available in the Zenodo database (https://doi.org/10.5281/zenodo.15151271).



Major Brain Region	Sub-region Abbreviation	Sub-region Full Name
Hypothalamus	AHC	Anterior hypothalamic area
	ARC	Arcuate nucleus
	DMH	Dorsomedial hypothalamus
	LH	Lateral hypothalamus
	MPO	Median preoptic area
	PVN	Hypothalamic paraventricular nucleus
	SCN	Suprachiasmatic nucleus
	SON	Supraoptic nucleus
	VMH	Ventromedial hypothalamus
Striatum	CS	Caudal striatum
	NAc	Nucleus accumbens core
	NAs	Nucleus accumbens shell
	RS	Rostral striatum
	TU	Olfactory tubercle
Hippocampus	CA1	Cornu Ammonis 1
	CA3	Cornu Ammonis 3
	DG	Dentate Gyrus
Cortex and Amygdala	MC	Motor cortex
	PFC	Prefrontal cortex
	Pir	Piriform cortex
	SSC	Somatosensory cortex
	MA	Medial amygdala

Fig 2.1 Experimental design and data analysis. (A) Schematic Representation: (Top Left) Mice were perfused and harvested at two-hour intervals over a 24-h period. The harvested mice were then sectioned coronally. (Bottom Left) Coronal brain sections at different brain levels. (Top Middle) The ciliary base was defined as the origin of the coordinate system, and the tip of the cilia was labeled. Cilia length was measured from the base to the tips, and the circular angle was determined. (Bottom Middle) The brain section of the mice was divided into left and right hemispheres. For cilia found in the right hemisphere, a counter-clockwise coordinate system was used to determine the circular angle (Right). For cilia found in the left hemisphere, a clockwise coordinate

system was used (Left). (Top Right) An example of the angle measurement from cilia found in the right hemisphere. (B) Representative images of immunofluorescence staining showing cilia labeled with the ADCY3 antibody (red) and the basal body (cilia base) labeled with the centrin 1 antibody (green). (C) Brain Regions analyzed for cilia length and angle. (D) The number of cilia analyzed in 22 different brain regions of the mice; underlying data are available on the Zenodo database (https://doi.org/10.5281/zenodo.15151271). (E) Cilia density in 22 brain regions, expressed as the percentage of ciliated cells relative to the total number of cells in each region, underlying data are available in S1 Data. Parts of Fig 1A are created with BioRender.com.

Methodological verification

To validate the accuracy of our automated system for measuring cilia length and angle, we conducted a comparative analysis with manual measurements. In each of the 22 brain regions analyzed, 10 cilia were measured manually. The average of these manual measurements was then compared to the automated measurements. This comparative analysis showed a recall of 93.46%, indicating high reliability in the automated detection of cilia. The MAE for cilia length was 1.33 μm, and the MAE for angle measurements was 7.759 degrees (S1 Data). We also estimated the instrumental error introduced by measuring 3D cilia structures in 2D. Detailed calculations are provided in the Supplementary results (Figs A–C in S1 Text).

Region-dependent variations in cilia density, length, and angle in the mouse brain

Our analysis demonstrated marked variability in cilia density across the 22 brain regions examined. The lowest density was observed in the LH, where only 35% of cells were ciliated, while the highest density was found in the CA1 region of the hippocampus, with 90% of cells containing cilia (Fig 1E and S1 Data).

We assessed the average cilia length within specific brain regions using two distinct approaches. First, in the direct regional average method, we calculated the average length of each cilium individually within each region, revealing a variation in cilia lengths from 4.79 μm in the NAs to 6.33 μm in the TU (panel a of Fig E in S1 Text). Across all brain regions, including over 10 million cilia, this method resulted in an overall mean cilia length of 5.15 μm.

Second, in the section-based average method, we calculated the average of lengths of all cilia within each section to obtain a single value per section, then used these sections' averages to calculate the overall mean cilia length for each region. The brain-wide cilia length average was 5.4 ± 0.01 μm, with regional averages ranging from 4.87 μm in the NAs to 6.3 μm in the TU (Fig 2A and S2 Data). Additionally, a frequency distribution analysis showed that approximately 40% of cilia across all examined regions had lengths within the 4.8–5.4 μm range (Fig 2B and 2C). However, the frequency distribution analysis revealed a varied distribution of cilia lengths across the 22 brain regions. Some regions, like the ARC, MPO, SCN, and NAs have most cilia lengths concentrated around a narrow

range, whereas other regions, like the CS and RS, exhibit a broader distribution, with cilia lengths spread across a wider range (panel b of Fig E in S1 Text).

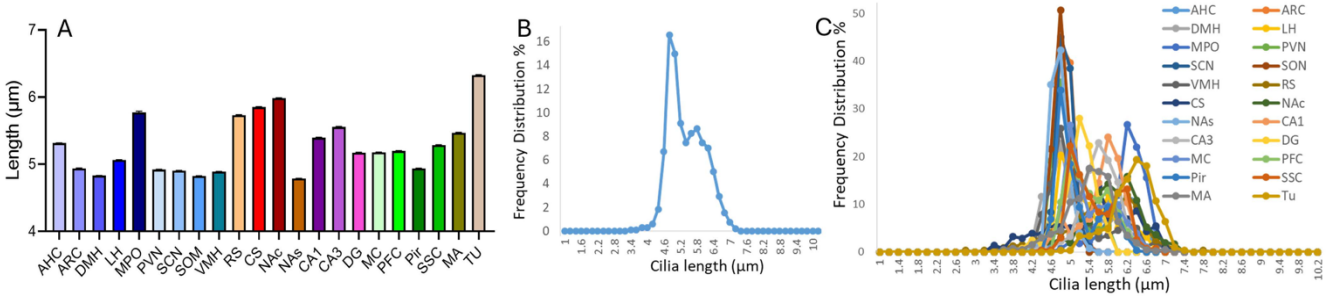


Fig 2.2 Cilia length analysis in different brain regions. (A) Histogram showing the means±SE of cilia length in the 22 brain regions based on the average length measured in each brain section. The x-axis represents cilia length in micrometers and the y-axis represents the percentage frequency of occurrence. (B and C) Histograms showing the frequency distribution of cilia length in (B) the entire brain and (C) the 22 individual brain regions, using the section-based average method. For each brain section, the lengths of all cilia were averaged to obtain a single value, which was then used to calculate the overall mean cilia length for each region. The mean cilia length was derived from the average lengths of both left and right hemisphere sections (3–4 sections per region). The x-axis represents cilia length in micrometers, and the y-axis shows the percentage frequency of occurrence; underlying data for Fig 2 are available in S2 Data.

Our analysis of individual cilia angles of over 10 million cilia showed a distinct pattern across all regions (Fig 3 and Fig F in S1 Text). Notably, the highest distribution of cilia orientation across the entire brain was toward 180° and 270°, indicating a primary medial and/or ventral orientation of cilia (Fig 3 and Fig F in S1 Text). However, cilia orientation did not exhibit uniform patterns across different brain regions (Fig 3). The RS, CS, MA, and CA3 showed a predominant cilia orientation toward 180°, and a secondary preference for 270°, whereas the NAc, TU, MPO, SCN, DG, and CA1 exhibited a primary

orientation toward 270°, followed closely by 180° (Fig 3). A more scattered distribution of cilia orientation was observed in the hypothalamic nuclei, various cortices, and the NAs.

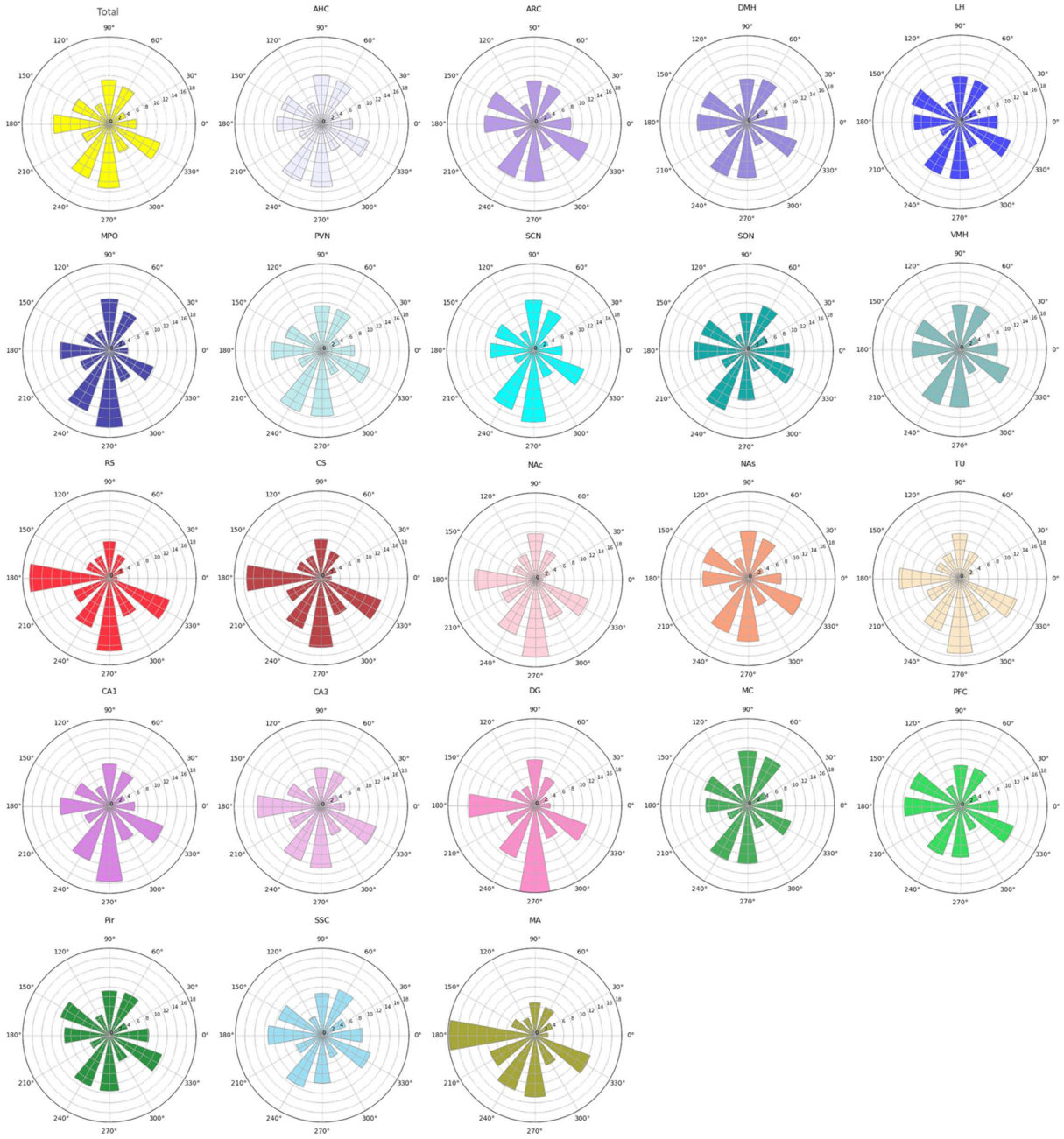
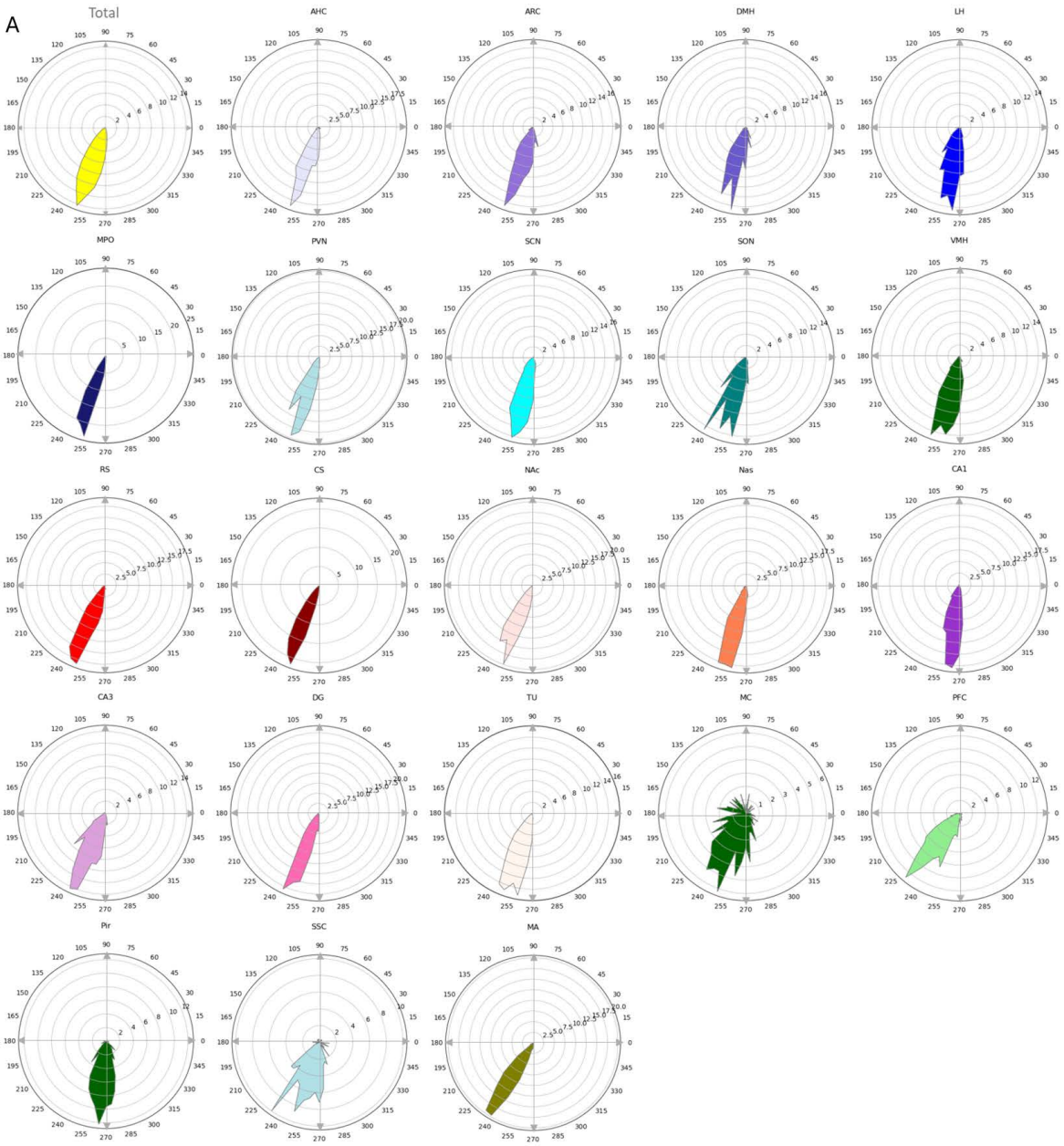


Fig 2.3. Cilia circular angle analysis, based on individual cilia measurements. Rose plot displaying the frequency distribution of cilia circular angles in individual brain regions from all individual measured cilia at 30° bins. Underlying data are available on the Zenodo database (https://doi.org/10.5281/zenodo.15151271).

When using the section-based averaging, where the circular mean of all cilia angles within each section was first determined and treated as a single value, cilia angle means and distributions revealed distinct patterns. Cilia angles predominantly favored the third quadrant (180°–270°), particularly around 250°, when measured relative to the horizontal line in coronal sections (Fig 4A, 4B and panel a of Fig G in S1 Text). The Pir exhibited the highest circular mean cilia angle (267°), whereas the MC displayed the lowest (219°) (Fig 4B and panel b of Fig G in S1 Text).


A
Total
AHC
ARC
DMH
LH
MPO
PVN
SCN
SON
VMH
RS
CS
NAc
Nas
CA1
CA3
DG
TU
MC
PFC
Pir
SSC
MA

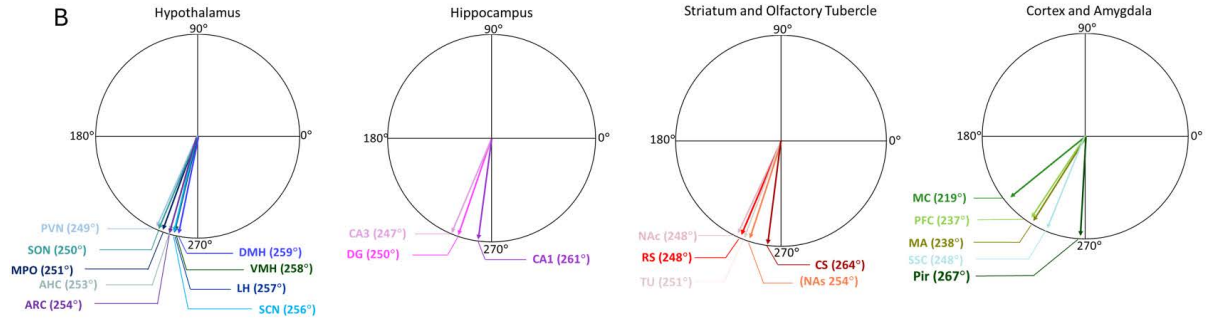

B
Hypothalamus
Hippocampus
Striatum and Olfactory Tubercle
Cortex and Amygdala
90°
180°
0°
270°
PVN (249°)
SON (250°)
MPO (251°)
AHC (253°)
ARC (254°)
DMH (259°)
VMH (258°)
LH (257°)
SCN (256°)
CA3 (247°)
DG (250°)
CA1 (261°)
NAc (248°)
RS (248°)
TU (251°)
CS (264°)
(NAs 254°)
MC (219°)
PFC (237°)
MA (238°)
SSC (248°)
Pir (267°)

Fig 2.4. Cilia circular angle analysis based on section-averaged circular means. (A) Radial plot showing the frequency distribution of cilia circular angles across the entire brain and individual brain regions. The analysis is based on section-averaged circular means, where the circular mean of all cilia angles within each section was first calculated and treated as a single value. Underlying data are available in S2 Data. (B) Radial plots displaying the mean cilia circular angles for the 22 brain regions, grouped into major categories: hypothalamus, hippocampus, cortices, and striatum. The average angle for each region was determined by calculating the circular angle means for each brain section. Underlying data are available in S2 Data.

We found no significant correlation between cilia density and cilia length (Pearson's coefficient, $r=-0.08$, $P=0.718$), whereas there was a trend toward a positive correlation between cilia density and orientation ($r=0.38$, $P=0.084$).

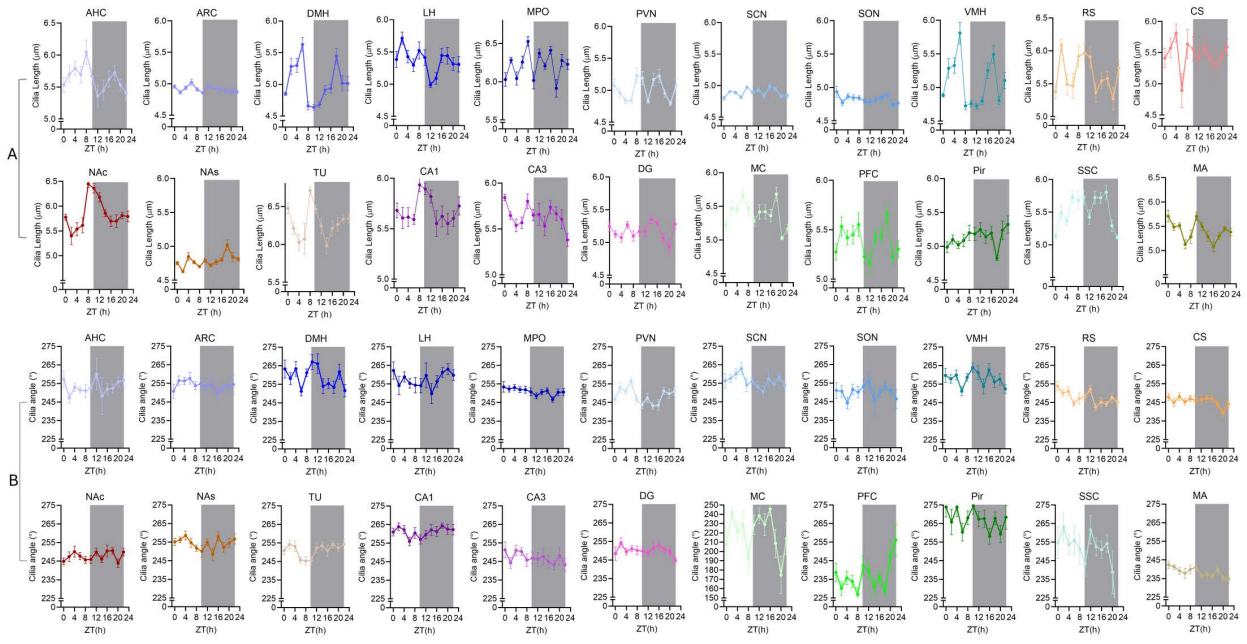
Temporal fluctuations and rhythmicity in cilia length and orientation across brain regions

We next analyzed cilia lengths and orientations at 2-h intervals over a 24-h period (S2 Data), and found complex, time-dependent fluctuations in both cilia length and orientation across various brain regions (Fig 5A and 5B). Notably, all regions except the AHC and CS exhibited significant variations in cilia length, with distinct fluctuation patterns observed during the light and dark phases (Fig 5A–5C).

Notably, the MA, LH, RS, CS, TU, AHC, CA3, and NAc reached their maximum cilia lengths at specific zeitgeber times (ZTs) during the light phase, whereas the ARC, DG, NAs, and PFC showed peak lengths at different ZTs during the dark phase (Fig 5A and 5C). Interestingly, both the DMH and VMH exhibited a bimodal pattern, with cilia length

peaks occurring at ZT 6 and ZT 18 during the light and dark phases, respectively (Fig 5A and 5C).

We observed significant time-dependent fluctuations in cilia angles within seven brain regions: DMH, PVN, RS, MC, PFC, SSC, and TU (Fig 5B and 5C). Notably, the DMH and PVN, two hypothalamic nuclei, displayed contrasting cilia angle patterns. The DMH reached its highest cilia angle between ZT 16–20, while the PVN showed its lowest angle during this same period. Conversely, at ZT 6, the DMH exhibited its lowest angle, and the PVN reached its highest (Fig 5B and 5C). The PFC's cilia angle changes were opposite to those in the SSC, with the PFC peaking at ZT 22, while the SSC reached its lowest angle at that time. The MC showed the most extensive range of cilia angle shifts, varying from 174° at ZT 20–245° at ZT 16 (Fig 5B and 5C).



Region		AHC	ARC	DMH	LH	MPO	PVN	SCN	SON	VMH	RS	CS	NAc	NAs	CA1	CA3	DG	MC	PFC	Pir	SSC	MA	TU
Length	(P value)	0.0504	0.0051	<0.0001	0.0057	<0.0001	<0.0001	<0.0001	0.0293	<0.0001	0.0002	0.1932	<0.0001	<0.0001	0.0179	0.0071	0.0039	<0.0001	0.0014	0.0402	<0.0001	<0.0001	<0.0001
Angle	(P value)	0.5127	0.8929	0.0119	0.5197	0.3963	0.0003	0.272	0.5903	0.0626	0.0028	0.085	0.2724	0.1127	0.258	0.6496	0.4146	0.0093	0.0016	0.2616	0.0023	0.0711	0.024

Fig 2.5. Fluctuation of cilia length and cilia circular angle across 24-hours' time.

(A and B) Diurnal fluctuations of cilia length (A) and angle (B): The plots show the

means ± SE of cilia length and angle over the course of 24-h day in different brain regions. The brain regions are grouped into major categories including, the Hypothalamus, Hippocampus, Cortices, and Striatum. The average length and angle are determined based on the measurements' means in each brain section; Zeitgeber time (ZT). One-way ANOVA test was used to compare the means of lengths and angles at different time points. P values were calculated using the False Discovery Rate (FDR) correction, employing the Two-stage linear step-up procedure of Benjamini, Krieger, and Yekutieli for multiple comparisons. (C) P values of one-way ANOVA test, used to assess the variability in cilia length and angle at different time points (in a,b), $P<0.05$: significant changes across the different time points over 24-h period. Underlying data for Fig 5 are available in S2 Data.

Our analysis revealed significant periodic fluctuations in cilia length within five specific regions: ARC, DMH, VMH, NAc, and SSC, with peak times varying among them: ARC at ZT 15, DMH at ZT 3.8, VMH at ZT 3.4, NAc at ZT 11, and SSC at ZT 12.16 (Fig 6). However, we found no evidence of rhythmic patterns in cilia angles in any of the regions studied (S3 Data).

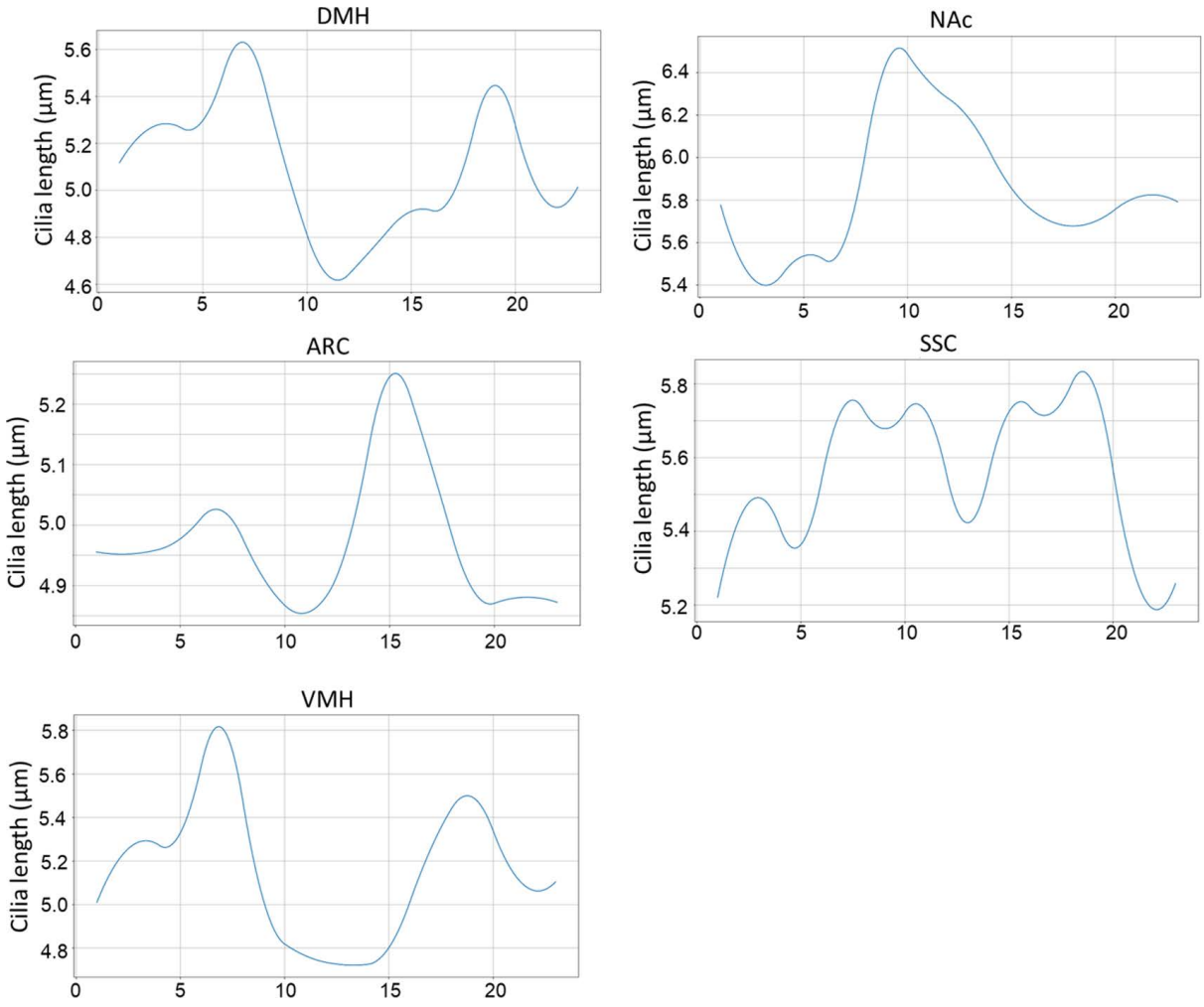


Fig 2.6. Circadian rhythms of cilia length. BioCycle analysis was used to examine the presence of rhythmic fluctuations in cilia length and revealed significant circadian patterns of cilia length variations across a 24-h period in five brain regions tested: ARC, DMH, VMH, NAc, and SSC, with $P<0.05$. Underlying data are available in S3 Data.

Correlation of cilia length and circular angle among various brain regions

We next assessed whether fluctuations in cilia length and angle over the 24-h period correlated across different brain regions. Our analysis revealed significant correlations in cilia length changes, with the DMH and VMH showing a particularly strong correlation.

Positive correlations were also observed between the PFC and several regions, including the DMH, VMH, LH, AHC, and MC, while CA1 cilia lengths negatively correlated with the DMH and VMH but positively with the RS, NAc, and DG (Fig 7A). Similarly, cilia angle fluctuations exhibited substantial correlations across various brain regions. The strongest correlation was observed between the DMH and VMH ($r=0.79$), with other notable correlations in hypothalamic regions such as AHC-LH, ARC-PVN, and PVN-SCN. Negative correlations were found between the PVN and VMH, and between cilia angles in the CA1 and TU regions (Fig 7B).

We next tested the hypothesis that more highly correlated brain regions, either in cilia length or angle, may be preferentially interconnected. Using the Louvain community detection algorithm on a network representation of the anatomical connections among these regions, we found three primary communities. The first and smallest community ("red") contained the three hippocampal regions DG, CA1, and CA3. The second community ("green") contained cortical regions, the striatum, and somewhat surprisingly, the SCN. The third community ("purple") contained all of the other regions, which overall had less strongly defined interconnectivity relationships (Fig 7D). Based on these data, we then asked if regions that had strong length correlations ($p<0.05$) were more likely to have stronger interconnectivity than regions with weak length correlations ($p>0.05$). We found no significant difference in normalized projection strength between pairs of regions correlated with cilia length versus those not correlated (Fig 7E), indicating that projection strength between regions does not influence cilia length.

We next examined all pairs of regions within and across different clusters and identified a bias toward regions having correlated cilia lengths if they were present within particular

communities; this relationship was most prominent between regions in the red and green communities (Fig 7F). The fraction of correlated pairs between red-green communities (0.111) was in the 9.1st percentile relative to the random distribution, indicating that cilia lengths were more likely than by chance to be correlated between pairs located in red and green communities (Fig 7F).

We next tested for the same relationship between cilia angle and connectivity. As with cilia length, we did not identify a significant difference in projection strength between pairs of regions correlated with cilia angle versus those not correlated (Fig 7G). We then assessed the relationship between community identity and cilia angle correlation and found that the fraction of correlated pairs within the purple community (0.107) was 7.4th percentile relative to the random distribution (Fig 7H). These data together indicate that while the connectivity strength between directly connected pairs did not appear to relate to cilia length or angle, the presence within particular communities did appear to relate to both cilia length and angle, indicating that the network architecture of the brain exhibits some relationship with cilia length and angle correlations across regions.

Given the lack of clear relationship between direct anatomical connectivity and cilia length or angle correlations, we next applied the network approach on the cilia length and angle correlation data directly. In order to do this, we built correlation networks using a log-scaled R value that yielded a nicer distribution for edge weights, and again used the Louvain community detection algorithm to assign communities (Fig 7I–7L). These results yielded four communities that did not distinctly track by anatomical connectivity, as evidenced by a different regional distribution across communities. Interestingly, we observed a number of regions that cluster together in both cilia length and angle

correlation networks. Notably, NAc, CA1, CA3, TU cluster together for both, as do AHC, PFC, MC, and SSC (Fig 7I–7L). The NAc and TU are both striatal regions while CA1 and CA3 are both hippocampal, and PFC, MC, and SSC are all cortical regions. However, the exact relationship between these sets of regions that co-cluster is not immediately apparent, again suggesting that factors other than direct connectivity likely influence the non-random correlations in cilia length and angle across regions.

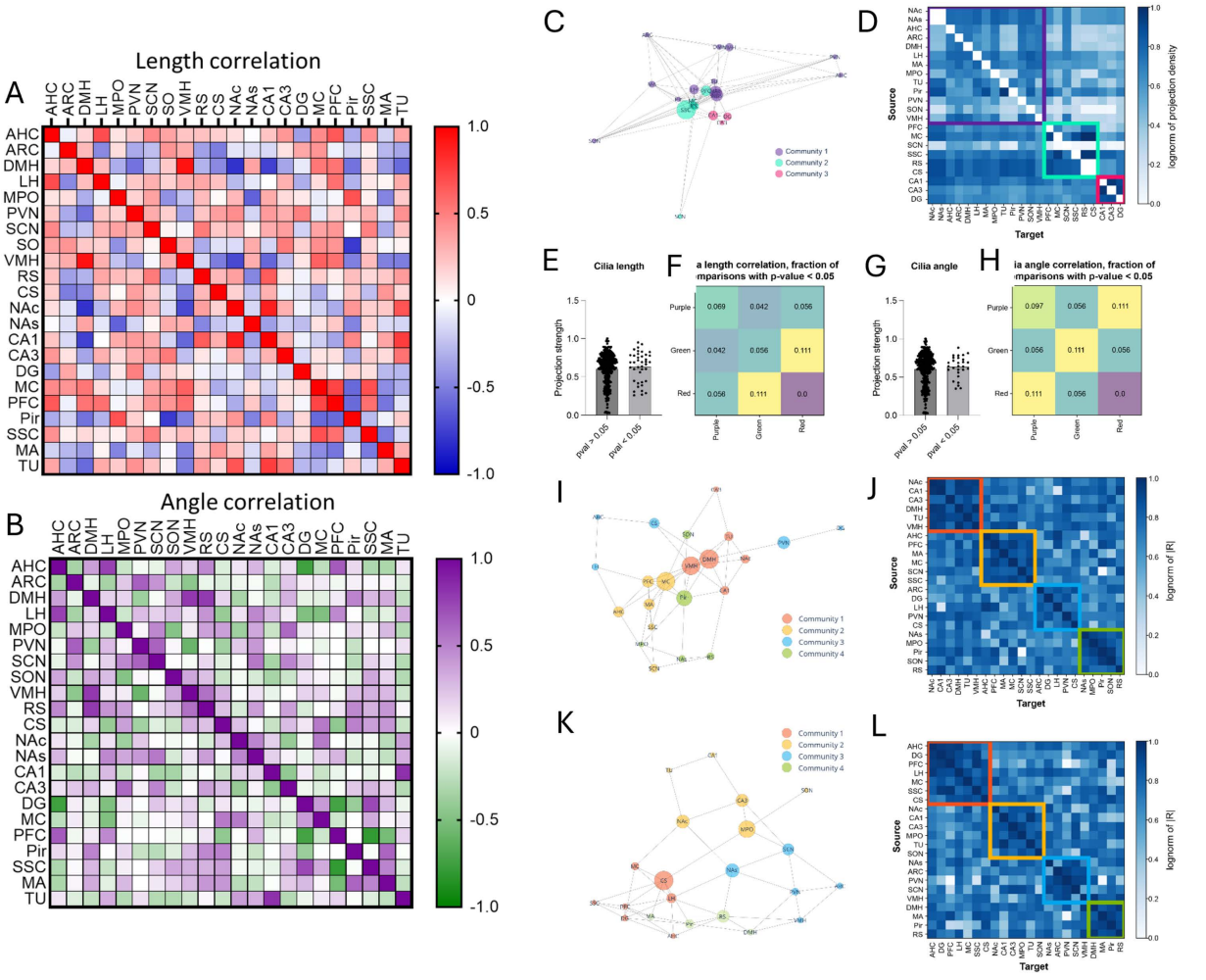


Fig 2.7. Correlation of cilia length and circular angle among various brain regions and relationship between cilia length/angle and network connectivity. (A) Heatmap showing the correlation of cilia length (based on the mean of the section means) among

different brain regions. The correlation coefficient ranges from 1 (indicating the most positive correlation, red) to −1 (indicating the most negative correlation, blue). Positive correlation implies that the cilia lengths in the two regions are on the longer and shorter side simultaneously. Negative correlation indicates that the two regions have opposite cilia length sizes; underlying data are available in S2 Data. (B) Heatmap displaying the correlation of cilia angle (based on the mean of the section circular means) among different brain regions. The correlation coefficient ranges from 1 (indicating the most positive correlation, purple) to −1 (indicating the most negative correlation, green); underlying data are available in S2 Data. (C) Anatomical network of the brain regions in our study. The network is embedded in 2D space using a spring embedding, in which highly connected nodes are pulled together as by a spring. Node size represents betweenness, a measurement of centrality based on the number of shortest paths between nodes that a particular node shows up on. Nodes are colored according to their community assignment, as determined by the Leiden algorithm. (D) Correlogram indicating the strength of input-output connections between all pairs of regions in the dataset. The color bar indicates the log-normalized projection density between any two regions. Regions are grouped according to their community membership. (E) Bar graph comparing projection strength between regions significantly correlated with cilia length vs. those not correlated. Projection strength equals the log normalization of normalized (by injection volume) projection density. (F) Fraction of region pairs significantly correlated by cilia length among all regions pairs between two communities. For example, a fraction of 0.111 means that 11.1% of all region pairs between the red and green communities are correlated by cilia length. (G) Bar graph comparing projection strength between regions significantly correlated with cilia angle versus those not

correlated. (H) Fraction of region pairs significantly correlated by cilia angle among all regions pairs between two communities. (I) Cilia length correlation network. The spring embedding puts regions more highly correlated closer together. Betweenness and community membership are shown as node size and color, respectively. (J) Cilia length correlogram shows the groupings of different regions by community, as well as their correlation patterns. (K) Cilia angle correlation network. Betweenness and community membership are shown as node size and color, respectively. (L) Cilia angle correlogram shows the groupings of different regions by community, as well as their correlation patterns. Underlying data of Fig 7C-L are available in S2 Data, and from the publicly available Allen Mouse Brain Connectivity Atlas Data.

Discussion

In our study, we examined the spatiotemporal patterns of cilia length and orientation across 22 mouse brain regions. Our findings revealed substantial variation in cilia length across these regions, and distinct temporal oscillation in certain regions. We also observed non-random distribution patterns in cilia orientation across the brain, suggesting a structured spatial organization.

To investigate spatiotemporal variability in primary cilia dynamics across mouse brain regions, we developed automated image analysis algorithms for high-throughput analysis of cilia length and orientation. These algorithms enabled the examination of over 10 million individual cilia, creating the largest spatial and temporal atlas of cilia metrics. Automated measurements were validated through manual measurements of cilia length and angles in each of the 22 brain regions examined.

Our study uncovered marked variations in cilia length among different brain regions, with the NAs exhibiting the shortest average cilia length and the TU the longest. Our cilia length findings are in agreement with those reported by Sipos and colleagues across most of the examined regions, though discrepancies were observed within the hypothalamus. Notably, our measurements were based on hundreds of thousands of cilia per region, compared to a maximum of 200 cilia analyzed in the earlier study [57]. Further, while Sipos and colleagues' study captured a static snapshot at a single time point, our analysis dynamically tracked cilia length variations every 2h over a 24-h period [57]. The discrepancy in cilia length within the hypothalamus between the two studies is especially interesting given the profound variability we observed in these regions over the course of the day. This highlights the importance of specifying the timing of the day when reporting cilia-related metrics.

The variations in cilia length across brain regions raise questions about their potential role in functional specialization tailored to the needs of each brain structure, including whether longer cilia might provide a larger surface area for receptor expression, thereby enhancing cellular sensitivity to extracellular signaling molecules. This prompts further investigation of whether the presence of the longest cilia in the TU reflects the critical role of cilia in olfaction [58-61]. Interestingly, the NAc displayed cilia lengths similar to those in the adjacent RS and CS, while the NAs had the shortest cilia lengths among all examined brain regions. This is noteworthy given the anatomical proximity of the TU, RS, CS, and NAc, which form one anatomical cluster, whereas the NAs is classified in a different anatomical cluster [62-65]. Further supporting this anatomical-functional relationship is the strong correlation observed in cilia length across the hypothalamic

regions particularly the DMH and VMH, regions known to share several anatomical and functional characteristics.

We observed notable variations in cilia angles, with the MC having the smallest average angle and the Pir the largest. The finding that cilia display distinct orientation patterns across various brain regions presents a novel discovery. The distribution of cilia angles and the dominant orientation toward the medial-ventral quadrants across most regions indicate that cilia orientation in the brain follows specific patterns rather than being random. Notably, there is a remarkable consistency in cilia orientation among anatomically or functionally linked structures. For example, cilia in striatal regions (RS, CS, NAc) and hippocampal areas (CA1, CA3, DG) predominantly exhibit orientations toward 180° and/or 270°. Interestingly, the TU, which is classified as a striatal structure, and the MA, known for its substantial neural connections with the striatum, both exhibit a cilia orientation pattern similar to that of the striatum. Conversely, hypothalamic nuclei, cortical regions, and NAs exhibit wider cilia orientation patterns, yet the majority tend toward the medial-ventral quadrant or align with the axis from 45° to 225°. Our results align with previous findings showing CA1 cilia orient along the apical-basal axis, while cortical cilia orient toward the pial surface [66,67].

Our findings suggest that shared connectivity, reflecting common functional or anatomical characteristics, may shape the pattern of cilia orientation. This supports the idea that cilia orientation distribution across the brain is not random and is associated with the unique functional or anatomical features of interconnected regions. The distinctive cilia orientation patterns across various brain regions may also relate to their specific locations or proximities to the associated ventricles. For example, cilia in the striatum, TU, and

hippocampus primarily orient toward the lateral ventricles, whereas those in the hypothalamic nuclei appear to align more with the third ventricle, and in the cortices, cilia orient toward both the ventricles and the subarachnoid space.

Our analysis demonstrated that cilia length and angle fluctuate throughout the day across brain regions. Except for the CS and AHC (P=0.05), all tested regions exhibited time-dependent variations in cilia length, with seven also showing fluctuations in orientation. Although changes in cilia length of 1–2 μm may seem modest, they can result in functional alterations of 10–20% [68-70]. These fluctuations across light and dark phases may reflect varying sensory or signaling needs during these periods. The finding that cilia angles also follow time-dependent fluctuations in certain brain regions is especially interesting, as it suggests that, beyond length adjustments, the direction of signal sensing or transmission by cilia may also shift throughout the day.

Our Bio-Cycle analysis identified significant rhythmicity in cilia length in five brain regions (NAc, ARC, DMH, VMH, and SSC), with no circadian patterns detected in cilia angle. While the reason for this region-specific rhythmicity remains unclear, it is noteworthy that all five regions are closely associated with rhythmic physiological processes. The NAc is a vital hub for motivation and reward-seeking behavior, which notably peak during the active phase (dark) and diminish during the inactive phase (light) in nocturnal mice. Notably, GPCRs located on cilia in the NAc are involved in regulating these behaviors, raising the question of whether oscillations in cilia length contribute or respond to the temporal modulation of reward-related processes, especially that cilia are known to play distinct roles in both the acute and long-term responses to reward-inducing drugs [71]. Our recent study demonstrated that many cilia-related transcripts exhibit circadian

rhythmicity in the mouse nucleus accumbens and hypothalamus, with notable overrepresentation in the nucleus accumbens compared to the background transcripts. We also found that the rhythmic patterns of cilia transcripts are shifted under conditions of dopamine system modulation, including D2 receptor deletion and cocaine administration [72].

The hypothalamic structures ARC, DMH, and VMH, which exhibit rhythmic oscillations in cilia length, are well known for regulating physiological functions that follow circadian rhythms, including sleep–wake cycles, feeding behavior, energy balance, body temperature regulation, hormone secretion, and stress responses [34–42,73–77].

Cilia in these regions have been implicated in the regulation of rhythmic physiological processes. For example, cilia in the VMH play a crucial role in maintaining energy balance and skeletal homeostasis [78], with their length dynamically responding to metabolic conditions. Notably, shorter cilia are more prevalent under metabolically unfavorable conditions, such as obesity and leptin resistance [79-80]. Evidence suggests that primary cilia on ARC neurons play a crucial role in regulating energy homeostasis by mediating GPCR signaling in response to peripheral hormonal stimuli, ultimately influencing food intake and metabolic balance [81].

It is noteworthy that CSF composition and flow dynamics exhibit time-of-day-dependent variations, which are regulated in part by the beating of motile cilia [82], with highest flow during the night, when animal activity is at its peak [83]. This raises the possibility that primary cilia dynamics may similarly contribute to the regulation of physiological processes with circadian-like patterns. Our findings that cilia length fluctuates in a rhythmic manner within these regions warrant further studies to determine whether

these changes are directly driven by circadian mechanisms or are secondary to other rhythmic physiological processes. The SSC is the only cortical structure that showed rhythmic fluctuations in cilia length. This is interesting in light of previous studies showing rhythmic synaptic changes in the SSC [84–87]. While the exact role of these oscillations remains unclear, emerging evidence suggests that primary cilia may play a direct role in circadian regulation. A recent study demonstrated that cilia in a subset SCN neurons, specifically neuromedin S–producing neurons, exhibit rhythmicity in abundance and length, and that genetic ablation of ciliogenesis in these neurons disrupts intercellular coupling, leading to a loss of circadian coherence and an increased susceptibility to external perturbations [88]. Given that we observed rhythmic cilia length fluctuations in multiple hypothalamic regions, it is possible that cilia in other brain areas also play a role in modulating circadian-regulated functions. However, further research is needed to determine whether these oscillations are directly involved in molecular clock mechanisms or reflect secondary effects of circadian-driven processes.

Cilia host numerous receptors like GPCRs and ion channels, crucial for detecting extracellular signals and initiating intracellular responses. Receptors like MC4R, MCHR1, NPY2R, NPY5R, SSTR3, 5HT6, and DRD1 play key roles in rhythmic functions such as sleep-wake cycles and feeding behavior [37,43–47]. The observed fluctuations in cilia length and orientation raise the question of whether these structural changes could influence receptor availability or sensitivity to ligands, thereby modulating signal transduction and time-dependent physiological processes.

One limitation of our study is its exclusive focus on ADCY3-positive cilia, which may overlook the diversity of cilia across brain structures and the full length of cilia. However, ADCY3 is a primary marker for cilia in the mature adult brain, especially in neurons, and cilia labeled with the ADCY3 antibody are often longer than those stained with other markers, such as ARL13 and Sstr3, in many brain regions [57,89], suggesting that our measurements of cilia length likely captured the majority of neuronal cilia and accurately represented their total length. Another limitation of our study is that our study did not identify the specific cell types associated with cilia of various lengths and angles. This work primarily aimed to map the spatiotemporal dynamics of cilia across brain regions, with a focus on changes in ciliary length and orientation throughout the circadian cycle; future research should prioritize examining ADCY3-negative cilia and identifying cell types with cilia that exhibit fluctuations in length and angle. Lastly, when interpreting cilia length and orientation data, it is important to consider potential errors from 2D imaging of 3D structures, as detailed in the supplementary material. However, since these errors are consistent across brain regions due to uniform tissue thickness, they likely do not affect comparative analyses, and thus do not compromise the reliability of the relative measurements.

In conclusion, we presented the largest spatiotemporal atlas of cilia to date, revealing complex regional differences and time-dependent fluctuations in cilia dynamics across the mouse brain. Our findings highlight time-dependent variations in cilia length and orientation, with rhythmic patterns observed in specific brain regions. While the functional implications of these dynamic properties remain to be fully understood, the observed patterns suggest that cilia may contribute to the temporal regulation of physiological

processes in a region-specific manner. Future research is needed to elucidate the mechanistic links between cilia dynamics, receptor signaling, and brain function over the light-dark cycle.

Chapter 3: Loss of Primary Cilia in the Nucleus Accumbens Increases Wakefulness and Reduces Locomotor Activity and NREM Sleep

Abstract

Primary cilia are specialized signaling organelles enriched with receptors that regulate neuronal function, yet their role in accumbal circuits controlling circadian behavior remains poorly understood. The nucleus accumbens core (NAcC) integrates dopaminergic and glutamatergic inputs to regulate arousal, motivated locomotion, and sleep-wake behavior, and both cilia-associated gene expression and cilia length oscillate with circadian periodicity in this region. Here we investigated the functional role of NAcC primary cilia in circadian behaviors by selectively ablating the intraflagellar transport protein IFT88 from CaMKII-expressing NAcC neurons using stereotaxic AAV-CamKII-Cre delivery in Ift88fl/fl mice.

Cilia ablation was confirmed by immunohistochemistry for adenylyl cyclase III. Wheel running monitored over 13 days revealed a selective reduction in dark-phase locomotor activity in KO mice, with reduced overall activity level and dampened day-night amplitude, while the timing, structure, and consistency of the LD-entrained locomotor rhythm were not detectably altered. Food intake was unaffected across all measures. EEG/EMG recordings over 48 hours demonstrated significantly increased wakefulness in KO mice, reduced NREM sleep, while REM sleep, sleep architecture, and EEG spectral power were preserved across all stages. These findings identify primary cilia in NAcC neurons as modulators of circadian behavioral output amplitude rather than circadian timing, consistent with a model in which ciliary GPCR signaling may fine-tune the gain of dopamine-driven motivated behavior and arousal regulation during the active phase without detectably altering the timing of the LD-entrained behavioral rhythm.

Introduction

Primary cilia are microtubule-based signaling organelles that concentrate G protein-coupled receptors (GPCRs) within a restricted subcellular compartment, acting as specialized signaling hubs that amplify and localize receptor-coupled cAMP cascades [1-3]. Neuronal primary cilia host a diverse repertoire of neuromodulatory receptors, including dopamine D1 and D2 receptors, melanin-concentrating hormone receptor 1 (MCHR1), melanocortin 4 receptor (MC4R), and adenosine A2A receptor [4, 5]. Dopamine signaling itself bidirectionally regulates ciliary morphology: D1R activation elongates cilia while D2R activation reduces cilia length, demonstrating that dopamine tone dynamically tunes the signaling capacity of these organelles [6, 7]. In our laboratory, we have shown that MCH signaling via MCHR1 dynamically shortens cilia length in NAcC and other striatal regions, directly linking neuropeptide pathways to ciliary morphology and circadian behavior [8].

Strikingly, several of these ciliary receptors are themselves subject to circadian regulation, and cilia-related gene expression follows a circadian pattern across the brain. Transcriptomic analyses across 22 primate brain regions revealed that approximately 73% of cilia-related genes exhibit circadian rhythmicity in at least one region, with significant enrichment in striatal areas [9]. A subsequent analysis of the circadian cilia transcriptome across mouse brain regions confirmed rhythmic expression of cilia-associated genes in the NAcC, and showed that D2R deletion significantly reduces the number of rhythmically expressed cilia genes, implicating dopamine signaling in cilia gene rhythmicity [10]. Most strikingly, our structural analysis demonstrated circadian oscillations in cilia length in the NAcC, with peak length around

ZT11, just before the onset of the active phase, suggesting that ciliary signaling capacity is temporally gated to peak precisely when dopamine-driven locomotion and arousal are highest [11]. Broader functional evidence further supports a role for cilia in behavioral and sleep regulation: selective ablation of cilia in striatal medium spiny neurons impairs motor skill acquisition and time-interval perception without affecting spontaneous locomotion [12]; inducible IFT88 deletion broadly across neurons alters sleep architecture, reduces EEG power, and impairs phase-amplitude coupling [13]; and adult deletion of Ift88 in striatal medium spiny neurons reduces long-range excitatory inputs and weakens glutamatergic transmission, highlighting the role of cilia in maintaining striatal circuit integrity [14].

Circadian rhythms are endogenous approximately 24-hour cycles that govern a wide range of physiological and behavioral processes, including sleep-wake patterns, locomotor activity, metabolism, and hormone secretion. Proper alignment of these rhythms with environmental cues is essential for behavioral homeostasis, and their disruption is associated with sleep disturbances, metabolic dysfunction, and neuropsychiatric disease. While the suprachiasmatic nucleus (SCN) serves as the master pacemaker, circadian outputs are shaped by a distributed network of secondary oscillators in limbic, striatal, and cortical regions that translate clock signals into behavioral expression. Among these regions, the nucleus accumbens core (NAcC) has emerged as a key node linking dopaminergic reward signaling to the expression of circadian locomotor and sleep-wake behaviors.

The NAcC, located in the ventral striatum, integrates dopaminergic input from the ventral tegmental area with glutamatergic projections from prefrontal cortex,

hippocampus, and amygdala to drive goal-directed actions [15]. Beyond its well-established role in reward processing, the NAcC is critically involved in sleep-wake regulation and circadian behavioral output. Lesions of the NAcC robustly increase wakefulness and reduce NREM sleep, particularly when restricted to the core subregion [16]. Activation of adenosine A2A receptor-expressing neurons in the NAcC promotes sleep while their inhibition suppresses it [17], and D1 receptor activation in the NAcC enhances wakefulness and food motivation through disinhibition of midbrain and lateral hypothalamic circuits [18, 19]. Furthermore, dopamine D2 receptors within the NAcC mediate the arousal and sleep-rebound effects of fentanyl [20], demonstrating that dopaminergic signaling in this region bidirectionally regulates sleep-wake state. The NAcC also contributes directly to circadian locomotor behavior; deletion of melanin-concentrating hormone receptors in the NAcC increases locomotor activity [21], and histone acetylation within the NAc shell modulates locomotor responses [22]. Together, these findings position the NAcC as a critical interface through which dopaminergic and neuromodulatory circuits shape the magnitude and timing of circadian behavioral expression. A key but underexplored feature of NAcC neurons is their possession of primary cilia concentrating precisely the receptor systems shown above to regulate sleep, locomotion, and arousal.

Given the abundance of circadian-regulated GPCRs on NAcC cilia, the rhythmic oscillations in NAcC cilia length, and the established role of the NAcC in sleep-wake and locomotor regulation, we hypothesized that cilia in NAcC CaMKII-expressing neurons modulate the amplitude of circadian behavioral expression without disrupting the underlying clock mechanism. To test this, we used stereotaxic delivery of AAV-

CamKII-Cre to ablate cilia selectively from NAcC neurons in Ift88fl/fl mice and assessed wheel running, food intake, and sleep-wake architecture across 48 hours of EEG/EMG recording.

Materials and Methods

2.1 Animals

Male Ift88fl/fl mice (Jackson Laboratories, stock #022409) carrying loxP sites flanking exons 4–6 of the Ift88 gene were used in this study. All procedures were approved by the Institutional Animal Care and Use Committee at the University of California, Irvine, and conducted in accordance with NIH and institutional guidelines. Mice were maintained on a 12:12 h light-dark cycle with food and water available ad libitum. A minimum of eight animals per group was used for wheel running (n = 8 WT, 8 KO) and food intake (n = 8 WT, 8 KO) experiments, which were conducted simultaneously in the same animals. For EEG/EMG recordings, a separate cohort of at least eight mice per group were implanted; animals with incomplete or technically compromised recordings were excluded from analysis (final n = 5 WT, 7 KO)

2.2 Stereotaxic surgery and viral delivery

To selectively ablate cilia from CaMKII-expressing NAcC neurons, Ift88fl/fl mice received bilateral stereotaxic injections of pENN.AAV.CamKII.HI.GFP-Cre.WPRE.SV40 (Addgene #105551-AAV9; gift from James M. Wilson). Mice were anesthetized with isoflurane and secured in a stereotaxic frame. After exposing the skull via midline incision, bilateral injections were made at coordinates relative to bregma: AP = +1.6 mm, ML = ±1.1 mm, DV = −4.5 mm. A total of 0.1 µL of virus was injected per site at a

constant rate, followed by a 5-min waiting period before needle withdrawal at 0.01 mm/sec to minimize backflow. Animals received Carprofen (5 mg/kg) and Dexamethasone (10 mg/kg) post-operatively. Wild-type littermates receiving the same viral injection served as controls.

2.3 EEG/EMG implantation and recording

EEG electrodes were implanted simultaneously with viral injections. Under isoflurane anesthesia, four stainless steel EEG screws (Pinnacle Technology) were placed in holes drilled above frontal cortex (AP = +1.5 mm, ML = ±1.5 mm) and parietal cortex (AP = −1.3 mm, ML = ±1.5 mm). EMG wires were placed in the trapezius muscle. Mice were handled 2 minutes twice daily for 4 days prior to recording to promote habituation. EEG recordings began 7 days after surgery. Signals were transmitted wirelessly via Bluetooth and acquired using Sirenia Software (Pinnacle Technology). Continuous 48-hour recordings were divided into 10-second epochs and manually scored as Wake, NREM, or REM sleep by an experimenter blind to genotype. Initial classification used a cluster-based scoring method; ambiguous epochs were subsequently verified by visual inspection. NREM sleep was identified by low-frequency, high-amplitude EEG activity (predominantly 1–4 Hz); REM by low-amplitude, theta-dominant activity (5–8 Hz); Wake by low-amplitude mixed-frequency activity accompanied by high EMG tone.

2.4 Wheel running and food intake

Mice were individually housed in cages equipped with running wheels (Med Associates) and food intake monitoring systems (TSE Systems, Germany) for 14 consecutive days under a 12:12 h light-dark cycle. Wheel running was recorded in 5-minute intervals and

food intake was recorded hourly. Wheel running data were acquired using Med Associates software and exported as 5-minute interval activity counts. Food intake was recorded by the TSE Systems software and exported as hourly gram values. Both parameters were recorded simultaneously throughout the experiment. ZT0 was defined as lights-on (06:30), with lights-off at ZT12 (18:30). Raw 5-minute wheel running data were reordered to align with ZT0 = lights-on prior to analysis.

2.5 Histology

Immunohistochemistry for adenylyl cyclase III (ADCY3) was performed to confirm cilia ablation. Mice were transcardially perfused with 0.9% saline followed by 4% paraformaldehyde. Brains were postfixed overnight, cryoprotected in 30% sucrose, and sectioned coronally at 30 μm on a microtome. Sections were blocked in 4% goat serum/PBS/0.3% Triton X-100 for 1 h, then incubated with rabbit anti-ADCY3 (LSBIO-C204505, 1:500, overnight), followed by Alexa Fluor 546 goat anti-rabbit (1:500) with DAPI (1:10,000). Sections were imaged on a Keyence BZ-9000 fluorescence microscope at 20× magnification.

2.6 Data analysis

Wheel running. Light-phase (ZT0–11) and dark-phase (ZT12–23) wheel running totals were compared between groups using two-way ANOVA with Bonferroni post-hoc tests. Single-component cosinor analysis was performed per animal on the mean 24-hour wheel running profile (averaged across 13 recording days) by fitting $Y = M + A \cdot \cos(2\pi t/24 - \varphi)$ using linear regression . (Python/SciPy), where M is the mesor (rhythm-adjusted mean), A is the amplitude, and φ is the acrophase (time of peak).

Group differences in mesor, amplitude, and acrophase were assessed using Welch's two-sample t-tests. Interdaily stability (IS) , a measure of day-to-day rhythm consistency, and intraday variability (IV) , a measure of within-day fragmentation , were calculated as non-parametric circadian indices from the hourly wheel running time series. Activity onset and offset were defined as the first and last hour within the dark phase in which activity exceeded 10% of the daily maximum; alpha was the duration between them. M10 was defined as the most active consecutive 10-hour window of the mean 24-hour profile. Daily wheel running totals were plotted across 13 days to assess temporal stability of group differences.

Food intake. Light-phase and dark-phase food intake were compared using two-way ANOVA with Bonferroni post-hoc tests. Cosinor analysis of the mean 24-hour food intake profile was performed as described above for wheel running.

Sleep stage amounts. Total Wake, NREM, and REM time (min) was calculated over 48 hours and separately for the light (ZT0–11) and dark (ZT12–23) phases. Group comparisons used two-way ANOVA.

Hourly sleep profiles. Hourly time in each stage was averaged across the two recording days for each mouse to produce a single 24-hour profile per animal (ZT0–23). Group mean profiles (±SEM) were plotted with single-component cosinor fits. Mesor, amplitude, and acrophase were extracted per mouse and compared between groups with Welch's t-tests.

Bout analysis. A bout was defined as an uninterrupted sequence of epochs scored in the same stage Bout number and mean bout duration (seconds) were calculated for

Wake, NREM, and REM over the full 48 hours and separately for light and dark phases. Group comparisons used two-way ANOVA.

Sleep latency. Latency to first NREM and first REM epoch was calculated as the time (min) from recording onset to the first epoch of each stage. Group comparisons used Welch's t-tests.

State transition probabilities. Epoch-by-epoch transitions between Wake, NREM, and REM were counted for each mouse. Transition matrices were normalized by row to yield transition probabilities, averaged across mice within each group, and visualized as heatmaps.

All analyses were performed in Python (NumPy, Pandas, SciPy, Matplotlib). Statistical significance was set at $\alpha = 0.05$. Results are reported as mean ± SEM unless otherwise stated. Primary outcomes were dark-phase wheel running and total Wake time. Secondary and exploratory analyses, including cosinor parameters, non-parametric circadian indices, bout analysis, sleep latency, and state transition probabilities, were not corrected for multiple comparisons and should be interpreted accordingly.

Results

3.1 Selective cilia ablation from NAcC CaMKII-expressing neurons

Stereotaxic injection of AAV-CamKII-Cre into the NAcC of Ift88fl/fl mice produced robust cilia ablation from CaMKII-expressing neurons, confirmed by immunostaining for adenylyl cyclase III (ADCY3), a ciliary marker enriched on neuronal primary cilia. KO mice showed an 88% reduction in ADCY3-positive cilia in the NAcC compared to WT

controls (WT: 94.5 ± 5.0 vs. KO: 11.5 ± 2.3 cilia; $p < 0.0001$, $n = 8$ per group, Fig. 1b), confirming successful and selective cilia ablation restricted to the targeted region.

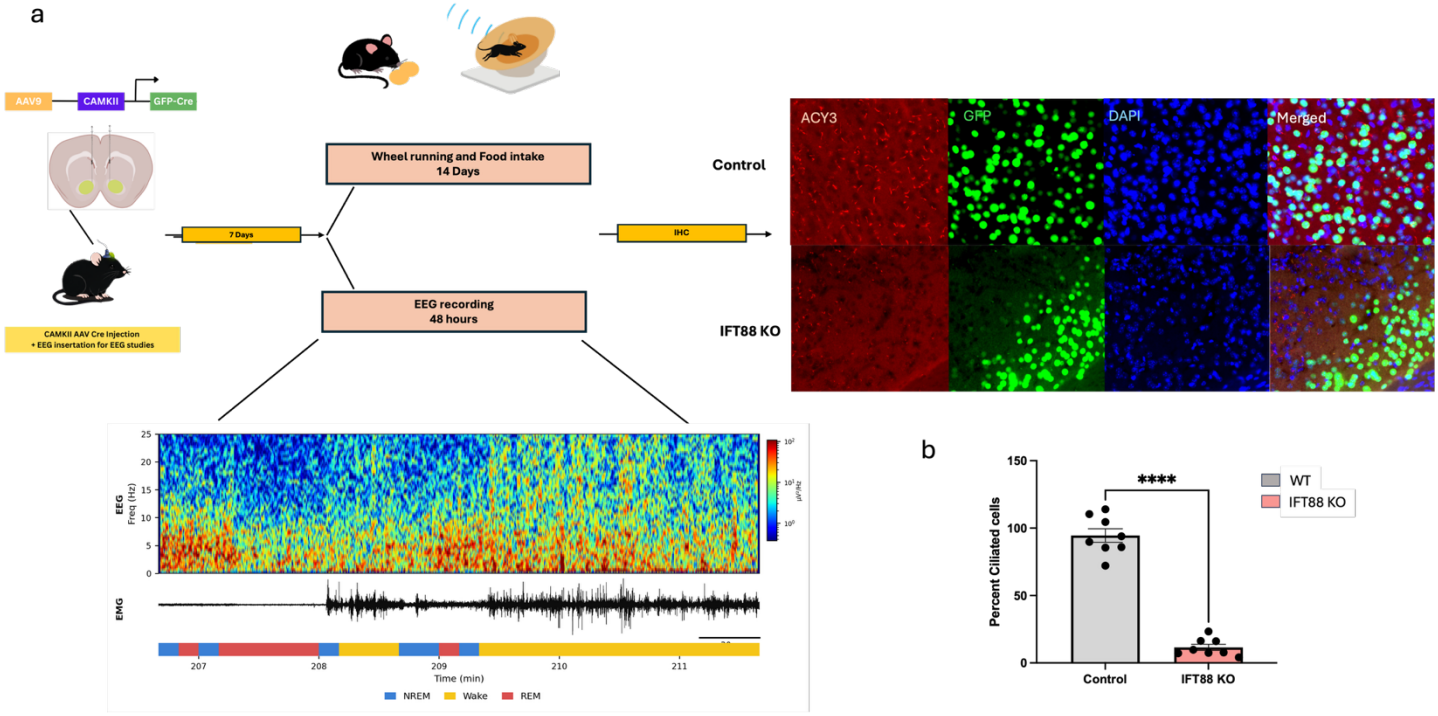


Figure 3.1. Stereotaxic AAV-mediated Cre delivery ablates primary cilia from CaMKII-expressing neurons in the NAcC. (A) AAV9-CaMKII-GFP-Cre was injected into the NAcC of Ift88fl/fl mice alongside EEG electrode implantation, followed by 7 days of recovery, 14 days of wheel-running and food-intake monitoring with concurrent 48-hour EEG/EMG recording and terminal immunohistochemistry (IHC). Representative confocal images show ADCY3 (ciliary marker), GFP (Cre-expressing neurons), DAPI (nuclei), and merged channels in control versus IFT88 KO NAcC, with IFT88 KO tissue showing a marked reduction in ADCY3 immunoreactivity. (b) Quantification confirms an 88% reduction in the percentage of ciliated cells in IFT88 KO mice relative to WT controls (WT: 94.5 ± 5.0% vs. KO: 11.5 ± 2.3%; ****$p < 0.0001$, unpaired t-test, $n = 8$ per group), confirming successful and selective cilia ablation restricted to the targeted region. Data are presented as mean ± SEM.

3.2 NAcC cilia ablation selectively reduces dark-phase wheel running without altering LD-entrained circadian timing

To determine whether NAcC cilia removal affects circadian locomotor behavior, wheel running was monitored continuously for 14 days under a 12:12 h light-dark cycle (minimum n = 8 per group). Actograms confirmed that both WT and KO mice showed robust circadian locomotor rhythms concentrated in the dark phase, with consistent daily patterns across the recording period (Fig. 2a). A significant effect of time of day was observed in both groups ($p < 0.0001$), confirming intact circadian patterning. Dark-phase wheel running was significantly reduced in KO mice relative to WT controls ($p = 0.048$, Fig. 2d), as was total wheel running (Fig. 2c) and light-phase running ($p = 0.025$, Fig. 2e).

Cosinor analysis of the mean 24-hour wheel running profile revealed a significantly reduced mesor in KO mice ($p = 0.025$, Fig. 2f) — the rhythm-adjusted 24-hour mean, reflecting an overall lower activity level — and a significantly reduced amplitude ($p = 0.021$, Fig. 2g), reflecting a dampened day-night contrast. Acrophase did not differ between groups ($p = 0.91$, Fig. 2h), demonstrating that the timing of peak activity was not detectably altered. Rhythm consistency and structure were equivalent between groups, with no significant difference in interdaily stability ($p= 0.994$, Fig. S1a) or intraday variability ($p = 0.711$, Fig. S1b). Peak locomotor capacity during the active phase was reduced in KO mice, as reflected by a significantly lower M10 value ($p = 0.022$, Fig. S1c).

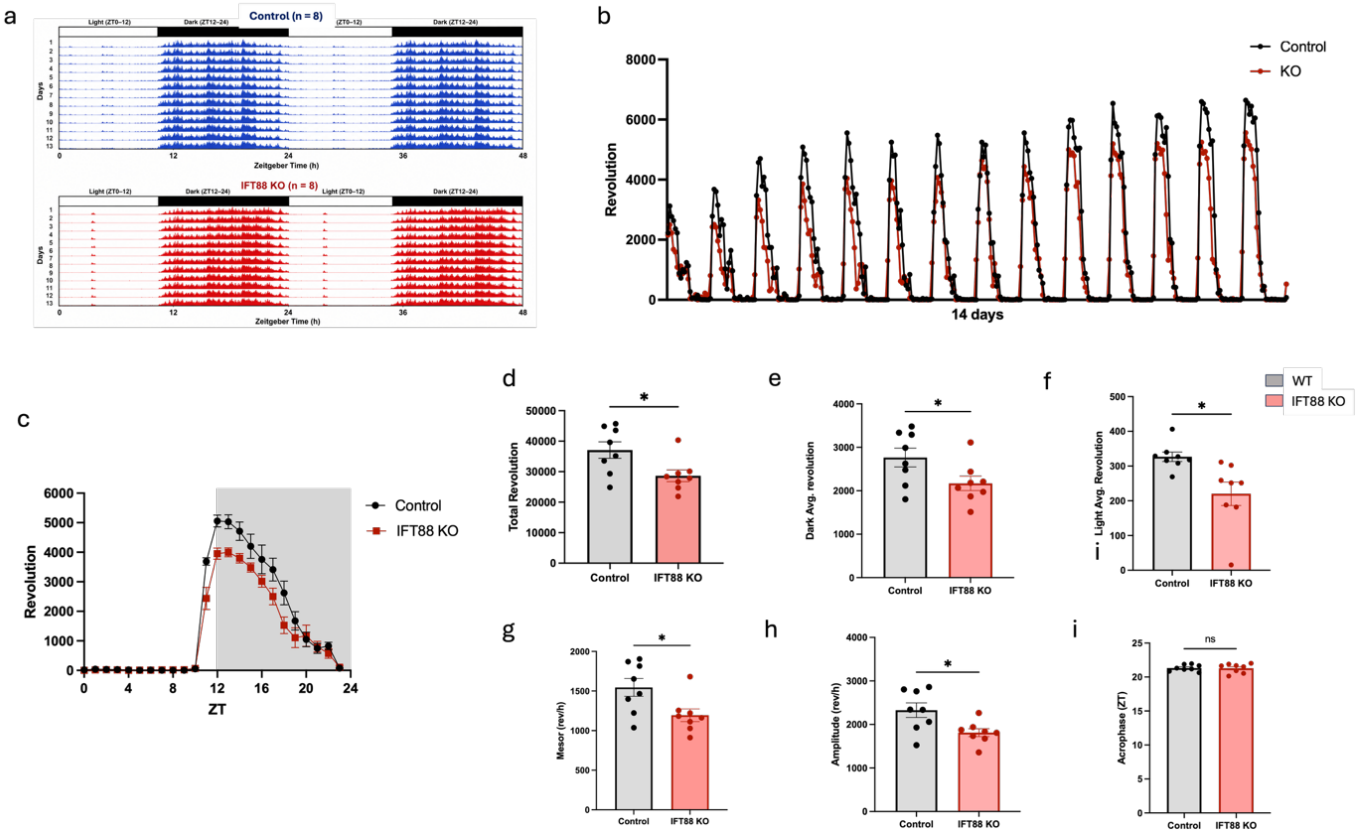


Figure 3.2. Wheel-running activity in control and NAcC IFT88 KO mice under a 12:12 h light-dark cycle. (A) Double-plotted actograms of wheel-running activity across 14 days in control (top, n = 8) and IFT88 KO (bottom, n = 8) mice. (B) Daily wheel-revolution time course over the 14-day recording period. (C) Mean 24-hour wheel-running profile (revolutions per hour) across Zeitgeber time, dark phase shaded. (D) Total wheel revolutions across the recording period. (E) Dark-phase wheel running. (F) Light-phase wheel running. (G) Mesor from cosinor analysis. (H) Amplitude from cosinor analysis. (I) Acrophase from cosinor analysis. *p < 0.05; ns, not significant. Data are presented as mean ± SEM; minimum n = 8 per group.

3.3 Food intake is unaffected by NAcC cilia ablation

Food intake was monitored continuously alongside wheel running over 14 days (n = 8 per group). Two-way ANOVA revealed no significant effect of genotype on food intake in either the total Food intake (Fig.3a) light phase ($p = 0.487$, Fig. 3b) or dark phase ($p = 0.794$, Fig. 3c) . Cosinor analysis confirmed the absence of significant changes in mesor, amplitude, or acrophase in KO mice relative to WT controls (Fig.3 e-g). Both groups showed the expected nocturnal concentration of feeding, with the majority of intake occurring during the dark phase. These findings indicate no detectable contribution of NAcC cilia to the circadian regulation of feeding behavior, suggesting a dissociation between motivated locomotion and metabolic homeostasis within the NAcC circuit.

To further characterize the independence of locomotor and feeding behavior, we examined the relationship between daily wheel running and daily food intake across individual mice. No significant correlation was observed between wheel running and food intake either overall ($r = 0.11$, $p = 0.72$) or within WT ($r = -0.05$, $p = 0.94$, $n = 5$) or KO ($r = 0.10$, $p = 0.82$, $n = 8$) groups, noting that the WT correlation was limited to the five animals with both measures available, providing no evidence that reduced locomotor output in KO mice reflected a general reduction in metabolic demand (Fig. 3h). . Together, these findings demonstrate that NAcC cilia removal selectively reduces the amplitude and overall level of circadian locomotor output during the active phase, while leaving the timing, structure, and consistency of the LD-entrained locomotor rhythm not detectably altered.

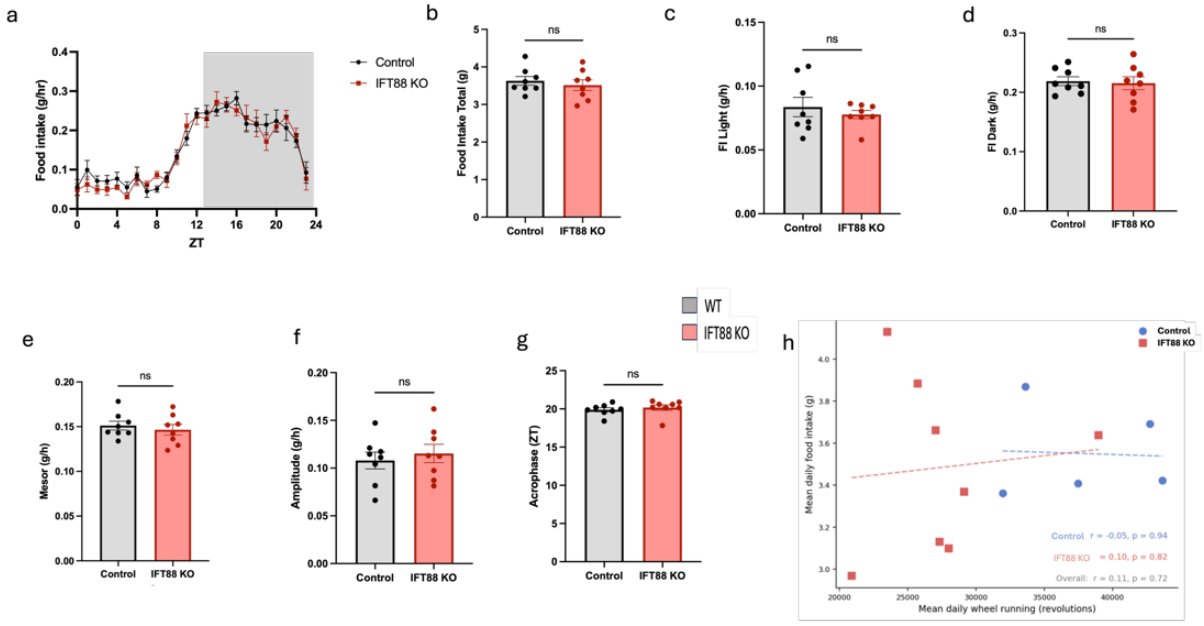


Figure 3.3. Food intake in control and NAcC IFT88 KO mice under a 12:12 h light-dark cycle. (A) Temporal profile of food intake (g/h) across Zeitgeber time in control versus IFT88 KO mice, dark phase shaded. (B) Total daily food intake. (C) Light-phase food intake. (D) Dark-phase food intake. (E) Mesor from cosinor analysis. (F) Amplitude from cosinor analysis. (G) Acrophase from cosinor analysis. (H) Scatterplot of mean daily wheel running against mean daily food intake for individual mice, with linear regression lines per genotype. ns, not significant. Data are presented as mean ± SEM; n = 8 per group (regression in H: n = 5 WT, n = 8 KO).

3.4 NAcC cilia ablation increases wakefulness without detectable changes in sleep architecture

EEG/EMG recordings were performed over 48 consecutive hours to characterize sleep-wake architecture (n = 5 WT, 7 KO, Fig. 5a-c). Representative EEG/EMG recordings during the light phase revealed sustained NREM sleep episodes with prominent delta

oscillations in WT mice, whereas IFT88 KO mice exhibited more frequent wake interruptions and fragmented NREM bouts (Fig 5.a) Total Wake time was significantly increased in KO mice compared to WT controls ($p = 0.008$, Fig. 5b). Phase analysis revealed that this increase was concentrated in the dark phase ($p = 0.0121$, 5g), while Wake time during the light phase did not differ significantly between groups ($p = 0.0595$). Total NREM sleep was significantly reduced in KO mice ($p = 0.0349$), while neither light nor dark phase NREM reached significance independently. REM sleep did not differ between groups in total or either phase (all $p > 0.99$). All sleep stage comparisons were performed using two-way ANOVA with Šídák's multiple comparisons test.

Cosinor analysis of the 24-hour Wake profile confirmed a significantly elevated Wake mesor in KO mice ($p = 0.008$, Fig. 6a), reflecting a higher rhythm-adjusted mean level of wakefulness, while Wake acrophase did not differ between groups, indicating that the timing of peak wakefulness was not detectably altered. NREM and REM cosinor parameters — mesor, amplitude, and acrophase — did not reach significance for either stage (Fig. 5).

Bout analysis revealed no significant differences in Wake, NREM, or REM bout number or mean bout duration over the full 48-hour period, within the light phase, or within the dark phase (all $p > 0.05$). Sleep latency to first NREM and first REM epoch was comparable between groups, and state transition probability matrices showed no significant differences in any Wake–NREM–REM transition, indicating no detectable alteration in sleep-wake cycling dynamics overall (Fig. S2).

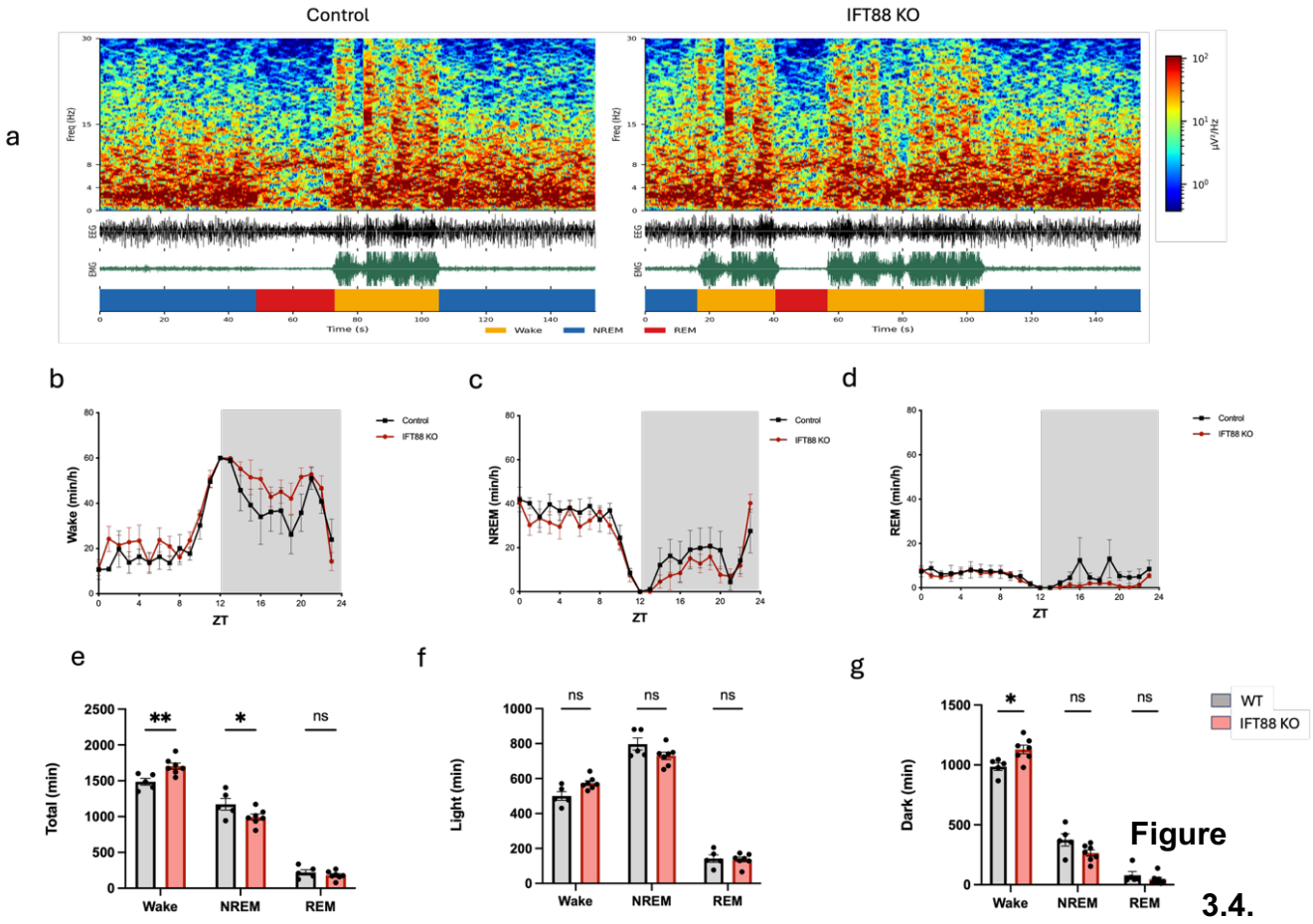


Figure 3.4.

Sleep-wake architecture in control and NAcC IFT88 KO mice assessed by EEG/EMG. (A) Representative EEG spectrograms, raw EEG and EMG traces, and corresponding hypnograms (wake, NREM, REM) during the light phase in control (left) and IFT88 KO (right) mice. (B) Wake time (min/h) across Zeitgeber time. (C) NREM time (min/h) across Zeitgeber time. (D) REM time (min/h) across Zeitgeber time. (E) Total time spent in wake, NREM, and REM across the 48-hour recording period. (F) Time spent in each state during the light phase. (G) Time spent in each state during the dark phase. *p < 0.05; **p < 0.01; ns, not significant (two-way ANOVA with Šídák's multiple comparisons test). Data are presented as mean ± SEM; n = 5 WT, 7 KO.

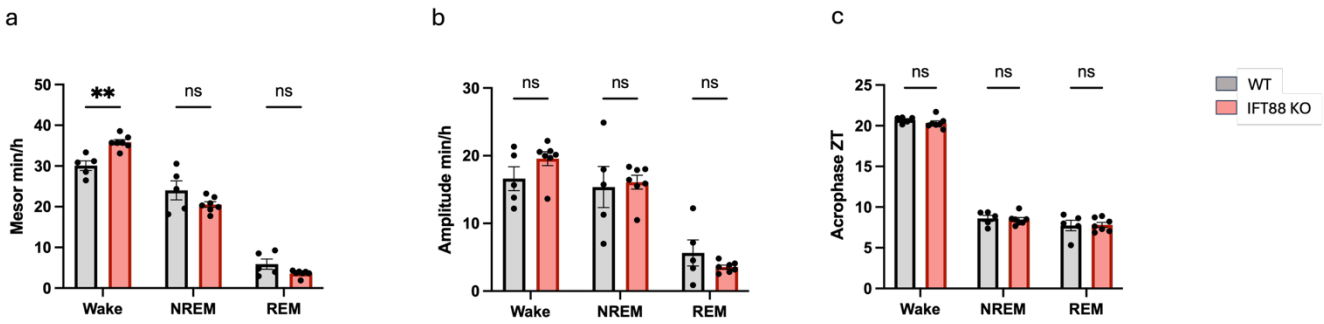


Figure 3.5. Cosinor analysis of sleep-wake states in control and NAcC IFT88 KO mice. (A) Mesor (24-hour rhythm-adjusted mean) for wake, NREM, and REM. (B) Amplitude for wake, NREM, and REM. (C) Acrophase (time of peak) for wake, NREM, and REM. **p < 0.01; ns, not significant (two-way ANOVA with Šídák's multiple comparisons test). Data are presented as mean ± SEM; n = 5 WT, 7 KO.

Discussion

In this study, we demonstrate that selective ablation of primary cilia from CaMKII-expressing NAcC neurons reduced the amplitude of circadian behavioral output, specifically dark-phase wheel running, total NREM sleep, increased wakefulness, without detectably altering the timing or structure of the LD-entrained rhythm, food intake, or EEG spectral composition. These findings identify NAcC primary cilia as gain modulators of motivated behavior and arousal regulation during the active phase, establishing a subcellular mechanism by which compartmentalized GPCR signaling within accumbal neurons shapes the magnitude of circadian behavioral expression. The central finding is a dissociation between amplitude and timing: every timing metric — acrophase, onset, offset, alpha, IS, and IV — was indistinguishable between groups, while every amplitude metric — cosinor mesor, cosinor amplitude, M10, and phase-specific running totals — was significantly reduced in KO mice, alongside increased

wakefulness. This pattern is consistent with a gain modulation defect rather than a clock defect. NAcC cilia, by concentrating D1R, D2R, adenosine A2A, and MCHR1 within a restricted signaling compartment, may serve as the molecular interface through which dopaminergic and adenosinergic tone during the active phase is converted into downstream cAMP cascades that sustain motivated locomotion and regulate arousal gating [4, 5]. Loss of this ciliary signaling hub reduces the gain without disturbing the timing.

The reduction in dark-phase wheel running is consistent with prior evidence that primary cilia support motivated and reward-driven locomotion rather than basic motor capacity. Ramos et al. (2021) showed that cilia loss in dopaminergic neurons blunted amphetamine-induced locomotor activation without affecting baseline locomotion, and Everett et al. (2024) reported reduced cocaine-induced locomotor sensitization following cilia disruption [23, 24]. In both studies, as in ours, baseline LD-entrained rhythm timing and structure were not detectably altered, confirming that cilia modulate the motivational component of locomotion. The NAcC is specifically implicated in this function: it integrates dopaminergic reward signals to drive voluntary locomotor output, and its D1-MSN population has been shown to promote locomotor activity through excitation of midbrain circuits [18]. Disruption of ciliary D1R signaling compartments may therefore specifically impair the motivational amplification of locomotor drive during the active phase without affecting the intrinsic capacity for movement.

The increased wakefulness and reduced NREM sleep in KO mice are consistent with prior lesion studies demonstrating that NAcC damage promotes arousal [16]. The NAcC normally contributes to sleep promotion through GABAergic projections to the lateral hypothalamus, ventral pallidum, and midbrain that inhibit wake-promoting circuits [25].

Primary cilia are required for normal inhibitory circuit formation, and loss of Arl13b-dependent ciliary signaling impairs GABAergic interneuron connectivity [26]. Disruption of ciliary GPCR signaling — particularly D2R and adenosine A2A pathways, both concentrated on NAcC cilia — may therefore impair the sleep-promoting output of accumbal GABAergic neurons, producing disinhibition of downstream arousal systems and reduced sleep consolidation during the active phase. Dopamine D2 receptors on NAcC cilia specifically mediate sleep-wake transitions and fentanyl-induced arousal rebound [20], and their loss may weaken homeostatic sleep drive, producing sustained wakefulness during the active phase consistent with our findings of increased Wake and reduced NREM.

The absence of any effect on food intake is mechanistically informative. Although D1R, leptin receptors, and MC4R are expressed on NAcC cilia, and hypothalamic cilia ablation disrupts feeding [27], our data indicate that NAcC cilia specifically support motivated locomotion and arousal regulation without contributing to metabolic control. This dissociation between wheel running (reduced) and food intake (intact) reveals that ciliary signaling in NAcC neurons is not a general circadian output regulator but rather specifically modulates behaviors driven by dopaminergic reward circuits — voluntary motivated locomotion and arousal gating — while leaving metabolically driven feeding behavior unaffected.

Preliminary EEG spectral analysis revealed no significant differences in delta or theta power across sleep stages, though full spectral analysis is pending verification of a band-export inconsistency identified during quality control. If confirmed, the absence of spectral differences would constrain the interpretation of the Wake increase and NREM reduction. If the wakefulness and NREM reduction reflected global disruption of sleep-

generating circuits, one would expect alterations in NREM delta power or theta power during REM, as these reflect the activity of sleep oscillation-generating networks. The absence of detectable spectral differences, if confirmed upon full reanalysis, would suggest that sleep oscillation quality was not measurably altered in KO mice, though this interpretation requires cautious consideration given the small sample size and pending verification of the spectral data.

Several limitations should be noted. The CaMKII promoter targets mixed MSN populations and may include interneurons; preliminary D1-specific cilia ablation did not recapitulate the present phenotypes but instead disrupted social behavior (unpublished observations), suggesting the circadian behavioral phenotype is not D1-mediated and pointing toward D2 or other CaMKII-expressing neurons as the relevant substrate. All data were collected under LD conditions, precluding conclusions about the endogenous free-running period without additional constant-condition experiments. The sleep cohort was modestly sized (n = 5 WT, following exclusion of two animals with technical issues), limiting power for smaller effect sizes, and full EEG spectral analysis is pending reprocessing due to a band-export inconsistency identified during quality control. Finally, the study was conducted in male mice only, and sex differences in ciliary signaling or NAcC-dependent circadian regulation remain unexplored.

In conclusion, primary cilia in NAcC CaMKII-expressing neurons modulate the amplitude of circadian behavioral output without detectably altering the timing of the LD-entrained behavioral rhythm. Loss of cilia reduces dark-phase motivated locomotion, reduces total NREM sleep, and increases nocturnal wakefulness, with no detectable changes in rhythm structure, sleep oscillation quality, or food intake, consistent with a model in which ciliary GPCR signaling may fine-tune the gain of accumbal circuit

function during the active phase. These findings establish a subcellular mechanism linking ciliary architecture to behavioral state regulation and suggest that ciliary dysfunction in accumbal circuits may contribute to conditions characterized by altered arousal, disrupted sleep-wake balance, or impaired reward-driven motivation.

Chapter 4: Cilia Loss in the nucleus accumbens impairs social behavior and disrupts cortical oscillatory coordination

Roudabeh Vakil Monfared, Anna Popa, Travis Dabbour, Dana Shevachman, Aaliyah Alzaim, Qun-Yong Zhou, Olivier Civelli, Amal Alachkar., **Cilia Loss in the nucleus accumbens impairs social behavior and disrupts cortical oscillatory coordination.**

Brain Communications

(in revision)

ABSTRACT

Social behavior requires the coordinated activity of distributed neural circuits that integrate motivational, sensory, and mnemonic information across time. While the circuit architecture underlying social behavior has been extensively characterized, the subcellular mechanisms that enable the temporal organization of neural activity during behavior remain poorly understood. Here, we identify primary cilia in the nucleus accumbens core (NAcC) as necessary for normal social behavior and for the neural dynamics associated with social behavior. Using region-specific deletion of the ciliary protein IFT88 in NAcC neurons, we show that loss of accumbal cilia impairs social approach motivation and social recognition memory. Concurrent local field potential (LFP) recordings reveal preserved baseline oscillatory structure but altered neural coordination during socially relevant epochs, including a selective reduction in parietal theta power during active social interaction, changes in delta-centered phase-amplitude coupling, and elevated frontal–parietal coherence across multiple frequency bands. Together, these findings support a role for accumbal primary cilia in both social behavior and the temporal coordination of neural activity during social behavior. They further support a link between cilia-dependent signaling and large-scale neural dynamics and suggest that ciliary dysfunction may contribute to disorders associated with impaired neural synchronization and social deficits.

Keywords: cilia, nucleus accumbens, social behavior, EEG, PAC

INTRODUCTION

Social behavior is a fundamental aspect of mammalian life, requiring the motivation to seek social contact, the ability to recognize individual conspecifics, and the formation and retrieval of social memories. Disruption of these processes is a core feature of multiple neuropsychiatric disorders, including autism spectrum disorder (ASD), schizophrenia, and major depressive disorder [1]. Despite their clinical relevance, the mechanisms by which neural circuits give rise to socially relevant behavior remain incompletely understood.

At the circuit level, social behavior depends on the coordinated activity of distributed brain networks that integrate motivational, sensory, and mnemonic information [1-4]. This coordination depends on which neurons are active and when they are active, and therefore require precise temporal organization of neural population dynamics across multiple timescales [5-7]. While this temporal coordination is increasingly recognized as fundamental to cognition and behavior [8,9], the cellular and molecular mechanisms that enable behaviorally relevant synchronization of neural activity remain largely unknown.

The nucleus accumbens core (NAcC) is a central hub for motivated behavior, integrating dopaminergic input from the ventral tegmental area with glutamatergic projections from the prefrontal cortex, hippocampus, and amygdala to drive goal-directed actions [1,2]. Beyond its established role in reward processing, accumulating evidence indicates that the NAcC is critically involved in social motivation and social memory encoding [3,10,11]. While the circuit-level organization of this region has been extensively characterized, the subcellular mechanisms that govern its dynamic recruitment during social behavior remain largely unexplored.

Primary cilia are microtubule-based organelles present on nearly all neurons, functioning as specialized signaling hubs that concentrate receptors and second messenger systems within a confined subcellular domain [12,13]. Cilia regulate key signaling pathways, including Sonic Hedgehog signaling and cAMP dynamics, and have been implicated in synaptic plasticity and cognition [14-16].

Beyond this canonical role, emerging evidence suggests that brain cilia are dynamic structures whose molecular composition, length, and organization vary across brain regions, physiological states, and timescales [17]. In the striatum, cilia have been implicated in timing-dependent functions [15].

Recent studies have begun to link cilia to large-scale neural coordination [13]. Global IFT88 ablation has been reported to impair hippocampal-dependent memory, disrupt sleep architecture, and alter cross-frequency coupling [16]. These findings raise the possibility that ciliary signaling influences network-level activity beyond single-cell mechanisms.

Here, we tested whether primary cilia in the NAcC are required for the temporal coordination of neural activity underlying social behavior. Using region- and cell-type-specific deletion of IFT88 in CaMKII-expressing neurons, we show that loss of accumbal cilia impairs social motivation and social recognition memory. Concurrent wireless local field potential (LFP) recordings from frontal and parietal cortex revealed altered neural coordination during social epochs, most notably a selective reduction in parietal theta power during active social interaction. Together, these findings identify NAcC primary cilia as contributors to both social behavior and the temporal coordination of neural activity during social behavior, and link cilia-dependent signaling to large-scale neural dynamics relevant to social cognition.

MATERIALS AND METHODS

2.1. Animals

Eight-week male Ift88fl/fl mice (Jackson Laboratories, stock #022409), carrying loxP-flanked exons 4–6 of the Ift88 gene, were used throughout this study. All procedures were approved by the Institutional Animal Care and Use Committee (IACUC) at the University of California, Irvine, and conducted in accordance with NIH guidelines. A minimum of eight animals per group was targeted. All mice received bilateral stereotaxic viral injection and electrode implantation as described below; wild-type (WT) littermates received the same surgical procedure and served as controls. Three Control and two KO animals removed their electrodes during the recording session, behavioral data from these animals were retained, but no electrophysiological data were available. The final sample was Control n = 8 and KO n = 9 for behavioral analyses, and Control n = 5 and KO n = 7 for electrophysiological analyses prior to signal quality verification (see below).

2.2. Viral Injection and Electrode Implantation

To selectively ablate primary cilia in CaMKII-expressing neurons of the NAcC, all mice received bilateral stereotaxic injections of AAV9.CaMKII.HI.GFP-Cre.WPRE.SV40 under isoflurane anesthesia (2–3%), secured in a stereotaxic frame. Bilateral coordinates targeting the NAcC were: AP = +1.6 mm, ML = ±1.1 mm, DV = −4.5 mm from bregma. A volume of 0.1 µL per hemisphere (titer 2.8 x 1013GC/mL) was injected over 5 minutes using a Hamilton syringe, followed by a 5-minute post-injection wait before needle withdrawal at 0.01 mm/s to minimize backflow. AAV9.CaMKII.HI.GFP-Cre.WPRE.SV40 was a gift from James M. Wilson (Addgene viral prep #105551-AAV9; RRID:Addgene_105551).

Immediately following viral injection and under the same anesthetic session, stainless steel screw electrodes (Pinnacle Technology) were implanted for wireless LFP recording. Two electrodes were placed bilaterally over frontal cortex (EEG1; anterior cingulate/prelimbic region; AP = +1.5 mm, ML = ±1.5 mm from bregma) and two over parietal cortex (EEG2; AP = −1.3 mm, ML = ±2.5 mm from bregma). EMG wires were placed bilaterally in the trapezius muscle. All animals received Carprofen (5 mg/kg) and Dexamethasone (10 mg/kg) post-operatively and were handled for 2 minutes twice daily for 4 days prior to the recording session, which commenced 7 days post-surgery.

2.3. Three-Chamber Social Behavior Test with Concurrent LFP/EMG Recording

Social behavior was assessed in a three-chamber Plexiglas apparatus (each chamber: 20 × 40 × 20 cm) separated by walls with 5-cm openings, as previously described 23,24. Wireless LFP and EMG data were acquired concurrently at 256 Hz during the light phase using Pinnacle telemetry hardware and Sirenia Acquisition software. Sample sizes are as stated in the Animals section above.

2.3.1. Behavioral assessment

Mice first underwent a 5-minute acclimation period in the center chamber with the dividers in place. Dividers were then removed for the social interaction phase (10 minutes), during which one side chamber contained a wire mesh cup with an unfamiliar conspecific and the opposite chamber contained an empty cup. After a brief inter-trial interval, mice were returned to the center chamber for the social novelty phase (10 minutes), in which the now-familiar conspecific remained in one cup and a novel unfamiliar mouse was placed in the previously empty cup. Active investigation was

defined as direct nose contact with, or approach within 3 cm of, a wire mesh cup and was scored using ANY-maze software (Stoelting). Cup position was counterbalanced across subjects. Discrimination indices were calculated as:

DI = (time with social/novel − time with empty/familiar) / (total interaction time) × 100

2.3.2. EEG Signal Quality Verification

Of the Control n = 5 and IFT88 KO n = 7 animals with intact electrode assemblies, EEG1 signal integrity was further assessed post hoc using amplitude range and the number of unique digitization levels across the full recording. Two IFT88 KO animals exhibited EEG1 amplitude range < 40 μV and < 125 unique levels (all other animals: range 222–961 μV, 641–2477 unique levels), consistent with electrode failure rather than electrode self-removal, and were excluded from all EEG1-dependent analyses. EEG2 and EMG signals from these two animals were independently verified as usable and were retained for EEG2- and EMG-based analyses. Accordingly, EEG1-dependent analyses (band power, spectral features, coherence, PSI, and EEG1 PAC) used Control n = 5 and IFT88 KO n = 5, whereas EEG2- and EMG-based analyses used Control n = 5 and IFT88 KO n = 7.

2.3.3. Spectral Analysis

Power spectral density (PSD) was estimated using Welch's method (scipy.signal.welch; 4 s windows, 50% overlap, Hann taper). Band power was computed by trapezoidal integration within canonical frequency bands: delta (1–4 Hz), theta (4–8 Hz), alpha (8–13 Hz), beta (13–30 Hz), and gamma (30–80 Hz). Relative power was calculated as band power divided by total 1–80 Hz power. The aperiodic 1/f slope was estimated by ordinary least-squares regression of log10(PSD) versus log10(frequency) over 2–40 Hz. Spectral entropy was computed over 0.5–80 Hz from the normalized power spectrum as

−Σ p(f) log2 p(f). Hjorth complexity was computed from the first and second temporal derivatives of the signal.

2.3.4. Coherence and Phase–Amplitude Coupling

Magnitude-squared coherence between EEG1 and EEG2 was computed using scipy.signal.coherence with parameters matched to PSD estimation. The phase slope index (PSI) was computed to assess the direction of information flow between frontal and parietal sites, where positive values indicate frontal-to-parietal propagation. Phase–amplitude coupling (PAC) was quantified using the Tort modulation index (MI) with 18 phase bins (Tort et al., 2010). Phase signals were extracted from theta (4–8 Hz) or delta (1–4 Hz) bands, and amplitude signals from gamma (30–80 Hz) or beta (13–30 Hz) bands. Phase convention was defined such that 0° corresponded to the peak of the bandpass-filtered slow oscillation, based on the angle of the analytic signal returned by the Hilbert transform. For descriptive validation of coupling above chance, 50 circularly time-shifted surrogates were generated per animal per epoch. Band pairs analyzed were θ×γ, δ×γ, δ×β, and θ×β for both EEG1 and EEG2.

2.3.5. EMG Analysis

The raw EMG signal was full-wave rectified and low-pass filtered (4th-order Butterworth, 10 Hz) to obtain an amplitude envelope. Bursts were defined as envelope excursions exceeding mean + 3 SD, with minimum duration 50 ms and minimum inter-burst interval 100 ms. Burst rate was expressed as bursts per minute within each epoch. Burst-locked EEG averages were computed from ±500 ms windows centered on burst onset.

2.4. Immunohistochemistry

Tissue preparation and staining: To verify cilia ablation, a subset of mice was transcardially perfused with 4% paraformaldehyde following completion of behavioral testing. Brains were cryosectioned coronally at 30 μm. Sections were blocked in 5% normal goat serum in PBS/0.3% Triton X-100 for 1 h, then incubated overnight at 4°C with a rabbit anti-ADCY3 primary antibody (LSBIO-C204505; 1:500), a canonical marker of neuronal primary cilia, as previously described 18. Sections were subsequently incubated with Alexa Fluor 546 goat anti-rabbit secondary antibody (1:500) and DAPI (1:10,000; Thermo Fisher) for 1 h at room temperature.

Imaging and quantification: Images were acquired on a Keyence BZ-9000 fluorescence microscope at 20× magnification. Cilia density was quantified as the percent of ADCY3-positive structures per DAPI-positive cell nucleus within GFP-positive (Cre-expressing) regions of the NAcC, across 3–4 sections per animal.

2.5. Statistical Analysis

Statistical analyses were performed using GraphPad Prism 9.4.0 (GraphPad Software, Inc.) and Python (scipy, pingouin). Data are presented as mean ± SEM. Statistical significance was defined as $p < 0.05$. Verification of cilia ablation was analyzed using unpaired Student's t-tests. Time spent investigating each chamber during the social interaction and social novelty phases was analyzed using two-way mixed ANOVA (between-factor: genotype; within-factor: chamber), followed by Bonferroni's post-hoc test for pairwise comparisons. Discrimination indices were compared between genotypes using unpaired Welch's t-tests. EEG and EMG group comparisons used two-sided Mann–Whitney U tests (exact method). Effect sizes are reported as Cohen's d and rank-biserial correlation (rrb), with positive values indicating WT > KO.

3. RESULTS

3.1. Targeted ablation of primary cilia in the NAcC

To examine the role of primary cilia in NAcC function, we selectively ablated neuronal cilia, using stereotaxic delivery of AAV-CamKII-GFP-Cre into IFT88^fl/fl mice (Fig. 1A). Immunofluorescent staining for ADCY3, a marker of neuronal primary cilia, revealed near-complete loss of cilia within GFP-positive regions of the NAcC in IFT88 KO mice, while surrounding regions and WT mice retained dense ciliation (Fig. 1B). Quantification of ADCY3-positive structures normalized to DAPI-positive nuclei demonstrated a significant reduction in cilia density in KO mice compared to WT mice (Fig. 1C; $p < 0.001$), confirming efficient and spatially restricted ablation. Importantly, cilia loss was confined to the injection site, preserving ciliation in adjacent brain regions.

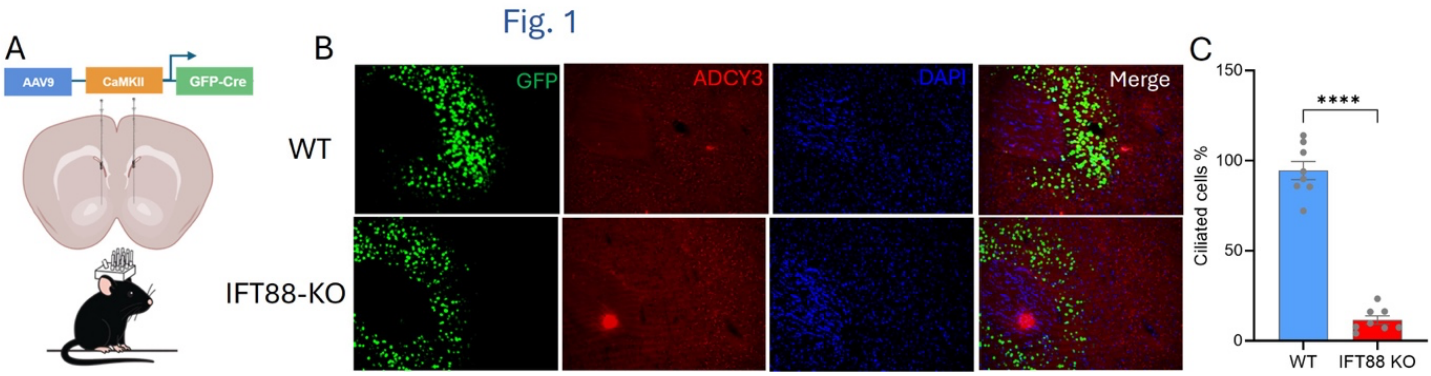


Figure 4.1. Selective ablation of primary cilia in CaMKII-expressing neurons of the nucleus accumbens core.

(A) Experimental schematic. AAV9.CaMKII.GFP-Cre was bilaterally injected into the NAcC of Ift88^fl/fl mice to selectively ablate primary cilia in CaMKII-expressing neurons. Immediately following viral injection and under the same anesthetic session, stainless

steel screw electrodes were implanted bilaterally over frontal cortex (EEG1; AP = +1.5 mm, ML = ±1.5 mm) and parietal cortex (EEG2; AP = −1.3 mm, ML = ±2.5 mm), with EMG wires placed in the trapezius muscle. Wild-type littermates underwent the same procedure and served as WT. (B) Representative fluorescence images from WT and IFT88 KO mice showing GFP (green), ADCY3 (red), DAPI (blue), and merged overlay. WT mice display abundant

ADCY3-positive cilia, whereas IFT88 KO mice show near-complete loss of ADCY3 signal in GFP-positive regions. (C) Quantification of cilia density (ADCY3-positive structures per DAPI-positive nucleus) within GFP-positive NAcC regions, across 3–4 coronal sections per animal (Control n = 8, KO n = 9; unpaired t- test, t= 15.06; ***p < 0.001). Bars represent mean ± SEM; dots indicate individual animals.

3.2. Loss of NAcC cilia impairs social motivation and social recognition memory

We assessed the behavioral consequences of NAcC cilia ablation using a three-chamber social interaction and social novelty paradigm (Fig. 2A; Supplementary Table 1).

During the social interaction phase, WT mice exhibited a robust preference for the chamber containing an unfamiliar conspecific (Figure 2B; $p < 0.0001$), whereas KO mice showed no significant preference (Figure 2B; $p > 0.05$). The social interaction discrimination index was significantly reduced in KO mice relative to WT mice (Figure 2C; $p < 0.0001$), indicating impaired social motivation.

During the social novelty phase, WT mice preferentially interacted with a novel conspecific over a familiar one (Figure 2D; $p < 0.01$; Supplementary Table 1), consistent with intact social recognition memory. In contrast, KO mice failed to discriminate

between novel and familiar mice (Figure 2D; $p > 0.05$), with a significantly reduced discrimination index compared to WT mice (Figure 2E; $p < 0.001$).

Together, these results demonstrate that primary cilia in the NAcC are required for both social approach motivation and social recognition memory.

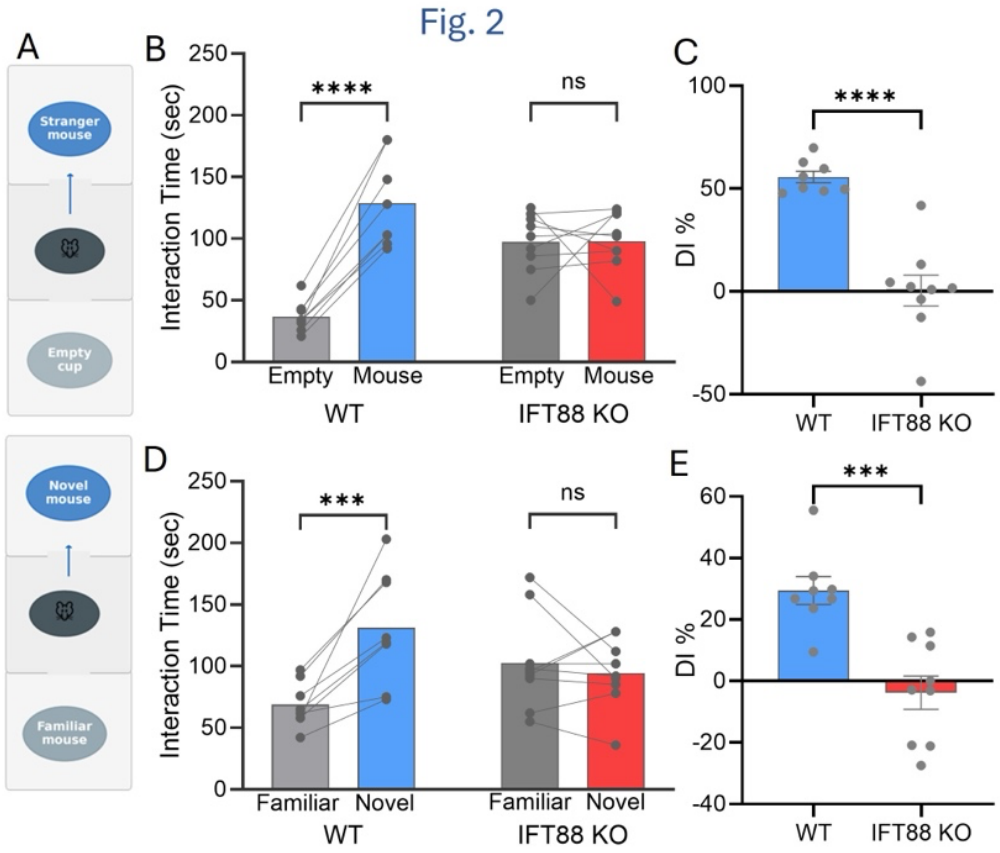


Figure 4.2. NAcC cilia KO mice exhibit deficits in social motivation and social memory.

(A) Schematic of the three-chamber social behavior test. (B) Time spent investigating the stranger mouse versus the empty cup (Control n = 8, IFT88 KO n = 9). Control mice showed a significant preference for the stranger, whereas IFT88 KO mice showed no preference (significant chamber effect ($F(1,15) = 29.22$, $p < 0.0001$) and genotype × chamber interaction ($F(1,15) = 28.25$, $p < 0.0001$). Post-hoc Bonferroni: Control mice

showed significant preference for the stranger (****p < 0.0001); (C) Social interaction discrimination index: DI = (stranger − empty) / (stranger + empty) × 100. (unpaired t-test t = 6.563; **** p < 0.0001, unpaired t-test). (D) Time spent investigating the novel versus familiar mouse during the social novelty phase. Two-way repeated-measures ANOVA revealed a significant chamber effect ($F(1,15) = 8.65$, $p = 0.010$) and a significant genotype × chamber interaction ($F(1,15) = 14.81$, $p = 0.0016$), with no significant main effect of genotype ($F(1,15) = 0.008$, $p = 0.931$). Post-hoc Bonferroni test: WT mice spent significantly more time with the novel mouse than the familiar mouse (* p < 0.05); IFT88 KO mice showed no significant preference (ns). Bars represent mean ± SEM; lines connect paired values from individual animals. (E) Social novelty discrimination index: DI = (novel − familiar) / (novel + familiar) × 100. ***p < 0.001, unpaired t-test (t = 4.632). Bars: mean ± SEM; dots indicate individual animals.

3.3. Cilia ablation preserves overall cortical spectral organization but reduces parietal theta power during social behavior

To determine whether loss of NAcC primary cilia affects cortical oscillatory activity during social behavior, we recorded LFP simultaneously from frontal and parietal electrodes in freely moving IFT88 KO and WT mice during acclimation, social interaction, and social novelty phases, and Trapezius EMG was recorded concurrently (Fig. 3A; Supplementary Table 2).

Global spectral structure was largely preserved following cilia ablation. Both groups showed the expected 1/f-like power spectra across EEG1 and EEG2 in all behavioral

epochs (Fig. 3B,C). Relative spectral composition was also similar between WT and cilia-ablated mice in both channels (Fig. 3D-G).

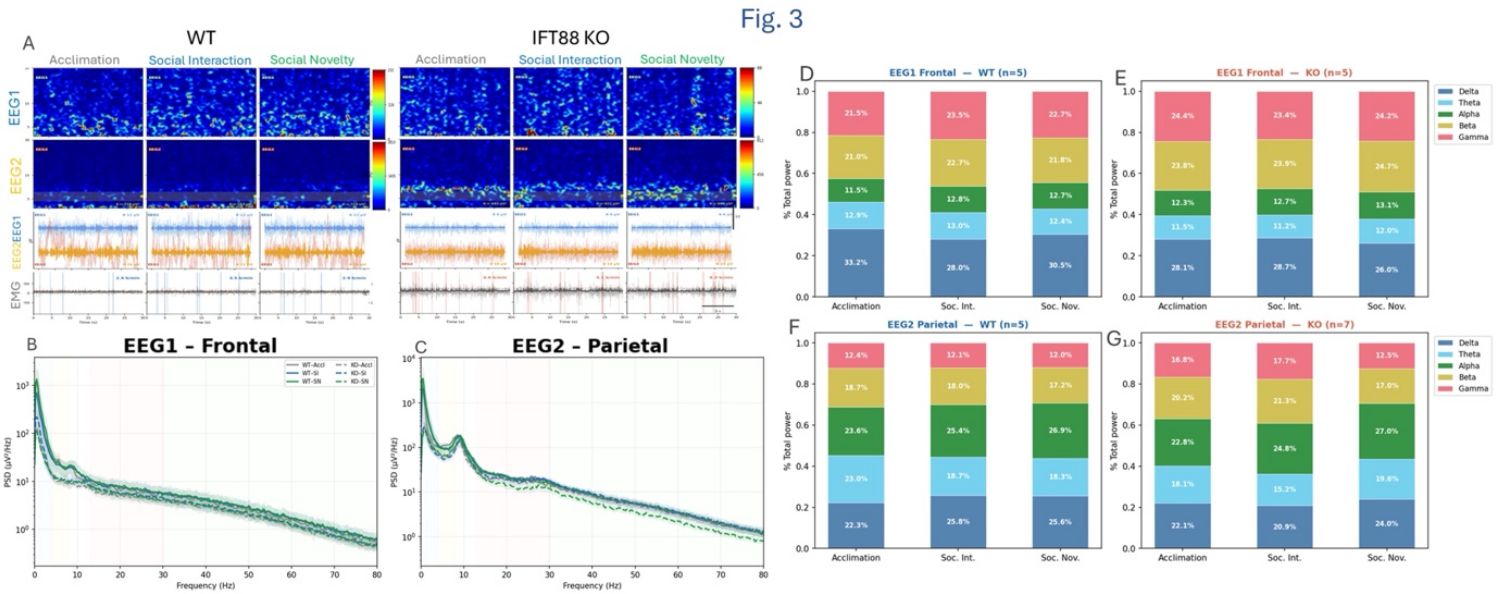


Figure 4.3. Preserved spectral organization in frontal and parietal cortex across social behavior epochs.

(A) Representative time–frequency spectrograms for frontal (EEG1) parietal (EEG2) recordings, EEG2/EEG1 power ratio, and EMG activity across acclimation, social interaction, and social novelty epochs in WT and IFT88 KO mice; Color scale indicates power (μV²/Hz). (B–C) Group-averaged power spectral density (PSD) for frontal and parietal recordings. estimated using Welch's method (4 s windows, 50% overlap, Hann taper). Thick lines indicate group means; shaded envelopes indicate ± SEM. Both genotypes exhibit typical 1/f-like power scaling across all groups and behavioral epochs, indicating preserved spectral organization. (D–G) Relative band power (% of total 1–80 Hz power) across behavioral epochs for frontal recordings (D) WT and (E) IFT88 KO, and parietal recordings (F) WT and (G) IFT88 KO recordings,

across behavioral epochs. Band distributions were comparable between WT and IFT88 KO mice across all conditions (all $p \geq 0.0.05$, Mann–Whitney U test).

Other spectral features, including entropy, aperiodic slope, theta/delta ratio, and Hjorth complexity, were likewise similar between WT and cilia-ablated mice in both channels (Fig. S1A-H; all $p > 0.05$). In EEG1, the aperiodic slope during social interaction was -0.78 ± 0.14 in WT and -0.70 ± 0.04 in cilia-ablated mice ($p > 0.05$, Fig. S1B), and the theta/delta ratio showed only a nonsignificant trend favoring WT during social novelty ($p > 0.05$, Fig. S1C). In EEG2, the largest numerical effect was a shallower aperiodic slope in cilia-ablated mice during social interaction (WT: -1.13 ± 0.06; IFT88 KO: -0.92 ± 0.09, Fig. S1F), but no comparison reached significance ($p > 0.05$). These findings indicate that cilia ablation did not broadly alter cortical spectral organization in either channel. Absolute power in the delta, theta, alpha, beta, and gamma frequency bands was quantified for frontal and parietal signals across acclimation, social interaction, and social novelty (Fig. 4). Frontal band power did not differ significantly between WT and cilia-ablated mice in any epoch (all $p > 0.05$; Fig. 4A-E). By contrast, parietal theta power was significantly reduced in cilia-ablated mice during social interaction (WT: 410.1 ± 49.2 μV^2; cilia-ablated: 252.0 ± 33.6 μV^2; $p = 0.030$, $d = +1.47$, $rrb = +0.77$), whereas the same comparison did not reach significance during acclimation or social novelty (Fig. 4G). No other EEG2 band differed significantly between groups (Fig. 4F-J).

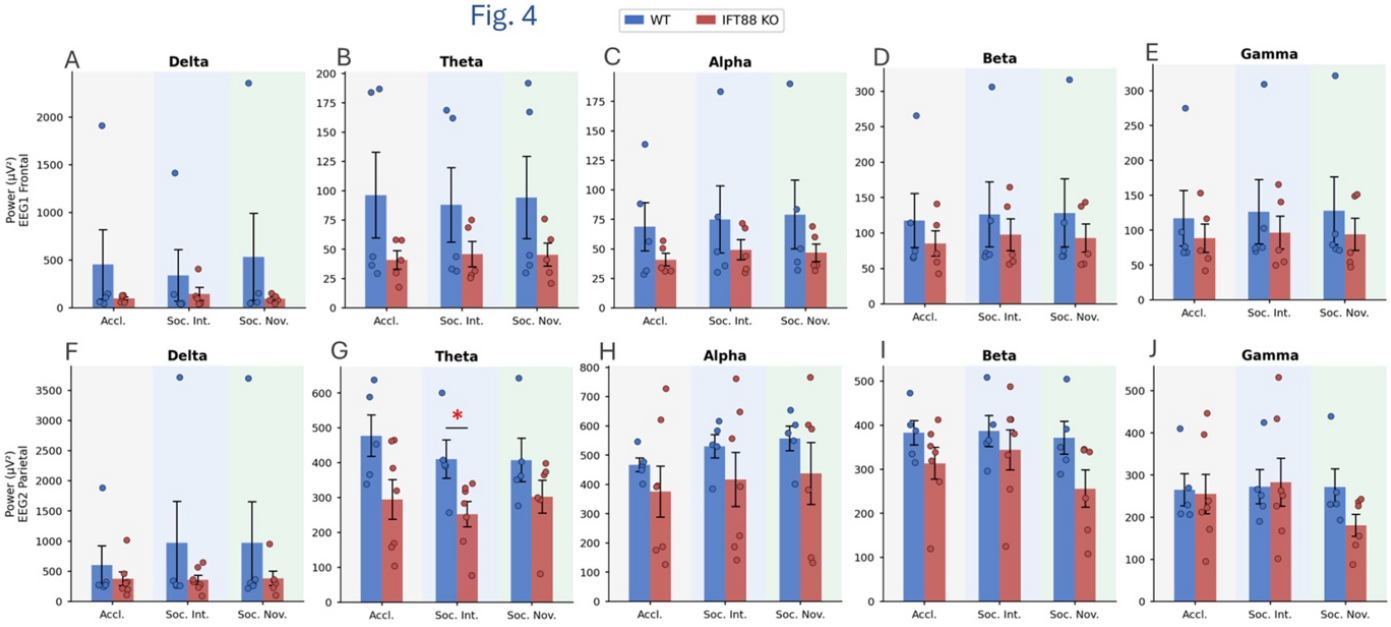


Figure 4.4. Absolute LFP band power across behavioral epochs.

(A-E) Frontal EEG1 and (F-J) parietal EEG2 power in (A,F) delta (1–4 Hz), (B,G) theta (4–8 Hz), (C,H) alpha (8–13 Hz), (D,I) beta (13–30 Hz), and (E,J) gamma (30–80 Hz) bands across acclimation (Accl.), social interaction (Soc. Int.), and social novelty (Soc. Nov.) epochs. (EEG1: Control n = 5, KO n = 5, EEG2: Control n = 5, KO n = 7). Bars represent group mean ± SEM; dots indicate individual animals. Band power was compared between using two-sided Mann–Whitney U tests. No significant differences were observed in frontal EEG across bands or epochs. In parietal recordings, theta power was significantly higher in Control mice compared to KO during the social interaction epoch ($p = 0.030$); all other comparisons were not significant; *$p < 0.05$; ns, not significant.

3.4. Frontal–parietal coherence is increased in cilia-ablated mice during social epochs

To test whether cilia loss altered interregional synchrony, magnitude-squared coherence between EEG1 and EEG2 was quantified across all five frequency bands for each epoch (Figs. 5; Supplementary Table 2). Coherence values were generally low in both groups, as expected for recordings from distinct cortical sites in freely moving animals, but IFT88 KO mice showed higher coherence than WT mice across multiple bands during social interaction and social novelty. No coherence differences were detected during acclimation (all $p > 0.0.05$; Fig. 5A). During social interaction, delta coherence was significantly elevated in IFT88 KO mice (IFT88 KO: 0.110 ± 0.068; WT: 0.007 ± 0.004; $p = 0.016$, $d = -0.86$, rrb = -0.92, Fig. 5B,D), while alpha, beta, and gamma coherence showed differences in the same direction that did not reach significance (alpha $p = 0.056$, $d = -1.71$; beta $p = 0.095$, $d = -1.39$; gamma $p = 0.095$, $d = -0.87$, Fig. 5B,F-H). During social novelty, theta, alpha, and beta coherence were also significantly higher in KO mice ($p = 0.016$, 0.032, and 0.016, respectively, Fig 5C,E-G), while gamma coherence showed a difference in the same direction that did not reach significance ($p = 0.056$; Fig. 5C,H). These data point to elevated frontal–parietal synchrony in cilia-ablated mice during social epochs.

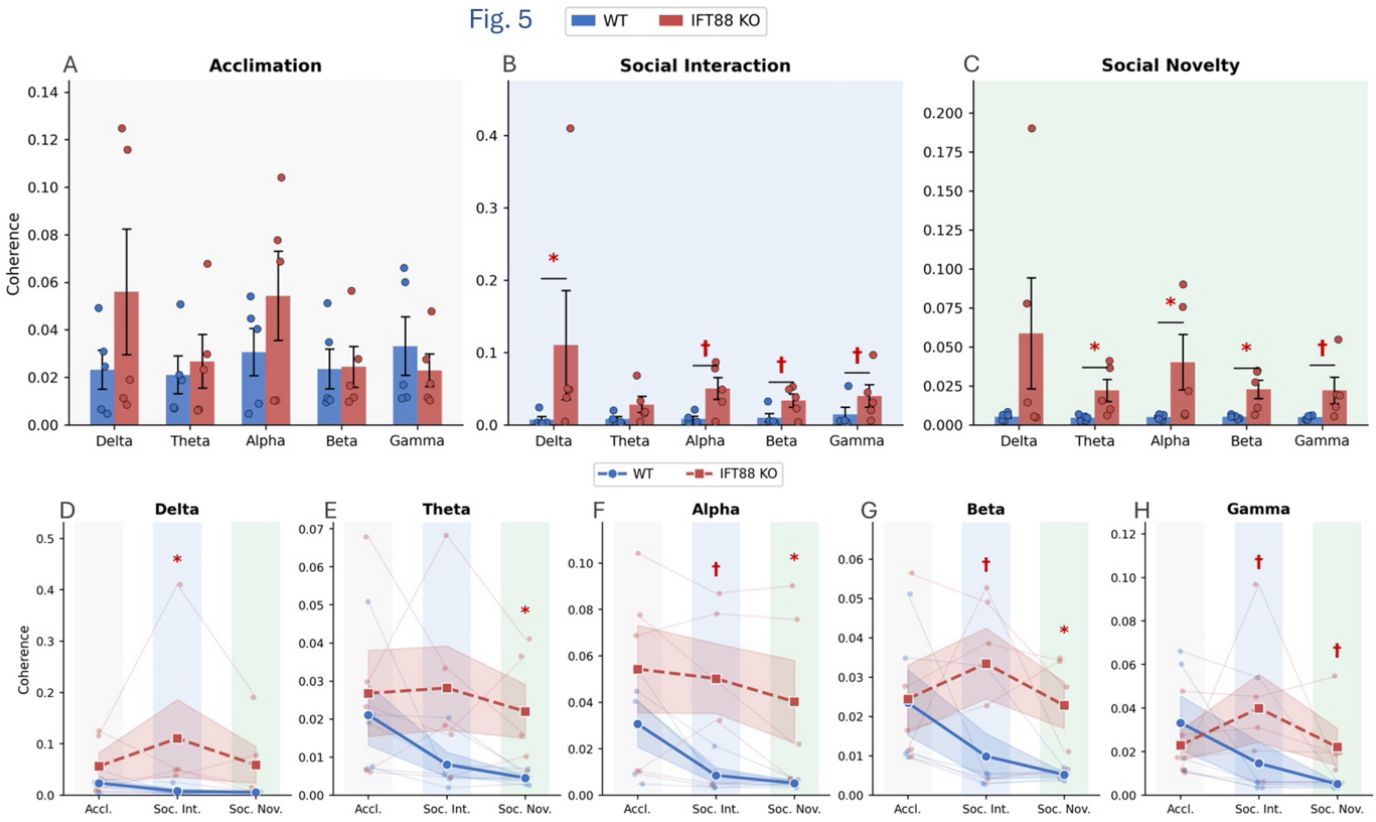


Figure 4.5. Elevated frontal–parietal coherence in IFT88 KO mice during social behavior epochs.

(A–C) Magnitude-squared coherence between frontal EEG1 and parietal EEG2 across frequency bands during (A) acclimation, (B) social interaction, and (C) social novelty epochs (Control n = 5, KO n = 5). Coherence was estimated using Welch's cross-spectral density method. Bars represent group mean ± SEM; dots indicate individual animals. Coherence values were generally low across conditions, consistent with recordings from distinct cortical regions in freely moving mice. KO mice exhibited higher frontal–parietal delta coherence than Control mice during social behavior, and higher theta, alpha, and beta coherence during social novelty (*p < 0.05, Mann–Whitney U

test). (D–H) Frontal–parietal coherence trajectories across behavioral epochs for (D) delta, (E) theta, (F) alpha, (G) beta, and (H) gamma bands. Thick lines represent group mean ± SEM; thin lines show individual animals. All five bands show a consistent directional pattern of higher coherence in KO animals during social interaction and social novelty epochs. Statistical comparisons by two-sided Mann–Whitney U test. *$p < 0.05$; † $p < 0.10$.

3.5. Cilia ablation is associated with selective increases in parietal phase–amplitude coupling

We next examined phase–amplitude coupling (PAC) as a measure of local cross-frequency coordination, quantified using the Tort modulation index for four band pairs: θ×γ, δ×γ, δ×β, and θ×β (Fig. 6; Supplementary Table 2). Phase–amplitude distributions showed that in both groups, high-frequency amplitude remained preferentially aligned near 0° of the slow oscillatory cycle, indicating that the preferred coupling phase was broadly preserved (Fig. 6). In the frontal EEG1 channel, PAC did not differ significantly between WT and cilia-ablated mice for any band pair in any behavioral epoch (all $p \geq 0.31$, Fig. 6A-D, I-L). In contrast, on the parietal EEG2 channel (Fig. 6E-H, M-P), cilia-ablated mice showed higher δ×γ PAC during acclimation than WT mice (IFT88 KO: $2.96 \times 10^{-4} \pm 1.41 \times 10^{-4}$; WT: $4.43 \times 10^{-5} \pm 3.57 \times 10^{-6}$; $p = 0.030$, $d = -0.81$, $rrb = -0.77$, Fig. 6F), and higher δ×β PAC during social interaction (IFT88 KO: $5.09 \times 10^{-4} \pm 2.49 \times 10^{-4}$; WT: $4.65 \times 10^{-5} \pm 5.80 \times 10^{-6}$; $p = 0.005$, $d = -0.84$, $rrb = -0.94$, Fig. 6G,O). The δ×β increase was restricted to the social interaction epoch and was not detected during acclimation or social novelty (Fig. 6E-H, M-P). Thus, cilia ablation was associated with

selective increases in parietal cross-frequency coupling in specific behavioral contexts, without disrupting the overall phase organization of PAC.

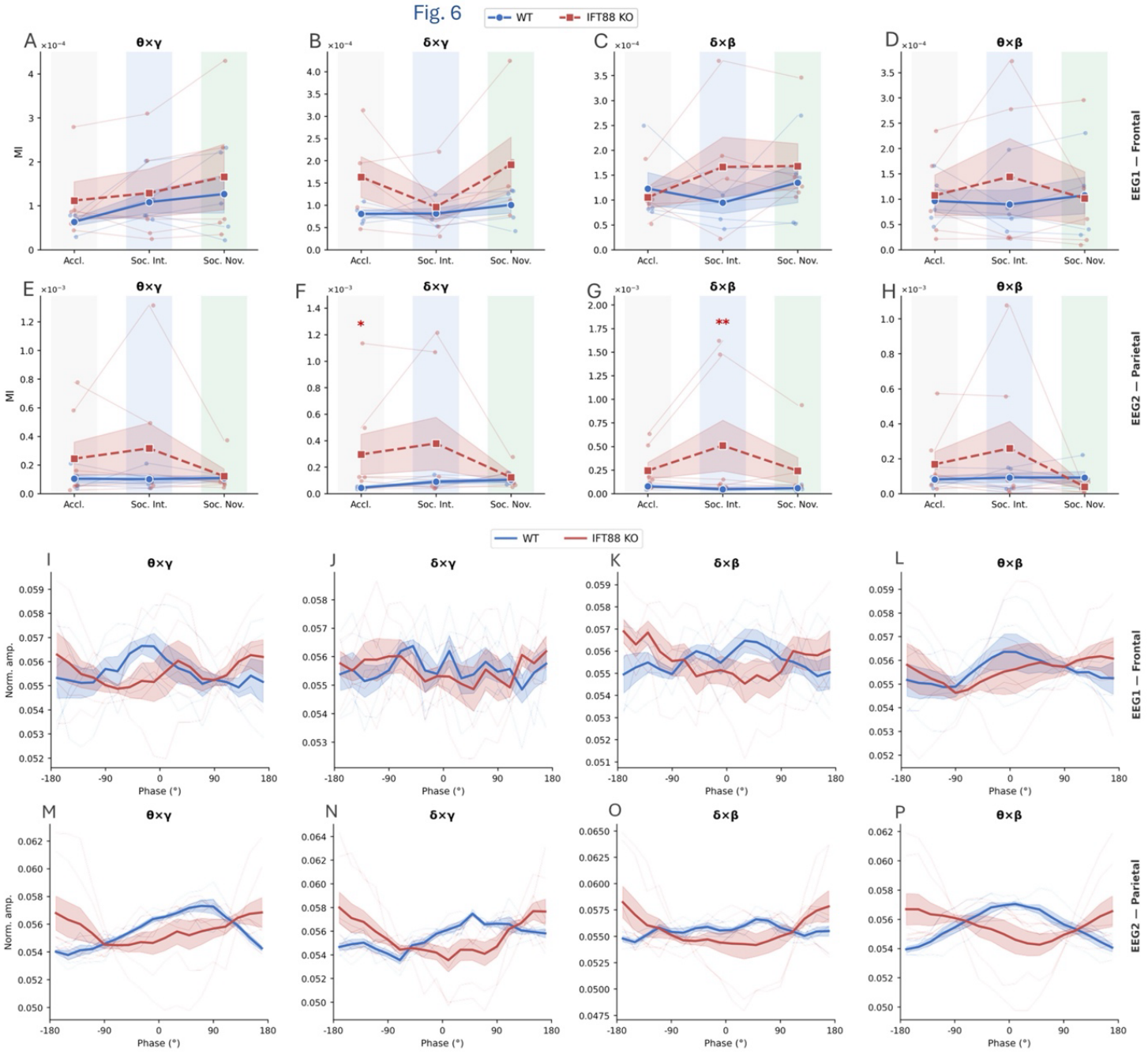


Figure 4.6. Phase–amplitude coupling across behavioral epochs and band pairs.

(A–H) Phase–amplitude coupling (PAC), quantified as modulation index (MI; Kullback–Leibler divergence method), across behavioral epochs for four band pairs: δ×γ (1–4 Hz × 30–80 Hz), θ×γ (4–8 × 30–80 Hz), δ×β (1–4 × 13–30 Hz), and θ×β (4–8 × 13–30 Hz). (A–D): EEG1 frontal channel (Control n =5, KO n = 5); (E–H): EEG2 parietal channel (Control n = 5, KO n = 7). Thick lines represent group mean ± SEM; thin lines indicate individual animals. KO mice showed differences in PAC strength across selected band pairs and epochs; Mann–Whitney U test, *p < 0.05, **p < 0.01. (I–P) Phase–amplitude distributions during the social interaction epoch for all four band pairs in (I–L) frontal and (M–P) parietal recordings. Normalized high-frequency amplitude (gamma or beta) is plotted as a function of low-frequency phase angle (delta or theta) from −180° to +180°. Grey dashed line indicates a uniform distribution expected under no coupling. In both groups of mice, high-frequency amplitude peaked near 0°, indicating that the preferred coupling phase is preserved across groups regardless of MI magnitude differences.

3.6. Baseline EMG-defined motor activity is elevated in cilia-ablated mice

before social exposure Trapezius EMG burst rate, used here as a proxy for upper-body motor output, was higher in cilia-ablated mice during acclimation (WT: 4.04 ± 0.41 bursts/min; cilia-ablated: 5.40 ± 0.37 bursts/min; p = 0.046, d = -1.31, rrb = -0.71; Fig. S2A; Supplementary Table 2). Burst rates were also numerically higher in cilia-ablated mice during social interaction and social novelty, but these differences did not reach significance (Fig. S2B). Because EMG was recorded from the trapezius, this measure should be interpreted as upper-body motor output rather than locomotion or a specific social behavior.

DISCUSSION

The present study provides evidence that primary cilia in the nucleus accumbens core are required for normal social motivation and social recognition memory, and that their loss is associated with selective alterations in the cortical oscillatory coordinations that accompany social behavior.

Using a targeted viral strategy to ablate cilia in the NAcC, we demonstrate that loss of accumbal cilia impairs both social motivation and social recognition memory and is accompanied by distinct electrophysiological alterations, most prominently reduced parietal theta power during active social interaction, elevations in frontal–parietal coherence, parietal phase–amplitude coupling, and baseline motor output. Together, these findings implicate primary cilia-dependent signaling in the NAcC in the regulation of both social behavior and the corticolimbic network dynamics that accompany it.

The NAcC serves as a major hub that integrates dopaminergic, glutamatergic, and serotonergic inputs to regulate motivational salience, reward processing, and action selection [1,2,25,26]. Our finding that targeted ablation of cilia from NAcC neurons abolished both social motivation and social recognition memory aligns with the view of primary cilia as transducers of neuromodulatory signals into cellular excitability changes. Primary neuronal cilia concentrate receptors for dopamine (D1R, D5R), serotonin (5-HT6R), somatostatin (SSTR3), and ADCY3, enabling compartmentalized cAMP-dependent integration of signals that would otherwise act on more distributed somatic receptors [27-30]. Disruption of this signaling hub in NAcC neurons would be expected to alter the kinetics of neuromodulatory signals, including dopaminergic reinforcement signals, and thereby impair the motivational drive necessary for social behavior. The impairment of social novelty discrimination in cilia-ablated mice suggests

an additional impairment in social recognition memory, a process known to depend largely on the hippocampal–accumbal–prefrontal circuit [31-33]. Primary cilia on striatal neurons have been shown to modulate hippocampal-dependent spatial memory and contextual memory, via cAMP-Protein kinase A (PKA) cascades [34,35], and disruption of ciliary ADCY3 impairs olfactory-dependent learning in rodents [36]. Whether the social recognition deficit observed here reflects a failure of reward-based reinforcement of social memories, an impairment in olfactory or contextual encoding, or both remains to be determined.

The most robust electrophysiological finding in this study was a significant reduction in parietal theta power in cilia-ablated mice during active social interaction, with no corresponding difference during acclimation or social novelty epochs. Theta oscillations (4–8 Hz) are widely regarded as a key neural correlate of goal-directed behavior, spatial navigation, and memory processes, particularly in hippocampal and medial temporal circuits [37,38]. Activity in the theta range over parietal cortex has been associated with attentional processing and the transformation of behaviorally relevant spatial information into action, including during visuospatial tasks that recruit frontoparietal networks [39,40]. The selective reduction in parietal theta power during social interaction, the epoch in which normal mice typically engage in active approach and investigation of a novel conspecific, may point at reduced recruitment of parietal cortical networks involved in attentional processing and sensorimotor integration during motivated social behavior.

The anatomical substrate and circuit mechanisms underlying the observed parietal theta reduction is unknown. In rodents, theta-range activity recorded over parietal cortex can be influenced by hippocampal theta rhythms through indirect pathways and volume

conduction, with strong hippocampal-prefrontal theta coherence implicated in coordinating goal-directed and memory-related processes [41,42]. Prefrontal–nucleus accumbens projections have also been shown to integrate social and spatial information [11]. One plausible interpretation is that primary cilia ablation in the NAcC disrupts dopaminergic or cAMP-mediated modulation of hippocampal–cortical network dynamics, leading to impaired recruitment of parietal theta during socially motivated states.

An unexpected finding was the elevated frontal–parietal coherence in cilia-ablated mice across multiple frequency bands during the social interaction and social novelty epochs, with several comparisons reaching statistical significance. Elevated inter-regional coherence in the context of impaired behavior is not straightforwardly interpretable. One possibility is that the increase reflects compensatory over-synchronization, a failure of the normal context-dependent modulation of frontal–parietal coupling that in WT animals allows flexible routing of information during social engagement.

Such alterations in cortical synchrony and directionality could contribute to impaired social information processing. In typical circuits, effective coordination between frontal and parietal regions is thought to rely on selective, frequency-specific coupling rather than broad elevations in synchrony [43-46]. Disruptions in selective oscillatory coordination have been proposed as a mechanism contributing to cognitive deficits in psychiatric disorders, particularly schizophrenia and autism-spectrum conditions [47-49]. Whether the coherence trends observed here reflect a similar disruption in the context of NAcC cilia ablation warrants further investigation with larger cohorts and combined behavioral-electrophysiological measures.

Two additional observations provide further context for the role of NAcC primary cilia in cortical dynamics. First, cilia-ablated mice showed increases in parietal δ×β, and δ×γ phase-amplitude coupling relative to WT mice. PAC reflects the nesting of fast oscillatory bursts within the excitable phase of slower oscillations and has been proposed as a mechanism for organizing information across temporal scales in neural networks [7,50]. In the present study, the preservation of the preferred coupling phase in both groups indicates that the basic architecture of PAC remained intact. The phenotype in cilia-ablated mice is, therefore, better described as a change in the magnitude or context dependence of selected parietal PAC measures (particularly δ×β during social interaction) rather than a generalized disruption of coupling structure. Second, cilia-ablated mice displayed a significantly higher EMG burst rate during acclimation, prior to any social exposure. Because EMG was recorded from the trapezius, this effect should not be interpreted directly as locomotion. However, it provides important context for the electrophysiological findings by suggesting that cilia-ablated mice may enter recording sessions in a different baseline arousal or motor state. Together, these observations raise the possibility that NAcC cilia ablation influences both tonic state regulation and the dynamic recruitment of parietal cortical networks during social behavior.

Primary neuronal cilia serve as specialized compartments that concentrate GPCR signaling components, including cAMP-generating and cAMP-sensing machinery, physically separated from the somatic membrane [51,52]. Ciliary dysfunction has been implicated in neurodevelopmental and psychiatric conditions characterized by social and cognitive impairment [53-57]. Mutations in ciliopathy genes have been associated with autism spectrum disorder, schizophrenia, and related disorders [53,57]. Consistent

with this, mice with cilia ablation exhibit deficits in hippocampal-dependent learning, reward processing, and dopamine-regulated behaviors [15,34,58-60].

The present findings add a circuit-level dimension to this body of evidence by showing that targeted cilia ablation in the NAcC is sufficient to alter corticolimbic network dynamics during social interaction, most notably a selective reduction in parietal theta power and changes in specific delta-modulated PAC measures, without gross disruption of spectral organization or excitability. These results support the view that primary cilia regulate ongoing neural state recruitment in adult circuits.

Several important limitations of this study must be acknowledged. The electrophysiological cohort was moderate. The wireless LFP recordings from frontal and parietal surface electrodes provide only coarse spatial resolution. Future experiments using multi-site depth electrodes or higher-resolution techniques will be necessary to localize the cellular generators of the observed oscillatory changes and to directly test the involvement of hippocampal, prefrontal, and accumbal circuits. Finally, the novelty deficit could reflect altered encoding, retrieval, or motivational salience; these possibilities will require phase-specific manipulations and more targeted behavioral assays to dissociate.

In summary, this study demonstrates that primary cilia on NAcC neurons are necessary for social motivation and social recognition memory and identifies selective alterations in cortical oscillatory coordination during social epochs as consistent neural correlates of this behavioral impairment. These findings support a role for NAcC primary cilia in social behavior and in the neural dynamics observed during social behavior. Further work combining higher-resolution recording, inducible ablation, and targeted circuit rescue

will be essential to determine the mechanisms, through which accumbal cilia influence corticolimbic dynamics during social behavior.

Chapter 5: Primary cilia on nucleus accumbens D1 neurons are required for social behavior but not circadian regulation

ABSTRACT

Primary cilia are neuronal signaling organelles that concentrate GPCRs — including D1 dopamine receptors — within a confined subcellular domain, and NAcC cilia exhibit circadian oscillations in length. D1 receptor-expressing medium spiny neurons (D1-MSNs) in the nucleus accumbens core (NAcC) are implicated in both social reward and circadian-sensitive dopamine signaling, yet whether their cilia contribute to either function remains unknown. Using cell-type-specific deletion of *IFT88* via a D1-Cre AAV construct, we selectively ablated cilia from NAcC D1-MSNs and assessed sleep architecture, circadian locomotor and food intake activity, social behavior and cortical dynamics during social behavior.

D1-cKO mice showed a complete loss of social approach preference and social novelty recognition, with discrimination indices indistinguishable from zero in both tasks. EEG recordings during social behavior revealed altered frontal cortical dynamics in D1-cKO mice, characterized by a steeper aperiodic slope, lower spectral entropy, and higher Hjorth complexity that were present before any social stimulus was introduced, with delta, beta, and gamma power differences emerging during social interaction and novelty. In contrast, wheel running rhythms, food intake, and sleep architecture were fully preserved. Sleep architecture was largely preserved, with reduced light-phase wakefulness and increased wake circadian amplitude, but no changes in total sleep amounts or EEG spectral power during sleep.

These results demonstrate that NAcC D1-MSN cilia are selectively required for social behavior, while circadian locomotor activity and feeding rhythms remain intact and sleep architecture is largely preserved, dissociating their contributions across these two

behavioral domains. The frontal — rather than parietal — EEG signature contrasts with the parietal theta deficit previously observed after broader CaMKII-neuron cilia ablation, suggesting that D1-MSN cilia loss disrupts the motivational state supporting social engagement rather than the encoding of social stimuli. These findings identify a cell-type-specific ciliary mechanism required for social behavior within the accumbal circuit.

1.Introduction

Primary cilia are microtubule-based organelles present on nearly all neurons, functioning as specialized signaling compartments that concentrate GPCRs and second messenger systems within a confined domain. D1 receptors localize to the ciliary membrane in striatal neurons, positioning cilia as a privileged site for dopaminergic signal transduction [1, 2]. Dopamine signaling dynamically regulates ciliary morphology: D1 receptor activation promotes cilia elongation, whereas D2 receptor activation shortens cilia, suggesting that opposing dopamine pathways bidirectionally regulate ciliary structure and signaling capacity [3, 4]. A large fraction of cilia-related transcripts exhibit circadian rhythmicity across primate brain regions, with particularly strong enrichment in the striatum, and primary cilia in the NAcC exhibit circadian oscillations in length, suggesting that ciliary signaling capacity is itself temporally regulated in a region-specific manner [5-7] . Beyond transcriptional regulation, cilia contribute to circadian and sleep regulation: disruption of ciliary signaling components such as adenylyl cyclase III alters sleep architecture, and temporal ablation of IFT88 disrupts brain rhythms and behavioral state organization [8, 9].

The nucleus accumbens core (NAcC) is a central hub that integrates dopaminergic input from the ventral tegmental area with glutamatergic projections from the prefrontal cortex, hippocampus, and amygdala to drive goal-directed behavior [10] [11, 12]. NAcC D1-MSNs also modulate voluntary locomotor activity and feeding behavior: activation of NAcC D1-expressing neurons facilitates effort for food reward and voluntary exercise while reducing food consumption, and D1 receptor signaling within the mNAc is required for motivated wheel running [13]. Within the NAcC, D1 receptor-expressing medium spiny neurons (D1-MSNs) are strongly implicated in social reward and affiliative motivation. Optogenetic activation of D1-MSNs promotes conditioned place preference for social stimuli, social experience enhances excitatory synaptic input onto this population, and disruption of oxytocin receptor signaling in D1-MSNs impairs social reward processing and social memor [11, 14, 15]. D1-MSNs also regulate arousal and sleep-wake transitions: lesions of the NAcC increase wakefulness and reduce REM and NREM sleep, while activation of D1 receptor-expressing neurons promotes arousal through disinhibition of midbrain and lateral hypothalamic circuits [16, 17]. At the molecular level, striatal clock gene disruption alters rest–activity rhythms, while D1 receptor signaling reciprocally regulates clock gene expression via CREB-dependent pathways [18-20]. Social behavior and circadian rhythms are both properties of NAcC D1-MSN circuits, though whether they share common cellular mechanisms remains unknown.

Given that D1-MSNs uniquely combine ciliary D1 receptor expression, dopamine sensitivity, and intrinsic circadian gene oscillations, primary cilia in this population represent a candidate mechanism for regulating D1-MSN-dependent behaviors.

Disruption of D2 receptor signaling alters the proportion and phase distribution of rhythmic cilia genes, further implicating dopaminergic tone in ciliary transcriptional timing. We previously demonstrated that broad deletion of IFT88 from CaMKII-expressing NAcC neurons impairs social approach and social recognition memory, increases wakefulness, and alters corticolimbic network dynamics during social interaction — including a reduction in parietal theta power during social exposure. However, CaMKII-driven manipulation targets heterogeneous neuronal populations, including D1- and D2-MSNs as well as interneurons, preventing identification of the responsible cell type and leaving unresolved whether social and circadian phenotypes arise from shared or separable mechanisms.

Here, we tested the hypothesis that primary cilia in D1-expressing NAcC neurons are required for social behavior and circadian outputs. Using D1-Cre–dependent AAV-mediated deletion of IFT88, we selectively ablated cilia from NAcC D1-MSNs and assessed social behavior, wheel running locomotor activity, home-cage feeding rhythms, and EEG/EMG-defined sleep architecture and neural dynamics during social interaction. We find that NAcC D1-MSN cilia are selectively required for social behavior, as D1-cKO mice fail to exhibit social approach or social novelty preference. In contrast, circadian locomotor rhythms, feeding rhythms, and baseline sleep architecture remain intact. EEG recordings during social behavior reveal a frontal-dominant shift in spectral state in D1-cKO mice that is present prior to social stimulus exposure, suggesting an altered baseline motivational or arousal state rather than a deficit in social information processing per se. Together, these findings identify NAcC D1-MSN cilia as a cell-type-

specific mechanism required for social behavior and dissociate their role in social versus circadian regulation within the accumbal circuit.

2. Materials and Methods

2.1 Animals

Eight-week-old male Ift88fl/fl mice (Jackson Laboratories, stock #022409) carrying loxP sites flanking exons 4-6 of the Ift88 gene were used in this study. All procedures were approved by the Institutional Animal Care and Use Committee at the University of California, Irvine, and conducted in accordance with NIH and institutional animal care guidelines.

To selectively eliminate primary cilia from D1 receptor-expressing neurons in the nucleus accumbens core (NAcC), wild-type and Ift88fl/fl mice received stereotaxic injections of a D1-MSN-specific Cre recombinase virus (pAAV-AiE0779m_3xC2-minBG-iCre(R297T)-BGHpA; Addgene #199776-PHPeB; a gift from the Allen Institute for Brain Science and Jonathan Ting). Ift88fl/fl mice receiving this virus are referred to throughout as D1-cKO mice; wild-type littermates receiving the same virus served as controls. This approach produces an adult-onset, regionally restricted conditional knockout of IFT88 in D1 receptor-expressing NAcC neurons, distinct from germline conditional knockout models in which ciliary loss occurs throughout development. A minimum of eight animals per group was used for food intake, wheel running, and social behavior

experiments. For EEG/EMG recordings, at least eight mice per group were implanted; animals with incomplete or disrupted recordings were excluded, yielding a final sample size of n = 7 per group for sleep/EEG analyses and n = 7 WT / n = 7 D1-cKO for the social behavior EEG paradigm.

2.2 Stereotaxic Surgery and EEG Implantation

2.2.1 Viral injection

Mice were anesthetized with isoflurane and secured in a stereotaxic frame. After disinfecting the scalp, a small midline incision was made to expose the skull. Bilateral injections of pAAV-AiE0779m_3xC2-minBG-iCre(R297T)-BGHpA were made into the NAcC using the following coordinates relative to bregma: AP = +1.6 mm, ML = +/-1.1 mm, DV = -4.5 mm. The skull was drilled at each coordinate, and the injection needle was slowly lowered at a rate of 0.01 mm/s. A total of 0.1 uL of virus was injected per site at a constant rate, followed by a 5-min waiting period before the needle was withdrawn at 0.01 mm/s to minimize backflow.

2.2.2 EEG/EMG implantation

EEG electrodes were implanted using a Pinnacle Technology headmount device with pre-positioned electrode contacts. The headmount was secured to the skull with dental cement following viral injections, with electrode contacts positioned over the frontal cortex and parietal cortex. The pre-drilled injection holes (AP = +1.6 mm, ML = ±1.1 mm) were used for both viral delivery and frontal electrode placement. EMG wires were

placed bilaterally in the trapezius muscle. Following electrode implantation, the wound was sutured and mice received Carprofen (5 mg/kg) and Dexamethasone (10 mg/kg) daily until recovery.

2.2.3 Postoperative care and habituation

Mice were handled for 2 minutes twice daily for 4 days before recordings to promote habituation to the experimenter and recording setup.

2.3 Experimental Timeline and Behavioral Assays

Following surgical recovery, mice underwent behavioral and physiological assessments in the following order: (1) wheel running and food intake recording for 14 consecutive days beginning 30 days after surgery; (2) social interaction and social novelty testing following completion of wheel running and food intake recording; (3) EEG/EMG sleep recording for 48 hours beginning after the completion of behavioral testing. This order was chosen to minimize stress carryover between assays and to ensure that EEG implants were fully healed prior to behavioral testing.

2.3.1 Wheel running and food intake

To assess circadian locomotor rhythmicity and feeding behavior, mice were individually housed in cages equipped with running wheels (Med Associates), automated food monitoring systems (TSE Systems, Germany) for 14 consecutive days under a standard 12:12 light-dark cycle (lights on at 06:30). Wheel-running revolutions were recorded continuously in 1-minute bins using Med Associates hardware and software and

subsequently summed into 1-hour bins for analysis. Food intake was measured continuously by the TSE PhenoMaster system, which records food weight at 30-minute intervals by means of a load cell-based sensor. Mice had ad libitum access to standard rodent chow and water throughout the recording period. Body weight was recorded at the beginning and end of the 14-day period.

Wheel running and food intake data were averaged across the 14-day recording period and analyzed as dark-phase average, light-phase average, and 24-hour total.

2.3.2 Social interaction and social novelty

Social behavior was assessed using a three-chamber Plexiglas apparatus (each chamber: 20 x 40 x 20 cm) separated by walls containing 5-cm openings to allow movement between chambers. Mice were first placed in the center chamber for a 5-minute acclimatization period with dividers closed. During the social interaction phase, one side chamber contained a wire mesh cup (9 x 10 cm) holding an unfamiliar conspecific of the same strain, age, and sex, while the other chamber contained an empty cup. The location of the stranger mouse was counterbalanced between trials. After acclimatization, dividers were removed and the test mouse was allowed to explore all three chambers freely for 10 minutes. Active interaction was defined as direct contact or approach within 3 cm of the cup. For the social novelty phase, a second unfamiliar mouse was placed in the previously empty cup, and the test mouse was allowed to explore freely for an additional 10 minutes. Time spent with each cup was recorded using ANY-maze software.

The effect of genotype and chamber on investigation time was evaluated as the primary analysis using two-way ANOVA with Šídák post-hoc correction, testing for main effects of genotype, chamber (mouse vs. empty cup for SI; novel vs. familiar for SN), and their interaction. A discrimination index (DI) was calculated for each animal as DI = (time with target − time with control) / (time with target + time with control) × 100. Group differences in DI were assessed using Welch's two-sample t-test. DI was also tested against zero using one-sample t-tests to confirm presence or absence of preference within each group.

2.3.3 Sleep and EEG recording

Following completion of social behavior testing, mice were individually housed in recording chambers connected to the Pinnacle Technology tethered EEG/EMG system. Continuous EEG and EMG signals were recorded for 48 hours beginning at light onset (ZT0) under a standard 12:12 light-dark cycle (lights on at 06:30AM). Food and water were available ad libitum throughout the recording period. Animals were allowed at least 48 hours of habituation to the recording tether prior to data collection. EEG and EMG signals were transmitted wirelessly via Bluetooth and acquired at 400 Hz using Sirenia Acquisition software (Pinnacle Technology) and subsequently down-sampled to 256 Hz for analysis.

2.4 Histology

Immunohistochemistry was performed to confirm cilia ablation in AAV-injected regions. Mice were deeply anesthetized with isoflurane and transcardially perfused with 0.9%

saline followed by 4% paraformaldehyde (PFA). Brains were post-fixed in PFA overnight and cryoprotected in 30% sucrose solution. Coronal sections (30 um) were cut using a microtome. Sections were blocked in goat serum in PBS containing 0.3% Triton X-100 for 1 h, then incubated overnight in blocking buffer containing rabbit anti-adenylate cyclase 3 (ADCY3) primary antibody (LSBio C204505, 1:500). After rinsing with PBS, sections were incubated with Alexa Fluor 546 goat anti-rabbit secondary antibody (Invitrogen, 1:500) and DAPI (Thermo Fisher Scientific, 1:10,000). Sections were washed, mounted on slides, and imaged using a Keyence BZ-9000 fluorescence microscope with a 20x objective.

2.5 Data Analysis

Sleep scoring

Continuous EEG and EMG recordings were divided into 10-second epochs and each epoch was semi-automatically classified as Wake, NREM sleep, or REM sleep based on the predominant waveform pattern (Sirenia Sleep Pro software). NREM sleep was characterized by high-amplitude, low-frequency delta activity (1-4 Hz); REM sleep by low-amplitude, theta-dominant activity (4-8 Hz); and wakefulness by low-amplitude, high-frequency activity with elevated EMG tone. All scoring was performed blind to genotype.

Sleep amount and phase analysis

Scored epochs were converted to 1-hour time bins and averaged across two consecutive recording days. Sleep stage amounts (Wake, NREM, REM) were computed separately for the light phase (ZT0-11) and dark phase (ZT12-23) as the mean number of epochs per hour within each phase. Phase comparisons were made using two-way ANOVA with genotype and phase as factors, followed by Sidak post-hoc tests. The significance of the genotype x phase interaction was evaluated as an index of circadian redistribution independent of total amount changes.

Cosinor analysis

To evaluate 24-hour rhythmicity of sleep-wake states and behavioral measures, a single-component cosinor analysis was applied to hourly time series data. For each animal, the hourly profile was fitted to the model Y = M + Acos(2pi*t/24 - phi) using ordinary least squares regression on sine and cosine components (numpy.linalg.lstsq, Python 3). M denotes the MESOR (mean level), A the amplitude (half the peak-to-trough range), and phi the acrophase (time of peak). Individual cosinor parameters were extracted per animal and compared between groups using Welch's two-sample t-test (two-tailed, alpha = 0.05).

Sleep bout analysis and latency

Bout number and mean bout duration were computed for each sleep stage across the full 48-hour recording and separately for the light and dark phases. A bout was defined as an uninterrupted sequence of consecutive epochs scored as the same state. Values were averaged across the two recording days per animal. Latency to first NREM and

first REM epoch was calculated from the start of each recording day and averaged across days. Sleep state transition probabilities were computed as the fraction of transitions from each state to each of the three possible subsequent states, yielding a 3x3 transition matrix per animal. All bout, latency, and transition comparisons between groups used Welch's two-sample t-test (two-tailed, alpha = 0.05).

Non-parametric circadian rhythm metrics

Additional circadian metrics were computed from wheel running data: M10 (mean activity during the most active 10 consecutive hours), L5 (mean activity during the least active 5 consecutive hours), relative amplitude (RA = (M10 − L5) / (M10 + L5)), interdaily stability (IS), intraday variability (IV), and activity onset, offset, and alpha duration. IS and IV were computed from the 48-hour Wake time series following Van Someren et al. (1999)[97].

EEG spectral power during sleep

EEG spectral power during sleep was assessed using pre-computed band power values exported from Sirenia software (Pinnacle Technology) for each 10-second scored epoch. Band power values were available for the following frequency ranges: delta (1-4 Hz), theta (4-8 Hz), alpha (8-13 Hz), beta (13-30 Hz), and gamma (30-80 Hz), along with total full-spectrum power. Relative band power was calculated per epoch as the ratio of each band to full-spectrum power. For each mouse, mean relative and absolute band power were computed separately for Wake, NREM, and REM epochs. Group comparisons used Welch's two-sample t-test (two-tailed, alpha = 0.05).

EEG analysis during social behavior

EEG and EMG signals recorded during the social behavior paradigm were imported as EDF files and processed in Python using MNE. Each recording was segmented into three epochs: acclimatization (Acc, 300 s), social interaction (SI, 600 s), and social novelty (SN, 600 s). One control mouse (EW19) was excluded from SN analyses due to insufficient recording duration, yielding n = 6 for SN EEG. Power spectral density was estimated using Welch's method (4-s Hann windows, 50% overlap). Band power, aperiodic slope, spectral entropy, Hjorth complexity, theta/delta ratio, frontal-parietal asymmetry index, coherence, phase-amplitude coupling, and EMG burst rate were computed as described in Supplementary Methods. All group comparisons used two-sided Mann-Whitney U tests (alpha = 0.05)

Supplementary methods Social behavior EEG and EMG Signal Processing

EEG and EMG signals recorded during the social behavior paradigm were imported as EDF files and processed in Python using MNE. Each recording was segmented into three epochs based on experimentally noted timestamps: acclimatization (Acc, 300 s), social interaction (SI, 600 s), and social novelty (SN, 600 s). One WT mouse (EW19) was excluded from the SN epoch only due to insufficient recording duration (409 s available), yielding n = 6 WT for SN EEG analyses; all other epochs used n = 7 per group.

For each epoch and each channel (EEG1: frontal; EEG2: parietal), power spectral density was estimated using Welch's method (4-s Hann windows, 50% overlap, scipy.signal.welch). Absolute band power was computed by integrating the PSD within

standard frequency bands (delta 1-4 Hz, theta 4-8 Hz, alpha 8-13 Hz, beta 13-30 Hz, gamma 30-80 Hz) using the trapezoidal rule. Relative band power was calculated as the ratio of each band to total power (1-80 Hz). As relative band powers sum to one, increases in one band necessarily reduce others; findings should be interpreted as spectral redistribution rather than independent band effects. The aperiodic component of the power spectrum was estimated by fitting a linear regression to the log-log PSD between 2 and 80 Hz; the resulting slope was used as an index of excitation-inhibition balance, with steeper (more negative) slopes indicating more inhibitory-dominant dynamics. Note that this sign convention is the inverse of the positive exponent reported by spectral parameterization software (specparam/FOOOF), where a larger exponent likewise reflects steeper aperiodic scaling. Spectral entropy was computed over 0.5–80 Hz as the Shannon entropy of the normalized power spectral density. The PSD was normalized by dividing each frequency bin by the total power across the 0.5–80 Hz range, yielding a probability distribution. Shannon entropy was then computed as $H = -\Sigma\, p(f) \log_2 p(f)$, where $p(f)$ is the normalized power at each frequency bin. Higher values indicate a more uniform (less predictable) spectral distribution; lower values indicate concentration of power in fewer frequency bins. Hjorth complexity was calculated as the ratio of the first-derivative signal mobility to the original signal mobility. The theta/delta ratio was computed as absolute theta power divided by absolute delta power.

Frontal-parietal coherence was estimated using magnitude-squared coherence (Welch method, same parameters as PSD) and averaged within each frequency band. Phase-amplitude coupling (PAC) was assessed using the Tort modulation index for four

frequency band pairs (theta x gamma, delta x gamma, delta x beta, theta x beta) in both channels. For each pair, the phase time series was extracted by bandpass filtering and computing the instantaneous phase via the Hilbert transform; the amplitude envelope was similarly extracted at the amplitude frequency. The modulation index was computed from the mean amplitude distribution across 18 phase bins, normalized to a uniform distribution. A frontal-parietal asymmetry index (AI) was computed for each frequency band as AI = (F − P) / (F + P), where F is frontal (EEG1) and P is parietal (EEG2) absolute band power for the corresponding epoch. Values range from −1 (purely parietal dominant) to +1 (purely frontal dominant). Group comparisons used two-sided Mann-Whitney U tests.

EMG burst rate was detected by rectifying the EMG signal, applying a low-pass filter (4th-order Butterworth, 10 Hz cutoff), and thresholding the resulting envelope at mean + 3 SD. Bursts with duration shorter than 50 ms or separated by less than 100 ms were merged or discarded. Burst rate is expressed as bursts per minute. One animal (EH44) was excluded from EMG analyses based on a pre-specified criterion of burst rate exceeding 3 interquartile ranges above the group median across all epochs (EH44: 18–22 bursts/min vs. group median of 3–7 bursts/min), consistent with electrode displacement or chronic artifact. This exclusion criterion was defined prior to statistical analysis. All remaining animals were retained. All group comparisons for EEG and EMG measures used two-sided Mann-Whitney U tests (alpha = 0.05). No correction for multiple comparisons was applied across epochs, as each epoch (acclimation, social interaction, social novelty) represents a distinct experimental condition; convergence of effects across epochs and independent spectral measures was used as evidence of

robustness. Although Acc, SI, and SN represent repeated epochs from the same animals, Mann-Whitney U tests were applied independently per epoch given the small sample size and non-normal distributions. All analyses were performed in Python 3 using NumPy, SciPy, MNE.

Results

3.1 Primary cilia are present on NAcC D1-MSNs and are selectively ablated by D1-Cre AAV

To confirm that primary cilia are present on D1 receptor-expressing neurons in the NAcC, we injected a D1-specific GFP-expressing AAV and performed immunofluorescence for AC3, a well-established marker of neuronal primary cilia. AC3-positive cilia were readily detected on GFP-labeled D1 neurons in the NAcC, confirming that this neuronal population bears primary cilia and is therefore a valid target for cell-type-specific ciliary ablation (Fig. 1b). To confirm selective cilia ablation in NAcC D1-MSNs, immunohistochemistry for adenylyl cyclase III (AC3), a marker of neuronal primary cilia, was performed on brain sections from AAV-injected mice. AC3-positive cilia were quantified across all DAPI-positive cells in the NAcC. D1-cKO mice showed a significant reduction in the proportion of AC3-positive cells compared to controls (ctrl: 91.25 ± 10.75%, D1-cKO: 48.00 ± 6.85%; $p < 0.0001$, Fig. 1b). The ~44% relative reduction is consistent with selective loss of cilia from D1-MSNs, which comprise approximately half of NAcC neurons, while AC3-positive cilia on non-D1 cells remain intact.

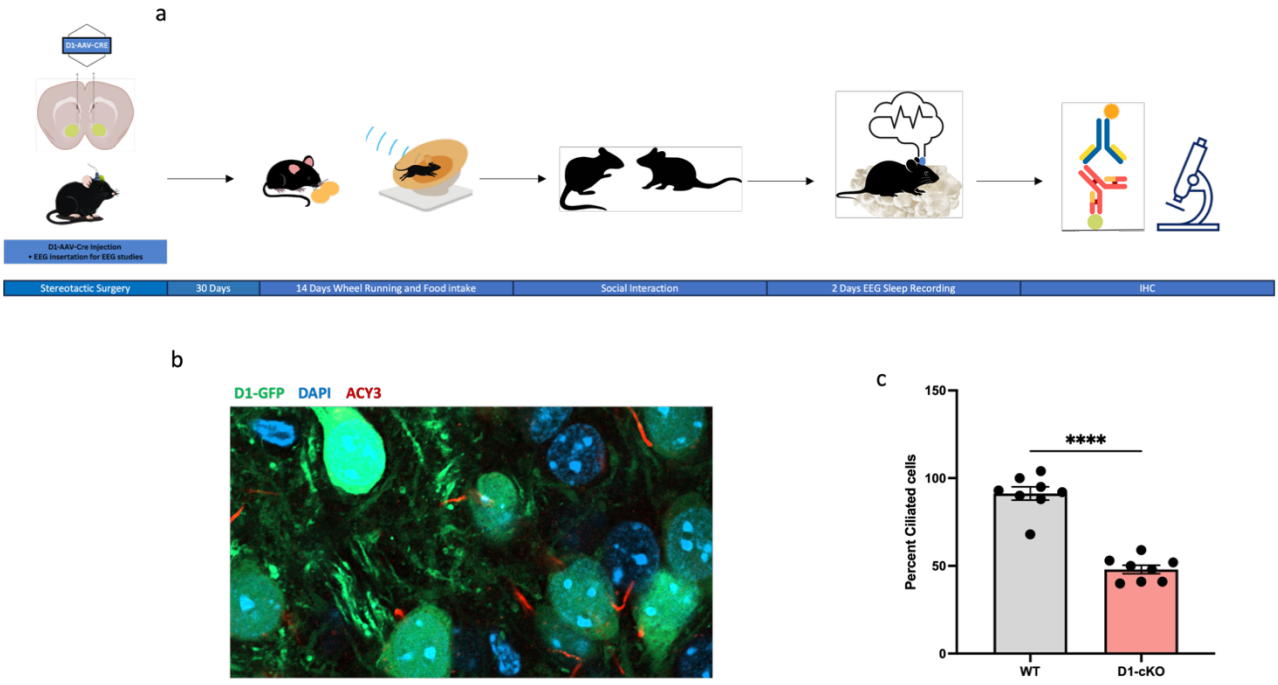


Figure 5.1. Validation of cell-type-specific cilia ablation in NAcC D1-MSNs. (A) Experimental timeline: bilateral stereotaxic injection of D1-specific AAV-Cre into the NAcC with concurrent EEG headmount implantation, followed by 30 days of recovery, 14 days of wheel-running and food-intake monitoring, social interaction and social novelty testing, 48 hours of EEG sleep recording, and terminal immunohistochemistry (IHC). (B) Representative widefield fluorescence image of NAcC tissue showing D1-GFP (green), DAPI (blue), and ACY3 (red, ciliary marker), with cilia visible on GFP-labeled D1 neurons. (C) Quantification of the percentage of ciliated cells in WT versus D1-cKO mice. ****$p < 0.0001$ (unpaired t-test). Data are presented as mean ± SEM; n = 8–9 per group.

3.2 D1-MSN cilia deletion does not alter wheel running or circadian locomotor rhythms

We assessed voluntary wheel running locomotor activity in a separate cohort of D1-cKO and control mice over 2 weeks of continuous wheel running recording. D1-cKO mice ran comparable total distances to controls ($p = 0.257$). Dark-phase running, which constitutes the majority of activity in mice, did not differ between groups ($p = 0.234$), nor did light-phase running ($p = 0.497$) (Fig. 2a-c). Both ctrl and D1-cKO mice showed robust 24-hour wheel running rhythms with peak activity during the dark phase, consistent with normal nocturnal entrainment (Fig. 2, S1 a-i).

3.3 D1-MSN cilia deletion does not alter food intake or circadian feeding rhythms

Food intake was measured continuously over 2 weeks in D1-cKO and control mice. Total food consumption did not differ significantly between groups ($p = 0.651$). Dark-phase intake, which represents the majority of feeding in nocturnal mice, was comparable between groups ($p = 0.855$), as was light-phase intake ($p = 0.166$) (Fig. 2e-h). Both ctrl and D1-cKO mice showed 24-hour feeding rhythms with peak intake during the dark phase consistent with normal nocturnal feeding patterns (Fig. 2d-f, Supplementary Figure S1 j-k).

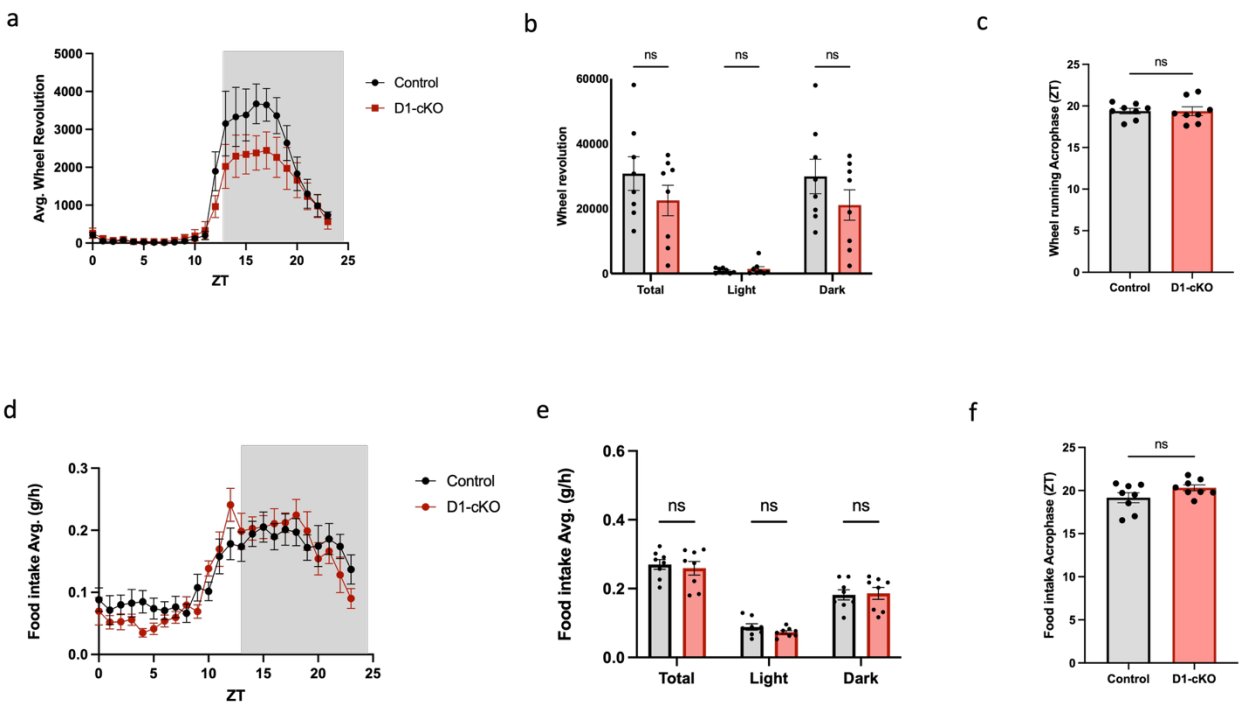


Figure 5.2. Wheel-running activity and food intake in control and D1-cKO mice under a 12:12 h light-dark cycle. (A) Mean 24-hour wheel-running profile (revolutions per hour) across Zeitgeber time, dark phase shaded. (B) Total, light-phase, and dark-phase wheel revolutions across the recording period. (C) Wheel-running acrophase (time of peak activity, from cosinor analysis). (D) Mean 24-hour food intake profile (g/h) across Zeitgeber time, dark phase shaded. (E) Total, light-phase, and dark-phase food intake across the recording period. (F) Food intake acrophase (time of peak feeding, from cosinor analysis). ns, not significant. Data are presented as mean ± SEM; n = 8 per group.

3.4 D1-MSN cilia deletion does not alter total sleep amounts but reduces light-phase wakefulness

Sleep architecture was largely preserved in D1-cKO mice over 48 hours of continuous EEG/EMG recording. Total Wake, NREM, and REM amounts did not differ between

groups ($p = 0.943$), and dark-phase sleep was unchanged ($p = 0.141$). However, light-phase wake was significantly reduced in D1-cKO mice compared to controls ($p = 0.024$), with a significant genotype × stage interaction in the light phase (Fig. 3e-g). Wake circadian amplitude was significantly larger in D1-cKO mice ($p = 0.0027$), while NREM and REM amplitudes and all other cosinor parameters did not differ between groups (Fig. 3h-j). Bout number, bout duration, sleep onset latency, state transition probabilities, EEG spectral power, interdaily stability, and intraday variability did not differ between groups (Supplementary Figures S2, S3, S4).

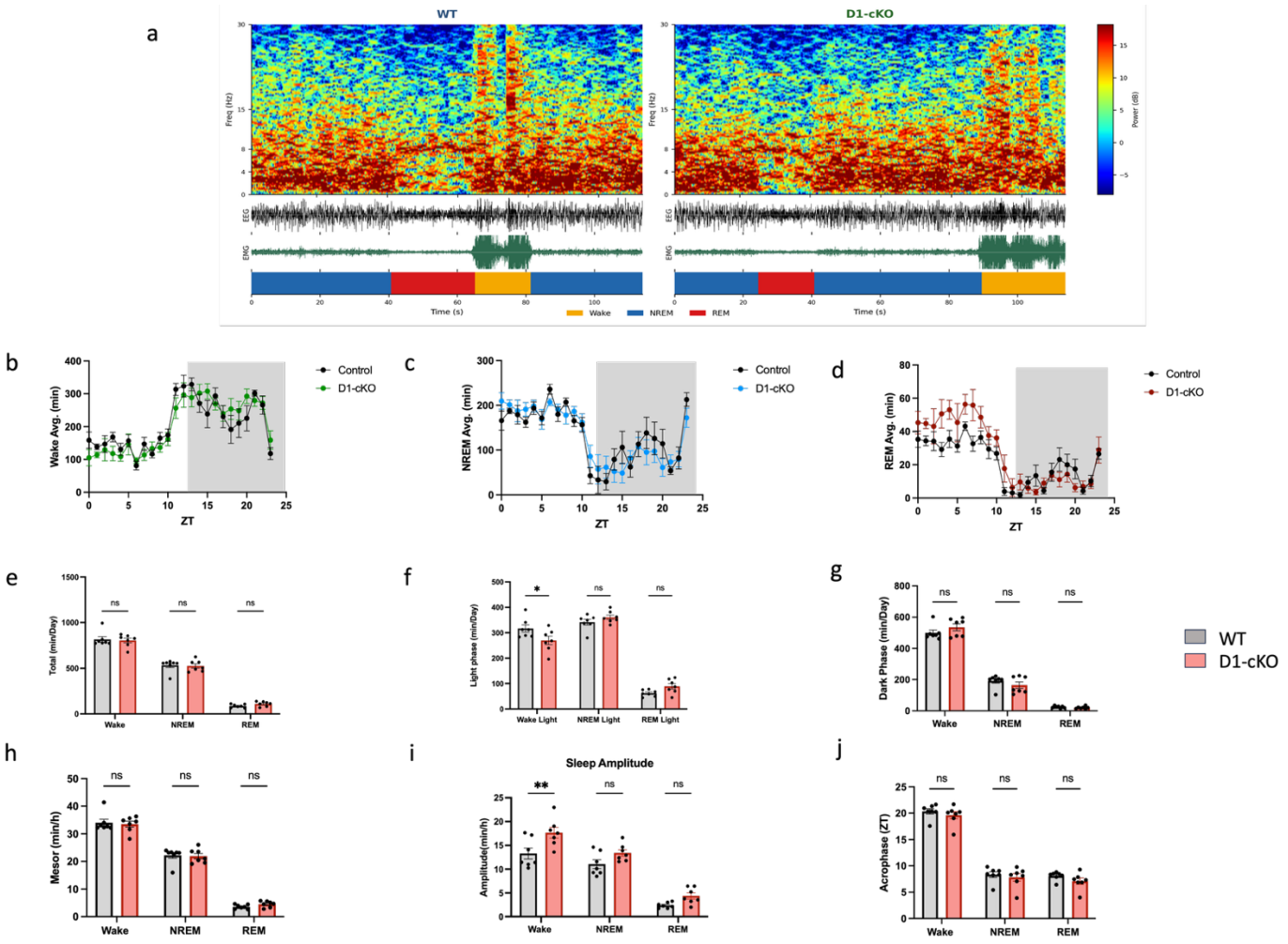


Figure 5.3. Sleep-wake architecture in control (WT) and D1-cKO mice assessed by EEG/EMG. (A) Representative EEG spectrograms, raw EEG and EMG traces, and corresponding hypnograms (wake, NREM, REM) in WT (left) and D1-cKO (right) mice. (B) Wake time (min) across Zeitgeber time. (C) NREM time (min) across Zeitgeber time. (D) REM time (min) across Zeitgeber time. (E) Total time spent in wake, NREM, and REM across the 48-hour recording period. (F) Time spent in each state during the light phase. (G) Time spent in each state during the dark phase. (H) Mesor for wake, NREM, and REM. (I) Amplitude for wake, NREM, and REM. (J) Acrophase for wake, NREM, and REM. *p < 0.05; **p < 0.01; ns, not significant (two-way ANOVA with Šídák's

multiple comparisons test). Data are presented as mean ± SEM; see Methods for group sizes per cohort.

3.5 D1-MSN cilia deletion abolishes social preference and social novelty recognition

We assessed social behavior in D1-cKO and control mice using a three-chamber social interaction and social novelty paradigm (Fig. 4a). Control mice showed a clear preference for the stranger mouse over the empty cup, spending significantly more time in social investigation ($p < 0.0001$), while D1-cKO mice showed no preference between the two chambers ($p = 0.460$), reflecting a significant genotype × chamber interaction ($p < 0.0001$; Fig. 4a-c). The discrimination index was significantly higher in control mice than D1-cKO mice ($p = 0.0005$), and differed significantly from zero in controls ($p = 0.0004$) but not in D1-cKO mice ($p = 0.148$), confirming a complete absence of social approach preference.

In the social novelty test, control mice preferentially investigated the novel conspecific over the familiar one ($p < 0.0001$), while D1-cKO mice showed no discrimination between the two mice ($p = 0.942$), reflecting a significant genotype × chamber interaction ($p = 0.0011$; Fig. 4d-e). The discrimination index was significantly higher in control mice than D1-cKO mice ($p = 0.0022$), and differed significantly from zero in controls ($p = 0.0018$) but not in D1-cKO mice ($p = 0.603$), indicating that D1-cKD mice failed to recognize the novel conspecific.

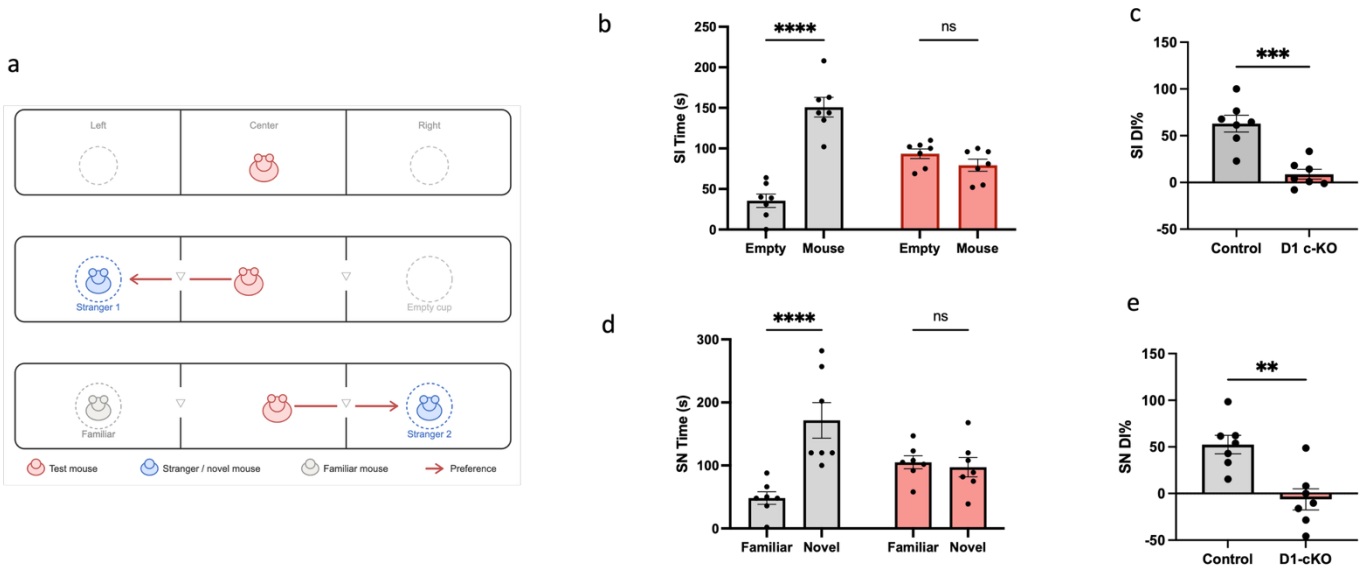


Figure 5.4. Social interaction and social novelty behavior in control and D1-cKO mice. (A) Schematic of the three-chamber apparatus and testing sequence: acclimatization, social interaction phase (stranger mouse vs. empty cup), and social novelty phase (familiar vs. novel conspecific). (B) Time spent investigating the empty cup versus the stranger mouse during the social interaction phase. (C) Discrimination index for social interaction (SI DI%). (D) Time spent investigating the familiar versus novel conspecific during the social novelty phase. (E) Discrimination index for social novelty (SN DI%). **p < 0.01; ***p < 0.001; ****p < 0.0001; ns, not significant (two-way ANOVA with Šídák's multiple comparisons test for B, D; unpaired t-test for C, E). Data are presented as mean ± SEM; n = 7 per group.

3.6 D1-MSN cilia deletion alters frontal cortical dynamics during social behavior

To examine cortical dynamics during social behavior, we recorded local field potentials from frontal (EEG1) and parietal (EEG2) cortex simultaneously with behavior across three epochs: acclimatization (Acc), social interaction (SI), and social novelty (SN). Representative EEG spectrograms and power spectral density curves are shown in Figure 5.

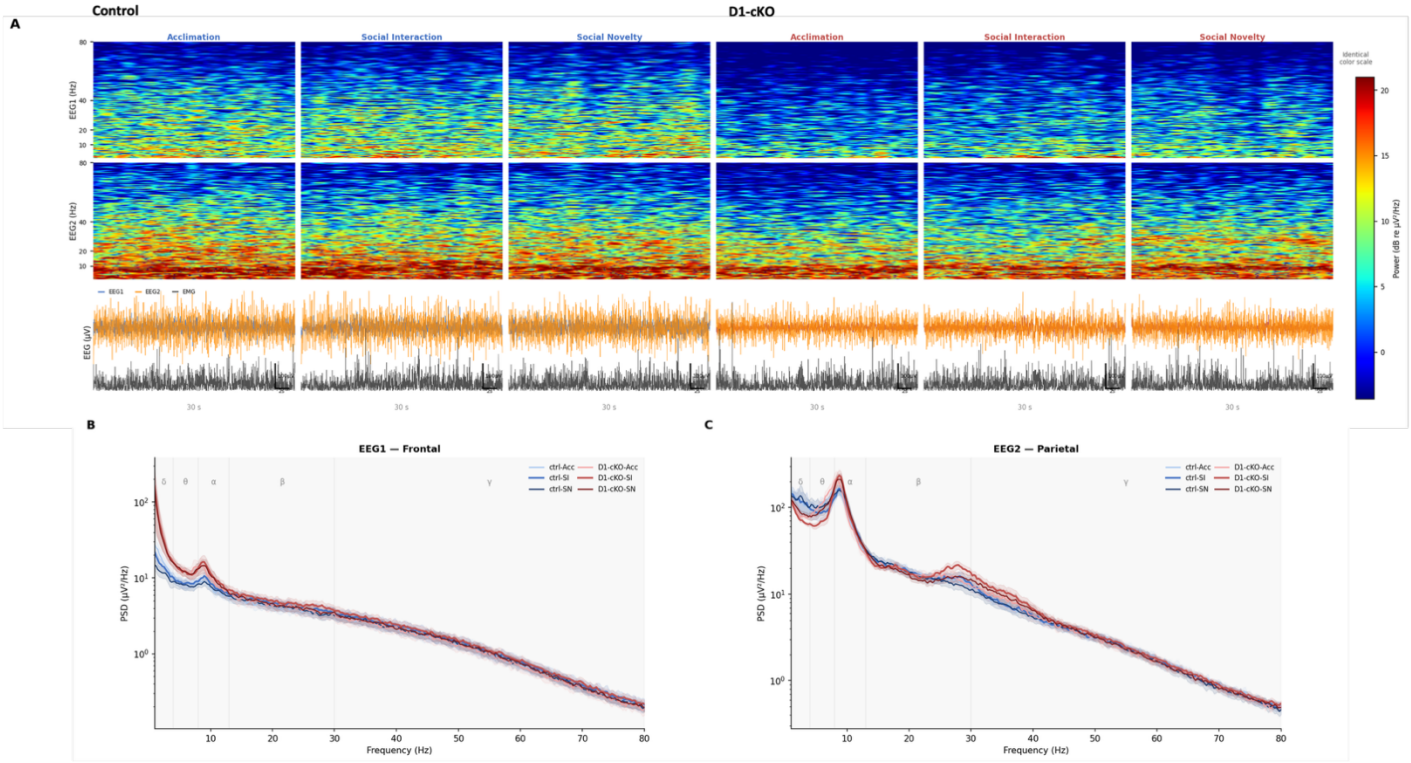


Figure 5.5. Cortical local field potential dynamics during social behavior in control and D1-cKO mice. (A) Representative EEG spectrograms from frontal (EEG1,

top) and parietal (EEG2, middle) cortex, with corresponding raw EEG (blue/orange) and EMG (gray) traces (bottom), shown for control (left) and D1-cKO (right) mice across the acclimatization, social interaction, and social novelty epochs; color scale is identical across all spectrograms. (B) Power spectral density (PSD) of frontal cortex (EEG1) across 1–80 Hz, plotted by genotype and epoch (Acc, SI, SN), with canonical frequency bands (δ, θ, α, β, γ) indicated. (C) Power spectral density (PSD) of parietal cortex (EEG2) across 1–80 Hz, plotted by genotype and epoch. Shaded regions represent SEM.

Frontal cortex (EEG1). D1-cKO mice showed a consistent pattern of altered frontal spectral dynamics across all three epochs, characterized by a steeper aperiodic slope, lower spectral entropy, and higher Hjorth complexity — differences that were already present during acclimatization before any social stimulus was introduced, indicating a baseline shift in frontal cortical state (Fig. 6a-d). During social interaction and novelty, elevated delta and reduced beta and gamma relative power were additionally observed (Fig. 6 e-i).

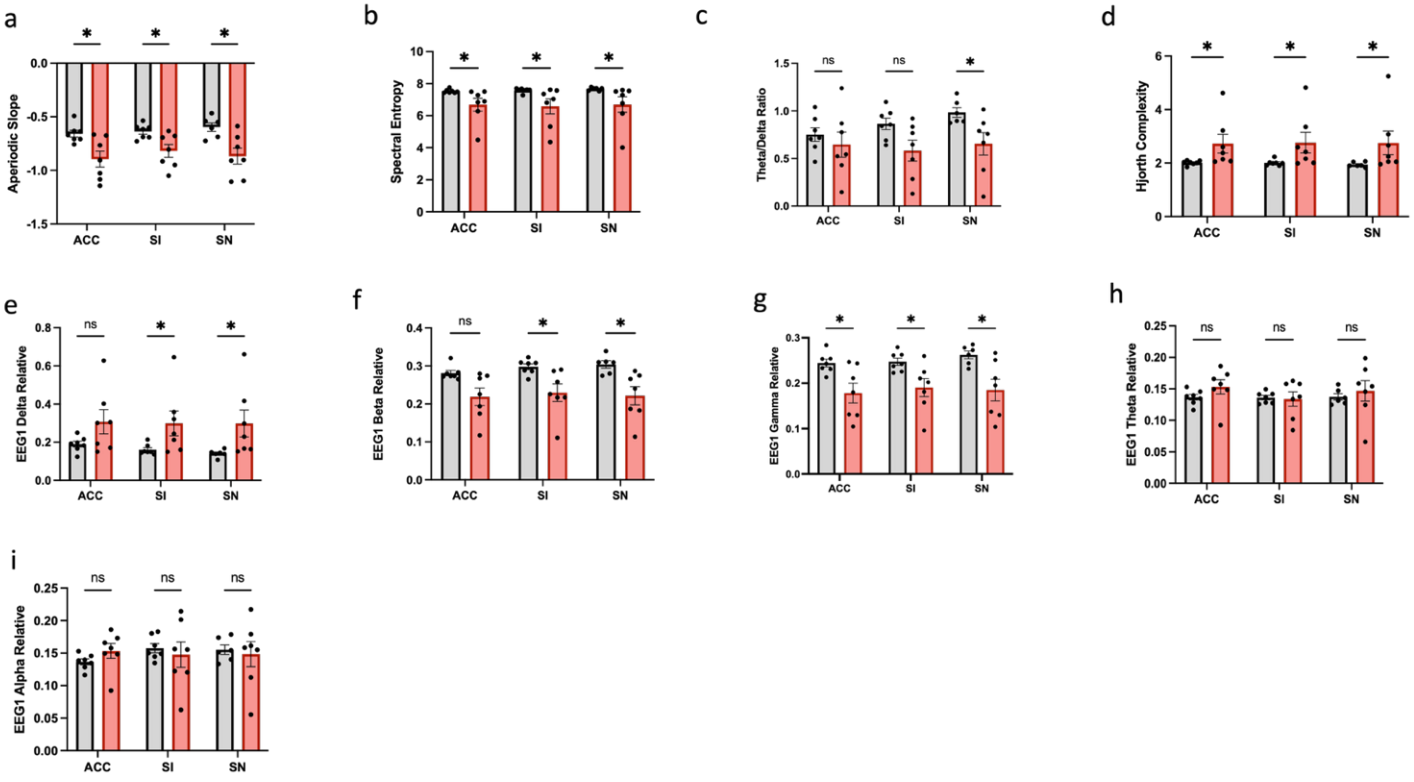


Figure 5.6. Frontal cortex (EEG1) spectral dynamics in control and D1-cKO mice across acclimatization (ACC), social interaction (SI), and social novelty (SN) epochs. (A) Aperiodic slope. (B) Spectral entropy. (C) Theta/delta ratio. (D) Hjorth complexity. (E) EEG1 relative delta power. (F) EEG1 relative beta power. (G) EEG1 relative gamma power. (H) EEG1 relative theta power. (I) EEG1 relative alpha power. *p < 0.05; ns, not significant. (Multiple Mann-Whitney tests) Data are presented as mean ± SEM; n = 7 per group.

Parietal cortex (EEG2). No significant differences were observed in any spectral measure in the parietal channel in any epoch (Supplementary Figure S5). The frontal-parietal asymmetry index confirmed a relative shift toward frontal delta dominance in

D1-cKO mice during SI (p = 0.007) and SN (p = 0.005), with a trend during Acc (p = 0.073), directly quantifying the regional specificity of the effect (Fig. 7a). Frontal-parietal coherence and phase-amplitude coupling did not differ between groups in any frequency band or epoch. EMG burst rate was comparable between groups across all epochs (Fig. 7b), and the novelty-evoked change in burst rate did not differ between groups (p = 0.378, Fig. 7c).

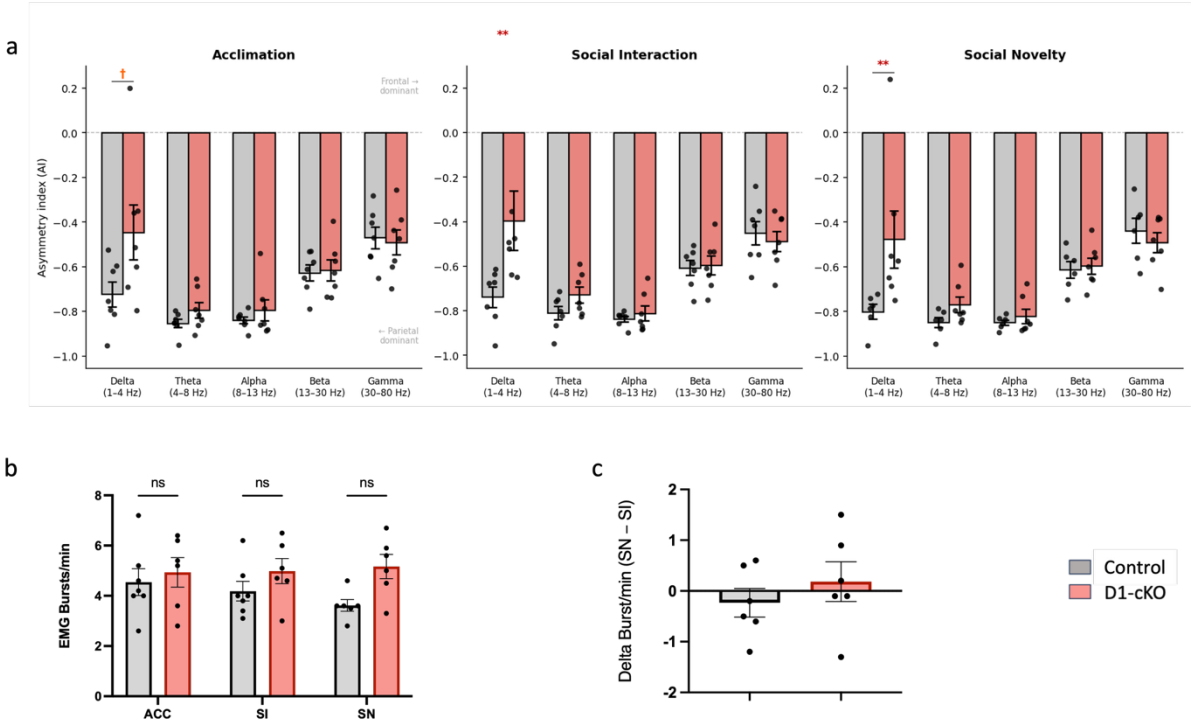


Figure 5.7. Frontal-parietal EEG asymmetry and EMG activity in control and D1-cKO mice. (A) Frontal-parietal asymmetry index (AI) for delta, theta, alpha, beta, and gamma bands during acclimation, social interaction, and social novelty epochs; positive values indicate frontal dominance, negative values indicate parietal dominance. (B) EMG burst rate (bursts/min) across acclimation, social interaction, and social novelty epochs. (C) Novelty-evoked change in delta burst rate, calculated as social novelty

minus social interaction (SN − SI). †p < 0.1; **p < 0.01; ns, not significant. (multiple Mann-Whitney tests) Data are presented as mean ± SEM; n = 7 per group.

Together, these results demonstrate that NAcC D1-MSN cilia are selectively required for social behavior but not for circadian locomotor activity, feeding rhythms, or sleep architecture. D1-cKO mice showed complete loss of social preference alongside a resting-state frontal cortical shift consistent with impaired motivational engagement, while circadian and sleep measures remained largely intact, identifying a cell-type-specific ciliary mechanism that dissociates social from circadian behavioral regulation within the accumbal circuit.

Discussion

The present study demonstrates that primary cilia on D1-MSNs in the nucleus accumbens core are selectively required for social behavior, while gross circadian locomotor activity and feeding rhythms show no detectable differences. Sleep architecture was largely preserved, with increased wake circadian amplitude but unchanged total sleep amounts, suggesting a more limited role of D1-MSN cilia in sleep-wake regulation. D1-cKO mice showed a loss of both social approach preference and social novelty recognition, with discrimination indices indistinguishable from zero in both tasks. EEG recordings during the social behavior paradigm revealed a consistent frontal cortical shift in D1-cKO mice that was present even before social stimulus exposure, indicating a baseline alteration in cortical state. Together, these findings suggest a cell-type-specific requirement for D1-MSN cilia in social behavior within the

accumbal circuit and establish a dissociation between social and circadian behavioral regulation.

The social behavioral deficit in D1-cKO mice was evident at both levels of social processing: social approach and social novelty discrimination. Control mice showed robust preference for social stimuli, whereas D1-cKO mice showed no preference in either assay. This pattern suggests impaired social reward valuation rather than sensory or motor impairment, as locomotion and EMG measures were intact.

D1-MSNs in the nucleus accumbens are well established as mediators of social reward processing. Prior work shows that activation of this population promotes social preference, that social experience enhances excitatory input onto D1-MSNs, and that disruption of neuromodulatory signaling within these neurons impairs social reward and social memory [77, 79, 96].

Primary cilia on D1-MSNs concentrate D1 receptors and associated signaling machinery, including cAMP-related pathways. Disruption of ciliary trafficking or localization of D1R impairs receptor signaling efficiency in striatal neurons [39, 64]. Together, these findings support a model in which ciliary compartmentalization of D1R signaling contributes to the computation of social reward salience in the nucleus accumbens core.

EEG recordings during the social behavior paradigm revealed altered frontal cortical dynamics in D1-cKO mice across all behavioral epochs, including baseline acclimatization. Specifically, D1-cKO mice exhibited increased delta power, reduced beta and gamma power, a steeper aperiodic 1/f slope, reduced spectral entropy, and increased signal regularity.

The aperiodic slope of the EEG power spectrum has been proposed to reflect excitation–inhibition balance, with steeper slopes associated with relatively increased inhibitory tone or reduced excitation [98]. Similarly, reductions in spectral complexity are generally associated with lower cortical responsiveness and reduced information processing capacity [92]. These observations are consistent with a baseline shift in frontal cortical state toward reduced engagement, which may reduce the propensity to initiate or sustain motivated social behavior. However, this interpretation remains indirect, as causal manipulation of prefrontal activity was not performed in this study. The prefrontal cortex is a key regulator of social motivation and decision-making, and alterations in excitation–inhibition balance in this region have been linked to social behavioral deficits in multiple models of neurodevelopmental and psychiatric disorders . We therefore propose that disruption of NAcC D1-MSN ciliary signaling may alter downstream cortico-striatal loop dynamics, shifting prefrontal cortical baseline state and thereby influencing behavioral readiness for social interaction.

The frontal EEG signature observed here differs from our previous findings following CaMKII-driven IFT88 deletion, which produced a parietal theta reduction specifically during the social interaction epoch [74]. These two phenotypes likely reflect distinct circuit mechanisms: a stimulus-locked encoding deficit in the CaMKII model versus a baseline motivational-state shift in the D1-MSN-specific model. This dissociation aligns with conceptual frameworks separating social perception/encoding from social motivation and action selection [99].

A key finding of this study is the preservation of circadian locomotor rhythms, feeding rhythms, and sleep architecture in D1-cKO mice. This is notable given prior evidence implicating NAcC D1-MSNs in arousal regulation, where activation promotes

wakefulness through downstream hypothalamic and midbrain circuits [83, 85], and where D1 receptor signaling reciprocally regulates clock gene expression in striatal neurons [90].

The absence of circadian and sleep phenotypes following ciliary disruption in D1-MSNs suggests that ciliary signaling is not essential for D1-MSN-mediated arousal regulation, or that non-ciliary D1R signaling pathways compensate for loss of ciliary compartmentalization.

Although total sleep amounts were preserved in D1-cKO mice, wake rhythmicity showed a larger circadian amplitude and D1-cKO mice showed reduced wakefulness during the light phase, consistent with a subtle redistribution of wake across the circadian cycle rather than a change in total arousal. In contrast, broader CaMKII-driven cilia ablation in the NAcC increased total wakefulness, indicating that wake-promoting effects of NAcC cilia loss depend on the specific neuronal population targeted, with D1-MSN cilia playing a more subtle modulatory role in sleep-wake organization.

Taken together with our prior CaMKII findings, these results suggest a functional dissociation within nucleus accumbens ciliary signaling pathways. D1-MSN cilia appear specifically required for social behavior, whereas non-D1 neuronal populations likely contribute to sleep and circadian phenotypes observed in broader CaMKII-based manipulations. D2-MSNs are known to regulate sleep–wake transitions via ventral pallidal and hypothalamic circuits [84], and cholinergic interneurons exert strong modulatory control over accumbal output and dopaminergic signaling dynamics [100, 101]. We propose that ciliary signaling in these populations may differentially regulate arousal-promoting and arousal-suppressing pathways within the accumbal microcircuit.

Several limitations should be noted. First, all experiments were conducted in male mice, and sex differences in accumbal dopamine signaling and social behavior may limit generalizability. Second, IFT88 deletion removes all primary cilia, not D1R-specific ciliary signaling. Third, potential off-target viral spread beyond the nucleus accumbens core cannot be fully excluded. Fourth, we did not directly measure cAMP signaling, D1 receptor localization dynamics, or ciliary morphology during social behavior, leaving mechanistic inference indirect. Additionally, controls were wild-type mice injected with the same Cre-expressing AAV rather than Ift88fl/fl mice injected with a Cre-null virus; although silent loxP insertions are not expected to alter behavior, this design does not fully isolate recombination as the sole variable.

In summary, primary cilia on nucleus accumbens D1-MSNs are required for social behavior and shape frontal cortical dynamics consistent with a motivational state deficit, while leaving circadian locomotor rhythms, feeding, and sleep architecture intact. These findings support a model in which neuronal primary cilia act as cell-type-specific signaling compartments that selectively regulate motivational aspects of social behavior without globally disrupting circadian organization. The dissociation established here between D1-MSN-dependent social behavior and non-D1-mediated circadian regulation provides a framework for understanding how primary cilia contribute to distinct behavioral functions within the same neural circuit.

Chapter 6: Conclusion and Perspectives

6.1 Revisiting the Question

This dissertation began with a simple observation and a harder question. The observation: primary cilia, long dismissed as vestigial cellular appendages, are in fact dynamic signaling organelles that concentrate the very receptors, D1 and D2 dopamine receptors, MCHR1, adenosine A2A, known to govern circadian behavior, motivation, and social engagement. The harder question: does this mean anything functionally? Does a microscopic, single organelle per neuron, ranging only a few micrometers in length, actually shape the large-scale behaviors an animal produces over the course of a day? And if it does, is it doing one job or several, and through which cells? Answering this required moving across four studies and several levels of resolution: from a brain-wide structural atlas, to circuit-level functional ablation, to cell-type-specific dissection. Each step narrowed the question further, and each answer reframed the one that came before it.

6.2 The Atlas: Cilia Are Not Static

The starting premise of this dissertation, that ciliary signaling capacity might be temporally regulated, rested on a structural claim that had not been established at scale. Chapter 2 addressed this directly, mapping primary cilia length and orientation across 22 mouse brain regions using a high-throughput imaging pipeline applied to over 10 million individual cilia. The result was the largest spatiotemporal atlas of primary cilia assembled to date, and it showed clearly that cilia are not fixed structures: their length and orientation vary substantially by brain region and fluctuate systematically across the 24-hour light-dark cycle. Critically, the nucleus accumbens core (NAcC) was among the

regions showing significant circadian oscillation in cilia length, with cilia reaching peak length in the hours just before the onset of the active phase.

This finding did more than confirm that cilia are dynamic; it identified the NAcC specifically as a region where ciliary structure appeared temporally poised to matter for behavior.

6.3 A Circuit Cut Broadly: Two Phenotypes Emerge

With the structural rationale established, The next chapters asked what happens when NAcC cilia are removed. Using AAV-CamKII-Cre-mediated deletion of IFT88, cilia were ablated broadly across CaMKII-expressing NAcC neurons, a population encompassing D1-MSNs, D2-MSNs, and other cell types.

The first phenotype to emerge was circadian. Chapter 3 showed that this broad ablation did not break the clock: the timing of the light-dark-entrained rhythm, its acrophase, its onset, its offset, its day-to-day stability, was untouched. What changed instead was amplitude. Cilia-ablated mice ran less during the dark phase, slept less during NREM, and were awake more, while food intake was entirely unaffected. This was not a broken oscillator; it was a quieter one. The behavioral rhythm persisted on schedule, but its output was blunted specifically during the active phase, when dopaminergic drive should have been at its highest.

The second phenotype, described in Chapter 4, was social. The same broad ciliary ablation abolished normal social approach motivation and social recognition memory. This impairment was accompanied by a specific electrophysiological signature: reduced parietal theta power during active social interaction, altered delta-centered phase-amplitude coupling, and elevated frontal-parietal coherence, changes concentrated in

the social interaction epoch itself, suggesting a deficit tied to the processing of social stimuli rather than a generalized change in cortical state.

Two real phenotypes, then, from one manipulation. But CaMKII is not a cell-type-specific promoter, it labels a mixed population, and Chapters 3 and 4 alone could not say whether one ciliated cell type was responsible for both effects, or whether two separate populations were each responsible for one.

6.4 Narrowing the Cell Type: A Dissociation

Chapter 5 resolved this directly by asking the same questions of a single, defined population: D1 receptor-expressing medium spiny neurons. Using D1-Cre-dependent AAV deletion of IFT88, cilia were removed specifically from NAcC D1-MSNs, and the full behavioral and electrophysiological battery, social behavior, wheel running, feeding, sleep architecture, and EEG during social interaction, was repeated.

The result was a clean dissociation. D1-MSN-specific cilia loss reproduced the social phenotype in its entirety: social approach preference and social novelty recognition were both abolished, with discrimination indices indistinguishable from zero. But the circadian phenotype did not follow. Wheel running rhythms, food intake, and sleep architecture were all largely preserved in D1-cKO mice, a striking contrast to the reduced activity and increased wakefulness seen after broad CaMKII ablation in Chapter 3.

The EEG data added a further layer. Rather than the parietal theta reduction seen after broad ablation, D1-MSN-specific cilia loss produced a frontal-dominant shift, a steeper aperiodic slope, lower spectral entropy, higher signal regularity; that was present even

before any social stimulus was introduced. Where the broad-ablation phenotype looked like a deficit in processing a social stimulus once it appeared, the D1-MSN-specific phenotype looked like an altered baseline state, present before the animal ever encountered another mouse.

Taken together, the story that emerges is this: the social phenotype might belong to D1-MSNs. The circadian phenotype does not. Something else within the CaMKII-labeled population, plausibly D2-MSNs, or cholinergic interneurons, both previously implicated in NAcC arousal and sleep-wake regulation, is responsible for the circadian gain deficit observed in Chapter 3. The single circuit turns out to be doing two jobs through two different ciliated populations, not one population doing double duty.

6.5 An Integrated Model

Bringing these findings together, this dissertation supports a model in which primary cilia function as cell-type-specific signaling compartments within the NAcC, and in which the same anatomical region achieves distinct behavioral outputs by routing ciliary signaling through different neuronal subpopulations rather than through a single shared mechanism. D1-MSN cilia appear necessary for the motivational and mnemonic processes underlying social behavior. A separate, still-unidentified ciliated population appears necessary for the circadian gain of motivated locomotor and arousal output. The distinct EEG signatures associated with each manipulation — parietal and stimulus-locked in one case, frontal and baseline-present in the other — suggest these two

functions are not only mediated by different cells but are expressed through at least partially different downstream circuit dynamics.

This reframes the original question from the introduction. It is not simply whether NAcC cilia matter for behavior, they clearly do. but how a single circuit can support multiple, behaviorally distinct outputs without those outputs interfering with one another. Cell-type-specific ciliary signaling offers one answer: compartmentalize not just within the cell, at the level of the organelle, but across cells, at the level of the circuit.

6.6 Limitations

Several limitations qualify these conclusions and are worth stating plainly rather than folding into the narrative above.

All experiments in this dissertation were conducted in male mice. Sex differences in accumbal dopamine signaling, in ciliary gene expression, and in social and circadian behavior are well documented in other contexts, and whether the findings reported here generalize to females is entirely untested.

IFT88 deletion removes the entire primary cilium, not D1 receptor ciliary localization specifically. This means the phenotypes observed cannot be attributed to loss of D1 receptor signaling alone; loss of other ciliary receptors known to be present on NAcC cilia, including D2R, MCHR1, and adenosine A2A, cannot be excluded as contributing factors, particularly in the CaMKII-driven experiments where the targeted population is heterogeneous.

The electrophysiological work throughout this dissertation relied on surface EEG and LFP electrodes, which offer only coarse spatial resolution. The cellular and circuit-level

generators of the parietal theta reduction (Chapter 4) and the frontal spectral shift (Chapter 5) remain unlocalized, and both findings are correlational with respect to the underlying ciliary manipulation rather than directly linked through causal circuit-level intervention.

The circadian experiments in Chapters 3 and 5 were conducted entirely under standard light-dark entrainment. Without constant-condition (free-running) recordings, conclusions about whether NAcC cilia loss affects the endogenous circadian period itself, rather than only the entrained behavioral output, cannot be drawn.

Finally, viral targeting carries inherent limitations: potential off-target spread beyond the NAcC cannot be fully excluded in any of the functional studies, and in several experiments, controls consisted of wild-type mice receiving the same Cre-expressing virus rather than Ift88fl/fl mice receiving a Cre-null virus, meaning recombination itself was not fully isolated as the sole experimental variable.

6.7 Future Directions

The findings of this dissertation open several concrete lines of investigation.

Identifying the circadian-relevant cell type. The most direct next step is to determine which non-D1 population within the CaMKII-labeled NAcC neurons is responsible for the circadian gain phenotype described in Chapter 3. D2-MSN-specific and cholinergic interneuron-specific cilia ablation, using the same IFT88-deletion strategy applied here to D1-MSNs, would directly test the candidates raised in this dissertation's discussion and would complete the cell-type map of NAcC ciliary function.

Localizing the circuit generators of the electrophysiological phenotypes. The parietal theta reduction observed after broad ablation and the frontal spectral shift observed after D1-MSN-specific ablation were both identified using surface electrodes with limited spatial resolution. Multi-site depth recordings, or simultaneous recording from the NAcC, prefrontal cortex, and hippocampus, would help determine whether these signatures originate locally in the cortex, are inherited from hippocampal or prefrontal afferents, or reflect broader corticolimbic network reorganization downstream of accumbal ciliary loss.

Establishing causal, real-time links between ciliary signaling and behavior. The current studies rely on constitutive or AAV-mediated deletion of IFT88, which removes ciliary signaling capacity permanently and prior to behavioral testing. Inducible or reversible ciliary manipulation, combined with in vivo imaging of ciliary cAMP dynamics or D1 receptor trafficking during ongoing social or circadian behavior, would allow the temporal relationship between ciliary signaling and behavioral state to be tested directly, rather than inferred from the consequences of its absence.

Testing generalizability across sex. Given that this dissertation was conducted exclusively in male mice, and given known sex differences in both dopaminergic signaling and social behavior circuits, repeating the D1-MSN and CaMKII ablation studies in female mice is a necessary next step before these findings can be considered general properties of NAcC ciliary function rather than male-specific ones.

Testing free-running circadian period. Because all circadian data here were collected under light-dark entrainment, follow-up studies using constant darkness would clarify whether NAcC ciliary signaling contributes to the intrinsic period of the circadian clock

itself, or is limited to shaping the entrained behavioral output, as the current data suggest.

Translational extension to psychiatric-relevant models. Given that ciliary gene dysregulation has been documented across schizophrenia, autism spectrum disorder, and other psychiatric conditions characterized by co-occurring social and circadian disturbance, an important future direction is to determine whether NAcC ciliary dysfunction is present in genetic or environmental models of these disorders, and whether restoring ciliary signaling in D1-MSNs specifically is sufficient to rescue social deficits in such models.

6.8 Closing Statement

What began as a question about a small, easily overlooked organelle ends with a circuit-level story: the nucleus accumbens core achieves two behaviorally distinct outputs, circadian and social, not through a single undifferentiated mechanism but through primary cilia acting in different cells for different purposes. D1-MSN cilia are necessary for social motivation and memory; a separate, still-to-be-identified ciliated population governs the gain of circadian behavioral output. In tracing this dissociation from a whole-brain atlas down to a single genetically defined cell type, this dissertation positions primary cilia not as a peripheral curiosity of cell biology, but as an active, cell-type-specific mechanism through which a single neural circuit can flexibly and separately support the many behaviors it is asked to produce.

Reference

Chapter 1 Reference:

1. Bloodgood, R.A., From central to rudimentary to primary: the history of an underappreciated organelle whose time has come. The primary cilium. Methods in cell biology, 2009. 94: p. 2-52.

2. Kiesel, P., et al., The molecular structure of mammalian primary cilia revealed by cryo-electron tomography. Nature structural & molecular biology, 2020. 27(12): p. 1115-1124.

3. Zimmermann, K.W., Beiträge zur Kenntniss einiger drüsen und epithelien. Archiv für mikroskopische Anatomie, 1898. 52(3): p. 552-706.

4. Sorokin, S., Centrioles and the formation of rudimentary cilia by fibroblasts and smooth muscle cells. The Journal of cell biology, 1962. 15(2): p. 363-377.

5. De Robertis, E., Electron microscope observations on the submicroscopic organization of the retinal rods. The Journal of Cell Biology, 1956. 2(3): p. 319-330.

6. KozMINSKI, K.G., et al., A motility in the eukaryotic flagellum unrelated to flagellar beating. Proceedings of the National Academy of Sciences, 1993. 90(12): p. 5519-5523.

7. Pazour, G.J., C.G. Wilkerson, and G.B. Witman, A dynein light chain is essential for the retrograde particle movement of intraflagellar transport (IFT). The Journal of cell biology, 1998. 141(4): p. 979-992.

8. Karalis, V., K.E. Donovan, and M. Sahin, Primary cilia dysfunction in neurodevelopmental disorders beyond ciliopathies. Journal of Developmental Biology, 2022. 10(4): p. 54.

9. Izawa, I., et al., Current topics of functional links between primary cilia and cell cycle. Cilia, 2015. 4: p. 1-13.

10. Ishikawa, H. and W.F. Marshall, Ciliogenesis: building the cell's antenna. Nature reviews Molecular cell biology, 2011. 12(4): p. 222-234.
11. Smith, C.E., A.V. Lake, and C.A. Johnson, Primary cilia, ciliogenesis and the actin cytoskeleton: a little less resorption, a little more actin please. Frontiers in Cell and Developmental Biology, 2020. 8: p. 622822.
12. Gonçalves, J. and L. Pelletier, The ciliary transition zone: finding the pieces and assembling the gate. Molecules and cells, 2017. 40(4): p. 243.
13. Conduit, S.E. and B. Vanhaesebroeck, Phosphoinositide lipids in primary cilia biology. Biochemical Journal, 2020. 477(18): p. 3541-3565.
14. DeMars, K.M., et al., Neuronal primary cilia integrate peripheral signals with metabolic drives. Frontiers in Physiology, 2023. 14: p. 518.
15. Kaiser, F., M. Huebecker, and D. Wachten, Sphingolipids controlling ciliary and microvillar function. FEBS letters, 2020. 594(22): p. 3652-3667.
16. Nachury, M.V. and D.U. Mick, Establishing and regulating the composition of cilia for signal transduction. Nature reviews Molecular cell biology, 2019. 20(7): p. 389-405.
17. Rosenbaum, J.L. and G.B. Witman, Intraflagellar transport. Nature reviews Molecular cell biology, 2002. 3(11): p. 813-825.
18. Lechtreck, K.F., IFT–cargo interactions and protein transport in cilia. Trends in biochemical sciences, 2015. 40(12): p. 765-778.
19. Mukhopadhyay, S., et al., TULP3 bridges the IFT-A complex and membrane phosphoinositides to promote trafficking of G protein-coupled receptors into primary cilia. Genes & development, 2010. 24(19): p. 2180-2193.

20. Nachury, M.V., E.S. Seeley, and H. Jin, Trafficking to the ciliary membrane: how to get across the periciliary diffusion barrier? Annual review of cell and developmental biology, 2010. 26: p. 59-87.
21. Marshall, W.F. and J.L. Rosenbaum, Intraflagellar transport balances continuous turnover of outer doublet microtubules: implications for flagellar length control. The Journal of cell biology, 2001. 155(3): p. 405-414.
22. Balla, T., Phosphoinositides: tiny lipids with giant impact on cell regulation. Physiological reviews, 2013. 93(3): p. 1019-1137.
23. Garcia-Gonzalo, F.R., et al., Phosphoinositides regulate ciliary protein trafficking to modulate hedgehog signaling. Developmental cell, 2015. 34(4): p. 400-409.
24. Prosseda, P.P., et al., Loss of OCRL increases ciliary PI (4, 5) P2 in Lowe oculocerebrorenal syndrome. Journal of cell science, 2017. 130(20): p. 3447-3454.
25. Abdul-Majeed, S. and S.M. Nauli, Dopamine receptor type 5 in the primary cilia has dual chemo-and mechano-sensory roles. Hypertension, 2011. 58(2): p. 325-331.
26. Miyoshi, K., et al., Lack of dopaminergic inputs elongates the primary cilia of striatal neurons. PloS one, 2014. 9(5): p. e97918.
27. Alhassen, W., et al., Regulation of Brain Primary Cilia Length by MCH Signaling: Evidence from Pharmacological, Genetic, Optogenetic, and Chemogenic Manipulations. Molecular Neurobiology, 2021: p. 1-21.
28. Brodsky, M., et al., 5-HT6 receptor blockade regulates primary cilia morphology in striatal neurons. Brain research, 2017. 1660: p. 10-19.
29. Bisgrove, B.W. and H.J. Yost, The roles of cilia in developmental disorders and disease. 2006.

30. Garcia-Gonzalo, F.R. and J.F. Reiter, Open sesame: how transition fibers and the transition zone control ciliary composition. Cold Spring Harbor perspectives in biology, 2017. 9(2): p. a028134.

31. Jenks, A.D., et al., Primary cilia mediate diverse kinase inhibitor resistance mechanisms in cancer. Cell reports, 2018. 23(10): p. 3042-3055.

32. Ma, R., et al., Primary cilia and ciliary signaling pathways in aging and age-related brain disorders. Neurobiology of disease, 2022. 163: p. 105607.

33. Rimkus, T.K., et al., Targeting the sonic hedgehog signaling pathway: review of smoothened and GLI inhibitors. Cancers, 2016. 8(2): p. 22.

34. Wheway, G., L. Nazlamova, and J.T. Hancock, Signaling through the primary cilium. Frontiers in cell and developmental biology, 2018. 6: p. 8.

35. Ávalos, Y., et al., Palmitic acid control of ciliogenesis modulates insulin signaling in hypothalamic neurons through an autophagy-dependent mechanism. Cell Death & Disease, 2022. 13(7): p. 659.

36. Berbari, N.F., et al., Identification of ciliary localization sequences within the third intracellular loop of G protein-coupled receptors. Molecular biology of the cell, 2008. 19(4): p. 1540-1547.

37. Corbit, K.C., et al., Vertebrate Smoothened functions at the primary cilium. Nature, 2005. 437(7061): p. 1018-1021.

38. Diniz, G.B., et al., Ciliary melanin-concentrating hormone receptor 1 (MCHR1) is widely distributed in the murine CNS in a sex-independent manner. Journal of neuroscience research, 2020. 98(10): p. 2045-2071.

39. Domire, J.S., et al., Dopamine receptor 1 localizes to neuronal cilia in a dynamic process that requires the Bardet-Biedl syndrome proteins. Cellular and Molecular Life Sciences, 2011. 68: p. 2951-2960.
40. Händel, M., et al., Selective targeting of somatostatin receptor 3 to neuronal cilia. Neuroscience, 1999. 89(3): p. 909-926.
41. DeCaen, P.G., et al., Direct recording and molecular identification of the calcium channel of primary cilia (vol 504, pg 315, 2013). NATURE, 2014. 513(7517).
42. Delling, M., et al., Primary cilia are specialized calcium signalling organelles. Nature, 2013. 504(7479): p. 311-314.
43. Saternos, H., S. Ley, and W. AbouAlaiwi, Primary cilia and calcium signaling interactions. International Journal of Molecular Sciences, 2020. 21(19): p. 7109.
44. Halls, M.L. and D.M. Cooper, Regulation by Ca2+-signaling pathways of adenylyl cyclases. Cold Spring Harbor perspectives in biology, 2011. 3(1): p. a004143.
45. Jiang, J.Y., et al., Direct visualization of cAMP signaling in primary cilia reveals up-regulation of ciliary GPCR activity following Hedgehog activation. Proceedings of the National Academy of Sciences, 2019. 116(24): p. 12066-12071.
46. Moore, B.S., et al., Cilia have high cAMP levels that are inhibited by Sonic Hedgehog-regulated calcium dynamics. Proceedings of the National Academy of Sciences, 2016. 113(46): p. 13069-13074.
47. Moore, E.R., et al., Adenylyl cyclases and TRPV4 mediate Ca2+/cAMP dynamics to enhance fluid flow-induced osteogenesis in osteocytes. Journal of molecular biochemistry, 2018. 7: p. 48.

48. Sadana, R. and C.W. Dessauer, Physiological roles for G protein-regulated adenylyl cyclase isoforms: insights from knockout and overexpression studies. Neurosignals, 2009. 17(1): p. 5-22.
49. Sherpa, R.T., et al., Sensory primary cilium is a responsive cAMP microdomain in renal epithelia. Scientific Reports, 2019. 9(1): p. 6523.
50. Green, J.A. and K. Mykytyn, Neuronal ciliary signaling in homeostasis and disease. Cellular and Molecular Life Sciences, 2010. 67: p. 3287-3297.
51. Liu, X., et al., Polycystin-2 is an essential ion channel subunit in the primary cilium of the renal collecting duct epithelium. elife, 2018. 7: p. e33183.
52. Lüscher, C. and P.A. Slesinger, Emerging roles for G protein-gated inwardly rectifying potassium (GIRK) channels in health and disease. Nature Reviews Neuroscience, 2010. 11(5): p. 301-315.
53. Napoli, G., et al., Potassium Channel KCNH1 activating variants cause altered functional and morphological ciliogenesis. Molecular Neurobiology, 2022. 59(8): p. 4825-4838.
54. Sánchez, A., D. Urrego, and L.A. Pardo, Cyclic expression of the voltage-gated potassium channel KV10. 1 promotes disassembly of the primary cilium. EMBO reports, 2016. 17(5): p. 708-723.
55. Alhassen, W., et al., Patterns of cilia gene dysregulations in major psychiatric disorders. Progress in Neuro-Psychopharmacology and Biological Psychiatry, 2021. 109: p. 110255.
56. Muñoz-Estrada, J., et al., Primary cilia formation is diminished in schizophrenia and bipolar disorder: a possible marker for these psychiatric diseases. Schizophrenia research, 2018. 195: p. 412-420.

57. Seo, S., et al., Requirement of Bardet-Biedl syndrome proteins for leptin receptor signaling. Human molecular genetics, 2009. 18(7): p. 1323-1331.
58. Davenport, J.R., et al., Disruption of intraflagellar transport in adult mice leads to obesity and slow-onset cystic kidney disease. Current Biology, 2007. 17(18): p. 1586-1594.
59. Lee, C.H., et al., Primary cilia mediate early life programming of adiposity through lysosomal regulation in the developing mouse hypothalamus. Nature Communications, 2020. 11(1): p. 5772.
60. Yang, D.J., J. Hong, and K.W. Kim, Hypothalamic primary cilium: A hub for metabolic homeostasis. Experimental & Molecular Medicine, 2021. 53(7): p. 1109-1115.
61. Yang, D., et al., Ciliary Type III Adenylyl Cyclase in the VMH Is Crucial for High-Fat Diet-Induced Obesity Mediated by Autophagy. Advanced Science, 2022. 9(3): p. 2102568.
62. Bernard, A., et al., MRAP2 regulates energy homeostasis by promoting primary cilia localization of MC4R. JCI insight, 2023. 8(2).
63. Wang, Y., et al., Melanocortin 4 receptor signals at the neuronal primary cilium to control food intake and body weight. The Journal of Clinical Investigation, 2021. 131(9).
64. Stubbs, T., et al., Disruption of dopamine receptor 1 localization to primary cilia impairs signaling in striatal neurons. Journal of Neuroscience, 2022. 42(35): p. 6692-6705.
65. Berbari, N.F., et al., Hippocampal and cortical primary cilia are required for aversive memory in mice. PLoS One, 2014. 9(9): p. e106576.
66. Lagos, P., et al., Effects on sleep of melanin-concentrating hormone (MCH) microinjections into the dorsal raphe nucleus. Brain research, 2009. 1265: p. 103-110.

67. Pascovich, C., et al., Microinjection of melanin-concentrating hormone (MCH) into the median raphe nucleus promotes REM sleep in rats. Sleep Science, 2021. 14(3): p. 229.

68. Chen, X., et al., Ablation of type III adenylyl cyclase in mice causes reduced neuronal activity, altered sleep pattern, and depression-like phenotypes. Biological psychiatry, 2016. 80(11): p. 836-848.

69. Strobel, M.R., et al., Temporal ablation of the ciliary protein IFT88 alters normal brainwave patterns. Scientific Reports, 2025. 15(1): p. 347.

70. Chen, K.J., Investigating primary cilia–dependent signaling in the striatum to define circuit connectivity, synaptic function, and molecular alterations. 2025, UC Irvine.

71. Ramos, C., et al., Neuron-specific cilia loss differentially alters locomotor responses to amphetamine in mice. Journal of neuroscience research, 2021. 99(3): p. 827-842.

72. Baldi, P., et al., Large-scale analysis reveals spatiotemporal circadian patterns of cilia transcriptomes in the primate brain. Journal of neuroscience research, 2021. 99(10): p. 2610-2624.

73. Chen, K., et al., Circadian cilia transcriptome in mouse brain across physiological and pathological states. Molecular Brain, 2024. 17(1): p. 67.

74. Monfared, R.V., et al., Cilia in the brain display region-dependent oscillations of length and orientation. PLoS Biology, 2025. 23(7): p. e3003197.

75. Avasthi, P., et al., A chemical screen identifies class a g-protein coupled receptors as regulators of cilia. ACS chemical biology, 2012. 7(5): p. 911-919.

76. Alhassen, W., et al., Cilia in the striatum mediate timing-dependent functions. Molecular Neurobiology, 2023. 60(2): p. 545-565.

77. Dölen, G., et al., Social reward requires coordinated activity of nucleus accumbens oxytocin and serotonin. Nature, 2013. 501(7466): p. 179-184.
78. Floresco, S.B., The nucleus accumbens: an interface between cognition, emotion, and action. Annual review of psychology, 2015. 66(1): p. 25-52.
79. Murugan, M., et al., Combined social and spatial coding in a descending projection from the prefrontal cortex. Cell, 2017. 171(7): p. 1663-1677. e16.
80. Trezza, V., et al., Nucleus accumbens μ-opioid receptors mediate social reward. Journal of Neuroscience, 2011. 31(17): p. 6362-6370.
81. Zachry, J.E., et al., D1 and D2 medium spiny neurons in the nucleus accumbens core have distinct and valence-independent roles in learning. Neuron, 2024. 112(5): p. 835-849. e7.
82. Zahm, D.S., Functional-anatomical implications of the nucleus accumbens core and shell subterritories. Annals of the New York Academy of Sciences, 1999. 877(1): p. 113-128.
83. Qiu, M.-H., et al., The role of nucleus accumbens core/shell in sleep-wake regulation and their involvement in modafinil-induced arousal. 2012.
84. Oishi, Y., et al., Slow-wave sleep is controlled by a subset of nucleus accumbens core neurons in mice. Nature communications, 2017. 8(1): p. 734.
85. Luo, Y.-J., et al., Nucleus accumbens controls wakefulness by a subpopulation of neurons expressing dopamine D1 receptors. Nature communications, 2018. 9(1): p. 1576.
86. Matikainen-Ankney, B.A., et al., Nucleus Accumbens D1 Receptor–Expressing Spiny Projection Neurons Control Food Motivation and Obesity. Biological psychiatry, 2023. 93(6): p. 512-523.

87. Sharma, R., et al., Dopamine D2 receptors in the accumbal core region mediates the effects of fentanyl on sleep-wakefulness. Neuroscience, 2024. 560: p. 11-19.
88. Chee, M.J., et al., Conditional deletion of melanin-concentrating hormone receptor 1 from GABAergic neurons increases locomotor activity. Molecular metabolism, 2019. 29: p. 114-123.
89. Sprow, G.M., J.A. Rinker, and T.E. Thiele, Histone Acetylation in the Nucleus Accumbens Shell Modulates Ethanol-Induced Locomotor Activity in DBA/2 J Mice. Alcoholism: Clinical and Experimental Research, 2014. 38(9): p. 2377-2386.
90. Imbesi, M., et al., Dopamine receptor-mediated regulation of neuronal “clock” gene expression. Neuroscience, 2009. 158(2): p. 537-544.
91. Roybal, K., et al., Mania-like behavior induced by disruption of CLOCK. Proceedings of the National Academy of Sciences, 2007. 104(15): p. 6406-6411.
92. Voytek, B., et al., Age-related changes in 1/f neural electrophysiological noise. Journal of neuroscience, 2015. 35(38): p. 13257-13265.
93. Fries, P., Rhythms for cognition: communication through coherence. Neuron, 2015. 88(1): p. 220-235.
94. Lisman, J.E. and O. Jensen, The theta-gamma neural code. Neuron, 2013. 77(6): p. 1002-1016.
95. Nishitani, N., et al., Medial nucleus accumbens dopamine receptors modulate motivation for wheel running in male mice. Neuropsychopharmacology, 2025: p. 1-11.
96. Francis, T.C., et al., Nucleus accumbens medium spiny neuron subtypes mediate depression-related outcomes to social defeat stress. Biological psychiatry, 2015. 77(3): p. 212-222.

Chapter 2 Reference:

1. Nachury MV, Mick DU. Establishing and regulating the composition of cilia for signal transduction. Nat Rev Mol Cell Biol. 2019;20(7):389–405. https://doi.org/10.1038/s41580-019-0116-4 PMID: 30948801

2. Liu Z, Tu H, Kang Y, Xue Y, Ma D, Zhao C, et al. Primary cilia regulate hematopoietic stem and progenitor cell specification through Notch signaling in zebrafish. Nat Commun. 2019;10(1):1839. https://doi.org/10.1038/s41467-019-09403-7 PMID: 31015398

3. Guo J, Otis JM, Higginbotham H, Monckton C, Cheng J, Asokan A, et al. Primary cilia signaling shapes the development of interneuronal connectivity. Dev Cell. 2017;42(3):286-300.e4. https://doi.org/10.1016/j.devcel.2017.07.010 PMID: 28787594

4. Nechipurenko IV, Doroquez DB, Sengupta P. Primary cilia and dendritic spines: different but similar signaling compartments. Mol Cells. 2013;36(4):288–303. https://doi.org/10.1007/s10059-013-0246-z PMID: 24048681

5. Berbari NF, O'Connor AK, Haycraft CJ, Yoder BK. The primary cilium as a complex signaling center. Curr Biol. 2009;19(13):R526-35. https://doi. org/10.1016/j.cub.2009.05.025 PMID: 19602418

6. Wheatley DN. Nanobiology of the primary cilium—paradigm of a multifunctional nanomachine complex. Methods Cell Biol. 2008;90:139–56. https:// doi.org/10.1016/S0091-679X(08)00807-8 PMID: 19195549

7. Han Y-G, Spassky N, Romaguera-Ros M, Garcia-Verdugo J-M, Aguilar A, Schneider-Maunoury S, et al. Hedgehog signaling and primary cilia are required for the formation of adult neural stem cells. Nat Neurosci. 2008;11(3):277–84. https://doi.org/10.1038/nn2059 PMID: 18297065

8. Breunig JJ, Sarkisian MR, Arellano JI, Morozov YM, Ayoub AE, Sojitra S, et al. Primary cilia regulate hippocampal neurogenesis by mediating sonic hedgehog signaling. Proc Natl Acad Sci U S A. 2008;105(35):13127–32. https://doi.org/10.1073/pnas.0804558105 PMID: 18728187

9. Oishi I, Kawakami Y, Raya A, Callol-Massot C, Izpisúa Belmonte JC. Regulation of primary cilia formation and left-right patterning in zebrafish by a noncanonical Wnt signaling mediator, duboraya. Nat Genet. 2006;38(11):1316–22. https://doi.org/10.1038/ng1892 PMID: 17013396

10. Kuhara A, Okumura M, Kimata T, Tanizawa Y, Takano R, Kimura KD, et al. Temperature sensing by an olfactory neuron in a circuit controlling behavior of C. elegans. Science. 2008;320(5877):803–7. https://doi.org/10.1126/science.1148922 PMID: 18403676

11. Humphries S. A physical explanation of the temperature dependence of physiological processes mediated by cilia and flagella. Proc Natl Acad Sci U S A. 2013;110(36):14693–8. https://doi.org/10.1073/pnas.1300891110 PMID: 23959901

12. O'Callaghan C, Achaval M, Forsythe I, Barry PW. Brain and respiratory cilia: the effect of temperature. Biol Neonate. 1995;68(6):394–7. https://doi.org/10.1159/000244261 PMID: 8721882

13. Clary-Meinesz CF, Cosson J, Huitorel P, Blaive B. Temperature effect on the ciliary beat frequency of human nasal and tracheal ciliated cells. Biol Cell. 1992;76(3):335–8. https://doi.org/10.1016/0248-4900(92)90436-5 PMID: 1305479

14. Nonaka S, Tanaka Y, Okada Y, Takeda S, Harada A, Kanai Y, et al. Randomization of left-right asymmetry due to loss of nodal cilia generating leftward flow of

extraembryonic fluid in mice lacking KIF3B motor protein. Cell. 1998;95(6):829–37. https://doi.org/10.1016/s0092-8674(00)81705-5 PMID: 9865700

15. Yoshiba S, Shiratori H, Kuo IY, Kawasumi A, Shinohara K, Nonaka S, et al. Cilia at the node of mouse embryos sense fluid flow for left-right determination via Pkd2. Science. 2012;338(6104):226–31. https://doi.org/10.1126/science.1222538 PMID: 22983710

16. Nauli SM, Jin X, AbouAlaiwi WA, El-Jouni W, Su X, Zhou J. Non-motile primary cilia as fluid shear stress mechanosensors. Methods Enzymol. 2013;525:1–20. https://doi.org/10.1016/B978-0-12-397944-5.00001-8 PMID: 23522462

17. McGlashan SR, Knight MM, Chowdhury TT, Joshi P, Jensen CG, Kennedy S, et al. Mechanical loading modulates chondrocyte primary cilia incidence and length. Cell Biol Int. 2010;34(5):441–6. https://doi.org/10.1042/CBI20090094 PMID: 20100169

18. Duffy MP, Sup ME, Guo XE. Adenylyl cyclase 3 regulates osteocyte mechanotransduction and primary cilium. Biochem Biophys Res Commun. 2021;573:145–50. https://doi.org/10.1016/j.bbrc.2021.08.033 PMID: 34411897

19. Ou Y, Ruan Y, Cheng M, Moser JJ, Rattner JB, van der Hoorn FA. Adenylate cyclase regulates elongation of mammalian primary cilia. Exp Cell Res. 2009;315(16):2802–17. https://doi.org/10.1016/j.yexcr.2009.06.028 PMID: 19576885

20. Tuxhorn J, Daise T, Dentler WL. Regulation of flagellar length in Chlamydomonas. Cell Motil Cytoskeleton. 1998;40(2):133–46. https://doi. org/10.1002/(SICI)1097-0169(1998)40:2<133::AID-CM3>3.0.CO;2-G PMID: 9634211

21. Brodsky M, Lesiak AJ, Croicu A, Cohenca N, Sullivan JM, Neumaier JF. 5-HT6 receptor blockade regulates primary cilia morphology in striatal neurons. Brain Res. 2017;1660:10–9. https://doi.org/10.1016/j.brainres.2017.01.010 PMID: 28087224

22. Alhassen W, Kobayashi Y, Su J, Robbins B, Nguyen H, Myint T, et al. Regulation of brain primary cilia length by MCH signaling: evidence from pharmacological, genetic, optogenetic, and chemogenic manipulations. Mol Neurobiol. 2022;59(1):245–65. https://doi.org/10.1007/s12035-021- 02511-w PMID: 34665407

23. Abdul-Majeed S, Nauli SM. Dopamine receptor type 5 in the primary cilia has dual chemo- and mechano-sensory roles. Hypertension. 2011;58(2):325–31. https://doi.org/10.1161/HYPERTENSIONAHA.111.172080 PMID: 21709211

24. Upadhyay VS, Muntean BS, Kathem SH, Hwang JJ, Aboualaiwi WA, Nauli SM. Roles of dopamine receptor on chemosensory and mechanosensory primary cilia in renal epithelial cells. Front Physiol. 2014;5:72. https://doi.org/10.3389/fphys.2014.00072 PMID: 24616705

25. Christensen ST, Pedersen SF, Satir P, Veland IR, Schneider L. The primary cilium coordinates signaling pathways in cell cycle control and migration during development and tissue repair. Curr Top Dev Biol. 2008;85:261–301. https://doi.org/10.1016/S0070-2153(08)00810-7 PMID: 19147009

26. Jones TJ, Adapala RK, Geldenhuys WJ, Bursley C, AbouAlaiwi WA, Nauli SM, et al. Primary cilia regulates the directional migration and barrier integrity of endothelial cells through the modulation of hsp27 dependent actin cytoskeletal organization. J Cell Physiol. 2012;227(1):70–6. https:// doi.org/10.1002/jcp.22704 PMID: 21837772

27. Schneider L, Cammer M, Lehman J, Nielsen SK, Guerra CF, Veland IR, et al. Directional cell migration and chemotaxis in wound healing response to PDGF-AA are

coordinated by the primary cilium in fibroblasts. Cell Physiol Biochem. 2010;25(2–3):279–92. https://doi.org/10.1159/000276562 PMID: 20110689

28. Dewan K, Benloucif S, Reid K, Wolfe LF, Zee PC. Light-induced changes of the circadian clock of humans: increasing duration is more effective than increasing light intensity. Sleep. 2011;34(5):593–9. https://doi.org/10.1093/sleep/34.5.593 PMID: 21532952

29. Wright KP Jr, McHill AW, Birks BR, Griffin BR, Rusterholz T, Chinoy ED. Entrainment of the human circadian clock to the natural light-dark cycle. Curr Biol. 2013;23(16):1554–8. https://doi.org/10.1016/j.cub.2013.06.039 PMID: 23910656

30. Damiola F, Le Minh N, Preitner N, Kornmann B, Fleury-Olela F, Schibler U. Restricted feeding uncouples circadian oscillators in peripheral tissues from the central pacemaker in the suprachiasmatic nucleus. Genes Dev. 2000;14(23):2950–61. https://doi.org/10.1101/gad.183500 PMID: 11114885

31. Buhr ED, Yoo S-H, Takahashi JS. Temperature as a universal resetting cue for mammalian circadian oscillators. Science. 2010;330(6002):379–85. https://doi.org/10.1126/science.1195262 PMID: 20947768

32. Casey T, Patel OV, Plaut K. Transcriptomes reveal alterations in gravity impact circadian clocks and activate mechanotransduction pathways with adaptation through epigenetic change. Physiol Genomics. 2015;47(4):113–28. https://doi.org/10.1152/physiolgenomics.00117.2014 PMID: 25649141

33. Robinson EL, Fuller CA. Gravity and thermoregulation: metabolic changes and circadian rhythms. Pflugers Arch. 2000;441(2-3 Suppl):R32-8. https://doi.org/10.1007/s004240000329 PMID: 11200977

34. Fuller CA. The effects of gravity on the circadian timing system. J Gravit Physiol. 1994;1(1):P1-4. PMID: 11538728

35. Gu W, Geddes BJ, Zhang C, Foley KP, Stricker-Krongrad A. The prolactin-releasing peptide receptor (GPR10) regulates body weight homeostasis in mice. J Mol Neurosci. 2004;22(1–2):93–103. https://doi.org/10.1385/JMN:22:1-2:93 PMID: 14742914

36. Nagata A, Hamamoto A, Horikawa M, Yoshimura K, Takeda S, Saito Y. Characterization of ciliary targeting sequence of rat melanin-concentrating hormone receptor 1. Gen Comp Endocrinol. 2013;188:159–65. https://doi.org/10.1016/j.ygcen.2013.02.020 PMID: 23467069

37. Omori Y, Chaya T, Yoshida S, Irie S, Tsujii T, Furukawa T. Identification of G Protein-Coupled Receptors (GPCRs) in primary cilia and their possible involvement in body weight control. PLoS One. 2015;10(6):e0128422. https://doi.org/10.1371/journal.pone.0128422 PMID: 26053317

38. Hughes JW, Cho JH, Conway HE, DiGruccio MR, Ng XW, Roseman HF, et al. Primary cilia control glucose homeostasis via islet paracrine interactions. Proc Natl Acad Sci U S A. 2020;117(16):8912–23. https://doi.org/10.1073/pnas.2001936117 PMID: 32253320

39. Lee H, Song J, Jung JH, Ko HW. Primary cilia in energy balance signaling and metabolic disorder. BMB Rep. 2015;48(12):647–54. https://doi. org/10.5483/bmbrep.2015.48.12.229 PMID: 26538252

40. Berbari NF, Pasek RC, Malarkey EB, Yazdi SMZ, McNair AD, Lewis WR, et al. Leptin resistance is a secondary consequence of the obesity in ciliopathy mutant mice. Proc Natl Acad Sci U S A. 2013;110(19):7796–801. https://doi.org/10.1073/pnas.1210192110 PMID: 23599282

41. Koemeter-Cox AI, Sherwood TW, Green JA, Steiner RA, Berbari NF, Yoder BK, et al. Primary cilia enhance kisspeptin receptor signaling on gonadotropin-- releasing hormone neurons. Proc Natl Acad Sci U S A. 2014;111(28):10335–40. https://doi.org/10.1073/pnas.1403286111 PMID: 24982149

42. Diniz GB, Battagello DS, Klein MO, Bono BSM, Ferreira JGP, Motta-Teixeira LC, et al. Ciliary melanin-concentrating hormone receptor 1 (MCHR1) is widely distributed in the murine CNS in a sex-independent manner. J Neurosci Res. 2020;98(10):2045–71. https://doi.org/10.1002/jnr.24651 PMID: 32530066

43. Brailov I, Bancila M, Brisorgueil MJ, Miquel MC, Hamon M, Vergé D. Localization of 5-HT(6) receptors at the plasma membrane of neuronal cilia in the rat brain. Brain Res. 2000;872(1–2):271–5. https://doi.org/10.1016/s0006-8993(00)02519-1 PMID: 10924708

44. Berbari NF, Lewis JS, Bishop GA, Askwith CC, Mykytyn K. Bardet-Biedl syndrome proteins are required for the localization of G protein-coupled receptors to primary cilia. Proc Natl Acad Sci U S A. 2008;105(11):4242–6. https://doi.org/10.1073/pnas.0711027105 PMID: 18334641

45. Domire JS, Green JA, Lee KG, Johnson AD, Askwith CC, Mykytyn K. Dopamine receptor 1 localizes to neuronal cilia in a dynamic process that requires the Bardet-Biedl syndrome proteins. Cell Mol Life Sci. 2011;68(17):2951–60. https://doi.org/10.1007/s00018-010-0603-4 PMID: 21152952

46. Händel M, Schulz S, Stanarius A, Schreff M, Erdtmann-Vourliotis M, Schmidt H, et al. Selective targeting of somatostatin receptor 3 to neuronal cilia. Neuroscience. 1999;89(3):909–26. https://doi.org/10.1016/s0306-4522(98)00354-6 PMID: 10199624

47. Varela L, Horvath TL. Neuronal cilia: another player in the melanocortin system. Trends Mol Med. 2018;24(4):333–4. https://doi.org/10.1016/j. molmed.2018.02.004 PMID: 29501261

48. Chen S, Alhassen W, Vakil Monfared R, Vachirakorntong B, Nauli SM, Baldi P, et al. Dynamic changes of brain cilia transcriptomes across the human lifespan. Int J Mol Sci. 2021;22(19):10387. https://doi.org/10.3390/ijms221910387 PMID: 34638726

49. Baldi P, Alhassen W, Chen S, Nguyen H, Khoudari M, Alachkar A. Large-scale analysis reveals spatiotemporal circadian patterns of cilia transcriptomes in the primate brain. J Neurosci Res. 2021;99(10):2610–24. https://doi.org/10.1002/jnr.24919 PMID: 34310750

50. Alhassen W, Chen S, Vawter M, Robbins BK, Nguyen H, Myint TN, et al. Patterns of cilia gene dysregulations in major psychiatric disorders. Prog Neuropsychopharmacol Biol Psychiatry. 2021;109:110255. https://doi.org/10.1016/j.pnpbp.2021.110255 PMID: 33508383

51. Oh SW, Harris JA, Ng L, Winslow B, Cain N, Mihalas S, et al. A mesoscale connectome of the mouse brain. Nature. 2014;508(7495):207–14. https://doi.org/10.1038/nature13186 PMID: 24695228

52. Muller B, Richards AJ, Jin B, Lu X. GOGrapher: a Python library for GO graph representation and analysis. BMC Res Notes. 2009;2:122. https:// doi.org/10.1186/1756-0500-2-122 PMID: 19583843

53. Hagberg AA. Exploring network structure, dynamics, and function using NetworkX. In: Proceedings of the 7th Python in Science Conference, Pasadena, CA, USA, 2008.

54. Sievert C. Interactive web-based data visualization with R, plotly, and shiny. 2020.

55. Agostinelli F, Ceglia N, Shahbaba B, Sassone-Corsi P, Baldi P. What time is it? Deep learning approaches for circadian rhythms. Bioinformatics. 2016;32(19):3051. https://doi.org/10.1093/bioinformatics/btw504 PMID: 27542773

56. Agostinelli F, Ceglia N, Shahbaba B, Sassone-Corsi P, Baldi P. What time is it? Deep learning approaches for circadian rhythms. Bioinformatics. 2016;32(12):i8–17. https://doi.org/10.1093/bioinformatics/btw243 PMID: 27307647

57. Sipos É, Komoly S, Ács P. Quantitative comparison of primary cilia marker expression and length in the mouse brain. J Mol Neurosci. 2018;64(3):397–409. https://doi.org/10.1007/s12031-018-1036-z PMID: 29464516

58. Joiner AM, Green WW, McIntyre JC, Allen BL, Schwob JE, Martens JR. Primary cilia on horizontal basal cells regulate regeneration of the olfactory epithelium. J Neurosci. 2015;35(40):13761–72. https://doi.org/10.1523/JNEUROSCI.1708-15.2015 PMID: 26446227

59. Pifferi S, Menini A, Kurahashi T. Signal transduction in vertebrate olfactory cilia. In: Menini A, Editor. The neurobiology of olfaction. Boca Raton (FL): Frontiers in Neuroscience. 2010.

60. Challis RC, Tian H, Wang J, He J, Jiang J, Chen X, et al. An olfactory cilia pattern in the mammalian nose ensures high sensitivity to odors. Curr Biol. 2015;25(19):2503–12. https://doi.org/10.1016/j.cub.2015.07.065 PMID: 26365258

61. Qiu L, LeBel RP, Storm DR, Chen X. Type 3 adenylyl cyclase: a key enzyme mediating the cAMP signaling in neuronal cilia. Int J Physiol Pathophysiol Pharmacol. 2016;8(3):95–108. PMID: 27785336

62. Berendse HW, Groenewegen HJ. Organization of the thalamostriatal projections in the rat, with special emphasis on the ventral striatum. J Comp Neurol. 1990;299(2):187–228. https://doi.org/10.1002/cne.902990206 PMID: 2172326

63. Zahm DS, Brog JS. On the significance of subterritories in the “accumbens” part of the rat ventral striatum. Neuroscience. 1992;50(4):751–67. https://doi.org/10.1016/0306-4522(92)90202-d PMID: 1448200

64. Siciliano CA, Calipari ES, Jones SR. Amphetamine potency varies with dopamine uptake rate across striatal subregions. J Neurochem. 2014;131(3):348–55. https://doi.org/10.1111/jnc.12808 PMID: 24988947

65. Shin R, Qin M, Liu Z-H, Ikemoto S. Intracranial self-administration of MDMA into the ventral striatum of the rat: differential roles of the nucleus accumbens shell, core, and olfactory tubercle. Psychopharmacology (Berl). 2008;198(2):261–70. https://doi.org/10.1007/s00213-008-1131-x PMID: 18389222

66. Sheu S-H, Upadhyayula S, Dupuy V, Pang S, Deng F, Wan J, et al. A serotonergic axon-cilium synapse drives nuclear signaling to alter chromatin accessibility. Cell. 2022;185(18):3390-3407.e18. https://doi.org/10.1016/j.cell.2022.07.026 PMID: 36055200

67. Kirschen GW, Liu H, Lang T, Liang X, Ge S, Xiong Q. The radial organization of neuronal primary cilia is acutely disrupted by seizure and ischemic brain injury. Front Biol (Beijing). 2017;12(2):124–38. https://doi.org/10.1007/s11515-017-1447-1 PMID: 28473847

68. Sherpa RT, Mohieldin AM, Pala R, Wachten D, Ostrom RS, Nauli SM. Sensory primary cilium is a responsive cAMP microdomain in renal epithelia. Sci Rep. 2019;9(1):6523. https://doi.org/10.1038/s41598-019-43002-2 PMID: 31024067

69. Sherpa RT, Atkinson KF, Ferreira VP, Nauli SM. Rapamycin increases length and mechanosensory function of primary cilia in renal epithelial and vascular endothelial cells. Int Educ Res J. 2016;2(12):91–7. PMID: 28529994

70. Abdul-Majeed S, Moloney BC, Nauli SM. Mechanisms regulating cilia growth and cilia function in endothelial cells. Cell Mol Life Sci. 2012;69(1):165–73. https://doi.org/10.1007/s00018-011-0744-0 PMID: 21671118

71. Ramos C, Roberts JB, Jasso KR, Ten Eyck TW, Everett T, Pozo P, et al. Neuron-specific cilia loss differentially alters locomotor responses to amphetamine in mice. J Neurosci Res. 2021;99(3):827–42. https://doi.org/10.1002/jnr.24755 PMID: 33175436

72. Chen K, Ashtiani KC, Monfared RV, Baldi P, Alachkar A. Circadian cilia transcriptome in mouse brain across physiological and pathological states. Mol Brain. 2024;17(1):67. https://doi.org/10.1186/s13041-024-01143-0 PMID: 39304885

73. Abe M, Herzog ED, Yamazaki S, Straume M, Tei H, Sakaki Y, et al. Circadian rhythms in isolated brain regions. J Neurosci. 2002;22(1):350–6. https://doi.org/10.1523/JNEUROSCI.22-01-00350.2002 PMID: 11756518

74. Myers MG Jr, Olson DP. Central nervous system control of metabolism. Nature. 2012;491(7424):357–63. https://doi.org/10.1038/nature11705 PMID: 23151578

75. Chou TC, Bjorkum AA, Gaus SE, Lu J, Scammell TE, Saper CB. Afferents to the ventrolateral preoptic nucleus. J Neurosci. 2002;22(3):977–90. https://doi.org/10.1523/JNEUROSCI.22-03-00977.2002 PMID: 11826126

76. Santoso P, Nakata M, Ueta Y, Yada T. Suprachiasmatic vasopressin to paraventricular oxytocin neurocircuit in the hypothalamus relays light reception to inhibit feeding behavior. Am J Physiol Endocrinol Metab. 2018;315(4):E478–88. https://doi.org/10.1152/ajpendo.00338.2016 PMID: 28174180

77. Acosta-Galvan G, Yi C-X, van der Vliet J, Jhamandas JH, Panula P, Angeles-Castellanos M, et al. Interaction between hypothalamic dorsomedial nucleus and the suprachiasmatic nucleus determines intensity of food anticipatory behavior. Proc Natl Acad Sci U S A. 2011;108(14):5813–8. https://doi.org/10.1073/pnas.1015551108 PMID: 21402951

78. Sun JS, Yang DJ, Kinyua AW, Yoon SG, Seong JK, Kim J, et al. Ventromedial hypothalamic primary cilia control energy and skeletal homeostasis. J Clin Invest. 2021;131(1):e138107. https://doi.org/10.1172/JCI138107 PMID: 33021968

79. Han YM, Kang GM, Byun K, Ko HW, Kim J, Shin M-S, et al. Leptin-promoted cilia assembly is critical for normal energy balance. J Clin Invest. 2014;124(5):2193–7. https://doi.org/10.1172/JCI69395 PMID: 24667636

80. Kang GM, Han YM, Ko HW, Kim J, Oh BC, Kwon I, et al. Leptin elongates hypothalamic neuronal cilia via transcriptional regulation and actin destabilization. J Biol Chem. 2015;290(29):18146–55. https://doi.org/10.1074/jbc.M115.639468 PMID: 26041775

81. Loktev AV, Jackson PK. Neuropeptide Y family receptors traffic via the Bardet-Biedl syndrome pathway to signal in neuronal primary cilia. Cell Rep. 2013;5(5):1316–29. https://doi.org/10.1016/j.celrep.2013.11.011 PMID: 24316073

82. Faubel R, Westendorf C, Bodenschatz E, Eichele G. Cilia-based flow network in the brain ventricles. Science. 2016;353(6295):176–8. https://doi.org/10.1126/science.aae0450 PMID: 27387952

83. Hablitz LM, Plá V, Giannetto M, Vinitsky HS, Stæger FF, Metcalfe T, et al. Circadian control of brain glymphatic and lymphatic fluid flow. Nat Commun. 2020;11(1):4411. https://doi.org/10.1038/s41467-020-18115-2 PMID: 32879313

84. Jasinska M, Woznicka O, Jasek-Gajda E, Lis GJ, Pyza E, Litwin JA. Circadian changes of dendritic spine geometry in mouse barrel cortex. Front Neurosci. 2020;14:578881. https://doi.org/10.3389/fnins.2020.578881 PMID: 33117123

85. Jasinska M, Jasek-Gajda E, Woznicka O, Lis GJ, Pyza E, Litwin JA. Circadian clock regulates the shape and content of dendritic spines in mouse barrel cortex. PLoS One. 2019;14(11):e0225394. https://doi.org/10.1371/journal.pone.0225394 PMID: 31730670

86. Jasinska M, Grzegorczyk A, Woznicka O, Jasek E, Kossut M, Barbacka-Surowiak G, et al. Circadian rhythmicity of synapses in mouse somatosensory cortex. Eur J Neurosci. 2015;42(8):2585–94. https://doi.org/10.1111/ejn.13045 PMID: 26274013

87. Jasinska M, Grzegorczyk A, Jasek E, Litwin JA, Kossut M, Barbacka-Surowiak G, et al. Daily rhythm of synapse turnover in mouse somatosensory cortex. Acta Neurobiol Exp (Wars). 2014;74(1):104–10. https://doi.org/10.55782/ane-2014-1977 PMID: 24718049

88. Tu H-Q, Li S, Xu Y-L, Zhang Y-C, Li P-Y, Liang L-Y, et al. Rhythmic cilia changes support SCN neuron coherence in circadian clock. Science. 2023;380(6648):972–9. https://doi.org/10.1126/science.abm1962 PMID: 37262147

89. Brewer KK, Brewer KM, Terry TT, Caspary T, Vaisse C, Berbari NF. Postnatal dynamic ciliary ARL13B and ADCY3 localization in the mouse brain. Cells. 2024;13(3):259. https://doi.org/10.3390/cells13030259 PMID: 38334651

Chapter 3 Reference:

1. Guemez-Gamboa, A., N.G. Coufal, and J.G. Gleeson, Primary cilia in the developing and mature brain. Neuron, 2014. 82(3): p. 511-521.

2. Lee, J.H. and J.G. Gleeson, The role of primary cilia in neuronal function. Neurobiology of disease, 2010. 38(2): p. 167-172.

3. Sterpka, A. and X. Chen, Neuronal and astrocytic primary cilia in the mature brain. Pharmacological research, 2018. 137: p. 114-121.

4. Berbari, N.F., et al., Identification of ciliary localization sequences within the third intracellular loop of G protein-coupled receptors. Molecular biology of the cell, 2008. 19(4): p. 1540-1547.

5. Domire, J.S., et al., Dopamine receptor 1 localizes to neuronal cilia in a dynamic process that requires the Bardet-Biedl syndrome proteins. Cellular and Molecular Life Sciences, 2011. 68: p. 2951-2960.

6. Avasthi, P., et al., A chemical screen identifies class a g-protein coupled receptors as regulators of cilia. ACS chemical biology, 2012. 7(5): p. 911-919.

7. Miyoshi, K., et al., Lack of dopaminergic inputs elongates the primary cilia of striatal neurons. PloS one, 2014. 9(5): p. e97918.

8. Alhassen, W., et al., Regulation of Brain Primary Cilia Length by MCH Signaling: Evidence from Pharmacological, Genetic, Optogenetic, and Chemogenic Manipulations. Molecular Neurobiology, 2021: p. 1-21.

9. Baldi, P., et al., Large-scale analysis reveals spatiotemporal circadian patterns of cilia transcriptomes in the primate brain. Journal of neuroscience research, 2021. 99(10): p. 2610-2624.

10. Chen, K., et al., Circadian cilia transcriptome in mouse brain across physiological and pathological states. Molecular Brain, 2024. 17(1): p. 67.

11. Monfared, R.V., et al., Cilia in the brain display region-dependent oscillations of length and orientation. PLoS Biology, 2025. 23(7): p. e3003197.

12. Alhassen, W., et al., Cilia in the striatum mediate timing-dependent functions. Molecular Neurobiology, 2023. 60(2): p. 545-565.

13. Strobel, M.R., et al., Temporal ablation of the ciliary protein IFT88 alters normal brainwave patterns. Scientific Reports, 2025. 15(1): p. 347.
14. Chen, K.J., Investigating primary cilia–dependent signaling in the striatum to define circuit connectivity, synaptic function, and molecular alterations. 2025, UC Irvine.
15. Floresco, S.B., The nucleus accumbens: an interface between cognition, emotion, and action. Annual review of psychology, 2015. 66(1): p. 25-52.
16. Qiu, M.-H., et al., The role of nucleus accumbens core/shell in sleep-wake regulation and their involvement in modafinil-induced arousal. 2012.
17. Oishi, Y., et al., Slow-wave sleep is controlled by a subset of nucleus accumbens core neurons in mice. Nature communications, 2017. 8(1): p. 734.
18. Luo, Y.-J., et al., Nucleus accumbens controls wakefulness by a subpopulation of neurons expressing dopamine D1 receptors. Nature communications, 2018. 9(1): p. 1576.
19. Matikainen-Ankney, B.A., et al., Nucleus Accumbens D1 Receptor–Expressing Spiny Projection Neurons Control Food Motivation and Obesity. Biological psychiatry, 2023. 93(6): p. 512-523.
20. Sharma, R., et al., Dopamine D2 receptors in the accumbal core region mediates the effects of fentanyl on sleep-wakefulness. Neuroscience, 2024. 560: p. 11-19.
21. Chee, M.J., et al., Conditional deletion of melanin-concentrating hormone receptor 1 from GABAergic neurons increases locomotor activity. Molecular metabolism, 2019. 29: p. 114-123.
22. Sprow, G.M., J.A. Rinker, and T.E. Thiele, Histone Acetylation in the Nucleus Accumbens Shell Modulates Ethanol-Induced Locomotor Activity in DBA/2 J Mice. Alcoholism: Clinical and Experimental Research, 2014. 38(9): p. 2377-2386.

23. Ramos, C., et al., Neuron-specific cilia loss differentially alters locomotor responses to amphetamine in mice. Journal of neuroscience research, 2021. 99(3): p. 827-842.
24. Everett, T., et al., Cilia loss on distinct neuron populations differentially alters cocaine-induced locomotion and reward. Journal of Psychopharmacology, 2024. 38(2): p. 200-212.
25. Lazarus, M., et al., How do the basal ganglia regulate sleep–wake behavior? Trends in neurosciences, 2012. 35(12): p. 723-732.
26. Guo, J., et al., Primary cilia signaling shapes the development of interneuronal connectivity. Developmental cell, 2017. 42(3): p. 286-300. e4.
27. Davenport, J.R., et al., Disruption of intraflagellar transport in adult mice leads to obesity and slow-onset cystic kidney disease. Current Biology, 2007. 17(18): p. 1586-1594.

Chapter 4 Reference:

1. Dölen G, Darvishzadeh A, Huang KW, Malenka RC. Social reward requires coordinated activity of nucleus accumbens oxytocin and serotonin. Nature. Sep 12 2013;501(7466):179-84. doi:10.1038/nature12518
2. Floresco SB. The nucleus accumbens: an interface between cognition, emotion, and action. Annual review of psychology. Jan 3 2015;66:25-52. doi:10.1146/annurev-psych-010213-115159
3. Okuyama T, Kitamura T, Roy DS, Itohara S, Tonegawa S. Ventral CA1 neurons store social memory. Science. 2016;353(6307):1536-1541. doi:doi:10.1126/science.aaf7003

4. Ko J. Neuroanatomical Substrates of Rodent Social Behavior: The Medial Prefrontal Cortex and Its Projection Patterns. Review. Frontiers in neural circuits. 2017-June-13 2017;Volume 11 - 2017doi:10.3389/fncir.2017.00041

5. Buzsáki G, Draguhn A. Neuronal oscillations in cortical networks. Science. Jun 25 2004;304(5679):1926-9. doi:10.1126/science.1099745

6. Fries P. Rhythms for Cognition: Communication through Coherence. Neuron. Oct 7 2015;88(1):220-35. doi:10.1016/j.neuron.2015.09.034

7. Canolty RT, Knight RT. The functional role of cross-frequency coupling. Trends in cognitive sciences. Nov 2010;14(11):506-15. doi:10.1016/j.tics.2010.09.001

8. Lisman JE, Jensen O. The θ-γ neural code. Neuron. Mar 20 2013;77(6):1002-16. doi:10.1016/j.neuron.2013.03.007

9. Voytek B, Knight RT. Dynamic Network Communication as a Unifying Neural Basis for Cognition, Development, Aging, and Disease. Biological psychiatry. 2015/06/15/ 2015;77(12):1089-1097. doi:https://doi.org/10.1016/j.biopsych.2015.04.016

10. Trezza V, Damsteegt R, Achterberg EJ, Vanderschuren LJ. Nucleus accumbens μ-opioid receptors mediate social reward. The Journal of neuroscience : the official journal of the Society for Neuroscience. Apr 27 2011;31(17):6362-70. doi:10.1523/jneurosci.5492-10.2011

11. Murugan M, Jang HJ, Park M, et al. Combined Social and Spatial Coding in a Descending Projection from the Prefrontal Cortex. Cell. Dec 14 2017;171(7):1663-1677.e16. doi:10.1016/j.cell.2017.11.002

12. Jurisch-Yaksi N, Wachten D, Gopalakrishnan J. The neuronal cilium – a highly diverse and dynamic organelle involved in sensory detection and neuromodulation.

Trends in neurosciences. 2024/05/01/ 2024;47(5):383-394. doi:https://doi.org/10.1016/j.tins.2024.03.004

13. Wu JY, Cho S-J, Descant K, et al. Mapping of neuronal and glial primary cilia contactome and connectome in the human cerebral cortex. Neuron. 2024/01/03/ 2024;112(1):41-55.e3. doi:https://doi.org/10.1016/j.neuron.2023.09.032

14. Siljee JE, Wang Y, Bernard AA, et al. Subcellular localization of MC4R with ADCY3 at neuronal primary cilia underlies a common pathway for genetic predisposition to obesity. Nature genetics. Feb 2018;50(2):180-185. doi:10.1038/s41588-017-0020-9

15. Alhassen W, Alhassen S, Chen J, Monfared RV, Alachkar A. Cilia in the Striatum Mediate Timing-Dependent Functions. Molecular neurobiology. Feb 2023;60(2):545-565. doi:10.1007/s12035-022-03095-9

16. Strobel MR, Zhou Y, Qiu L, Hofer AM, Chen X. Temporal ablation of the ciliary protein IFT88 alters normal brainwave patterns. Scientific reports. 2025/01/02 2025;15(1):347. doi:10.1038/s41598-024-83432-1

17. Rocha C, Prinos P. Post-transcriptional and Post-translational Modifications of Primary Cilia: How to Fine Tune Your Neuronal Antenna. Frontiers in cellular neuroscience. 2022;16:809917. doi:10.3389/fncel.2022.809917

18. Monfared RV, Abdelkarim S, Derdeyn P, et al. Cilia in the brain display region-dependent oscillations of length and orientation. PLoS biology. Jul 2025;23(7):e3003197. doi:10.1371/journal.pbio.3003197

19. Chen S, Alhassen W, Vakil Monfared R, et al. Dynamic Changes of Brain Cilia Transcriptomes across the Human Lifespan. International journal of molecular sciences. Sep 27 2021;22(19)doi:10.3390/ijms221910387

20. Chen K, Ashtiani KC, Monfared RV, Baldi P, Alachkar A. Circadian cilia transcriptome in mouse brain across physiological and pathological states. Molecular brain. Sep 20 2024;17(1):67. doi:10.1186/s13041-024-01143-0

21. Alhassen W, Kobayashi Y, Su J, et al. Regulation of Brain Primary Cilia Length by MCH Signaling: Evidence from Pharmacological, Genetic, Optogenetic, and Chemogenic Manipulations. Molecular neurobiology. Jan 2022;59(1):245-265. doi:10.1007/s12035-021-02511-w

22. Baldi P, Alhassen W, Chen S, Nguyen H, Khoudari M, Alachkar A. Large-scale analysis reveals spatiotemporal circadian patterns of cilia transcriptomes in the primate brain. Journal of neuroscience research. Oct 2021;99(10):2610-2624. doi:10.1002/jnr.24919

23. Wang L, Zhang Y, Wang C, et al. A Natural Product with High Affinity to Sigma and 5-HT(7) Receptors as Novel Therapeutic Drug for Negative and Cognitive Symptoms of Schizophrenia. Neurochemical research. Nov 2019;44(11):2536-2545. doi:10.1007/s11064-019-02873-7

24. Sanathara N, Alhassen L, Marmouzi I, et al. Oxytocin-MCH circuit regulates monosynaptic inputs to MCH neurons and modulates social recognition memory. Neuropharmacology. Feb 15 2021;184:108423. doi:10.1016/j.neuropharm.2020.108423

25. Mogenson GJ, Jones DL, Yim CY. From motivation to action: Functional interface between the limbic system and the motor system. Progress in neurobiology. 1980/01/01/ 1980;14(2):69-97. doi:https://doi.org/10.1016/0301-0082(80)90018-0

26. Schall TA, Wright WJ, Dong Y. Nucleus accumbens fast-spiking interneurons in motivational and addictive behaviors. Molecular psychiatry. Jan 2021;26(1):234-246. doi:10.1038/s41380-020-0683-y

27. Marley A, Choy RW, von Zastrow M. GPR88 reveals a discrete function of primary cilia as selective insulators of GPCR cross-talk. PloS one. 2013;8(8):e70857. doi:10.1371/journal.pone.0070857

28. Domire JS, Green JA, Lee KG, Johnson AD, Askwith CC, Mykytyn K. Dopamine receptor 1 localizes to neuronal cilia in a dynamic process that requires the Bardet-Biedl syndrome proteins. Cellular and molecular life sciences : CMLS. Sep 2011;68(17):2951-60. doi:10.1007/s00018-010-0603-4

29. Jiang JY, Falcone JL, Curci S, Hofer AM. Direct visualization of cAMP signaling in primary cilia reveals up-regulation of ciliary GPCR activity following Hedgehog activation. Proceedings of the National Academy of Sciences. 2019;116(24):12066-12071. doi:doi:10.1073/pnas.1819730116

30. Barbeito P, Garcia-Gonzalo FR. HTR6 and SSTR3 targeting to primary cilia. Biochemical Society transactions. Feb 26 2021;49(1):79-91. doi:10.1042/bst20191005

31. Phillips ML, Robinson HA, Pozzo-Miller L. Ventral hippocampal projections to the medial prefrontal cortex regulate social memory. eLife. May 21 2019;8doi:10.7554/eLife.44182

32. Hitti FL, Siegelbaum SA. The hippocampal CA2 region is essential for social memory. Nature. Apr 3 2014;508(7494):88-92. doi:10.1038/nature13028

33. Park G, Ryu C, Kim S, et al. Social isolation impairs the prefrontal-nucleus accumbens circuit subserving social recognition in mice. Cell reports. 2021;35(6)doi:10.1016/j.celrep.2021.109104

34. Einstein EB, Patterson CA, Hon BJ, et al. Somatostatin signaling in neuronal cilia is critical for object recognition memory. The Journal of neuroscience : the official journal

of the Society for Neuroscience. Mar 24 2010;30(12):4306-14. doi:10.1523/jneurosci.5295-09.2010

35. Wang Z, Phan T, Storm DR. The type 3 adenylyl cyclase is required for novel object learning and extinction of contextual memory: role of cAMP signaling in primary cilia. The Journal of neuroscience : the official journal of the Society for Neuroscience. Apr 13 2011;31(15):5557-61. doi:10.1523/jneurosci.6561-10.2011

36. Liu X, Zhou Y, Yang D, Li S, Liu X, Wang Z. Type 3 adenylyl cyclase in the MOE is involved in learning and memory in mice. Behavioural brain research. Apr 6 2020;383:112533. doi:10.1016/j.bbr.2020.112533

37. Buzsáki G, Moser EI. Memory, navigation and theta rhythm in the hippocampal-entorhinal system. Nature neuroscience. 2013/02/01 2013;16(2):130-138. doi:10.1038/nn.3304

38. Colgin LL. Mechanisms and functions of theta rhythms. Annual review of neuroscience. Jul 8 2013;36:295-312. doi:10.1146/annurev-neuro-062012-170330

39. Yang FC, Jacobson TK, Burwell RD. Single neuron activity and theta modulation in the posterior parietal cortex in a visuospatial attention task. Hippocampus. Mar 2017;27(3):263-273. doi:10.1002/hipo.22691

40. Sellers KK, Yu C, Zhou ZC, et al. Oscillatory Dynamics in the Frontoparietal Attention Network during Sustained Attention in the Ferret. Cell reports. Sep 13 2016;16(11):2864-2874. doi:10.1016/j.celrep.2016.08.055

41. Siapas AG, Lubenov EV, Wilson MA. Prefrontal Phase Locking to Hippocampal Theta Oscillations. Neuron. 2005/04/07/ 2005;46(1):141-151. doi:https://doi.org/10.1016/j.neuron.2005.02.028

42. Benchenane K, Peyrache A, Khamassi M, et al. Coherent Theta Oscillations and Reorganization of Spike Timing in the Hippocampal- Prefrontal Network upon Learning. Neuron. 2010/06/24/ 2010;66(6):921-936. doi:https://doi.org/10.1016/j.neuron.2010.05.013

43. Daitch AL, Sharma M, Roland JL, et al. Frequency-specific mechanism links human brain networks for spatial attention. Proceedings of the National Academy of Sciences. 2013;110(48):19585-19590. doi:doi:10.1073/pnas.1307947110

44. Marshall TR, Bergmann TO, Jensen O. Frontoparietal Structural Connectivity Mediates the Top-Down Control of Neuronal Synchronization Associated with Selective Attention. PLoS biology. Oct 2015;13(10):e1002272. doi:10.1371/journal.pbio.1002272

45. Antzoulatos EG, Miller EK. Synchronous beta rhythms of frontoparietal networks support only behaviorally relevant representations. eLife. 2016/11/14 2016;5:e17822. doi:10.7554/eLife.17822

46. Fiebelkorn IC, Pinsk MA, Kastner S. A Dynamic Interplay within the Frontoparietal Network Underlies Rhythmic Spatial Attention. Neuron. 2018/08/22/ 2018;99(4):842-853.e8. doi:https://doi.org/10.1016/j.neuron.2018.07.038

47. Uhlhaas PJ, Singer W. Abnormal neural oscillations and synchrony in schizophrenia. Nature reviews Neuroscience. Feb 2010;11(2):100-13. doi:10.1038/nrn2774

48. Uhlhaas Peter J, Singer W. Neuronal Dynamics and Neuropsychiatric Disorders: Toward a Translational Paradigm for Dysfunctional Large-Scale Networks. Neuron. 2012/09/20/ 2012;75(6):963-980. doi:https://doi.org/10.1016/j.neuron.2012.09.004

49. Sha Z, Wager TD, Mechelli A, He Y. Common Dysfunction of Large-Scale Neurocognitive Networks Across Psychiatric Disorders. Biological psychiatry. 2019/03/01/ 2019;85(5):379-388. doi:https://doi.org/10.1016/j.biopsych.2018.11.011

50. Tort AB, Komorowski R, Eichenbaum H, Kopell N. Measuring phase-amplitude coupling between neuronal oscillations of different frequencies. Journal of neurophysiology. Aug 2010;104(2):1195-210. doi:10.1152/jn.00106.2010

51. Ramos C, Roberts JB, Jasso KR, et al. Neuron-specific cilia loss differentially alters locomotor responses to amphetamine in mice. Journal of neuroscience research. Mar 2021;99(3):827-842. doi:10.1002/jnr.24755

52. Stubbs T, Bingman JI, Besse J, Mykytyn K. Ciliary signaling proteins are mislocalized in the brains of Bardet-Biedl syndrome 1-null mice. Frontiers in cell and developmental biology. 2022;10:1092161. doi:10.3389/fcell.2022.1092161

53. Lee JE, Gleeson JG. A systems-biology approach to understanding the ciliopathy disorders. Genome medicine. Sep 26 2011;3(9):59. doi:10.1186/gm275

54. Alhassen W, Chen S, Vawter M, et al. Patterns of cilia gene dysregulations in major psychiatric disorders. Progress in neuro-psychopharmacology & biological psychiatry. Jul 13 2021;109:110255. doi:10.1016/j.pnpbp.2021.110255

55. Huang AS, Li ASM, Hor CHH. Primary cilia in the mature brain: emerging roles in Alzheimer’s disease pathogenesis. Review. Frontiers in cell and developmental biology. 2025-September-24 2025;Volume 13 - 2025doi:10.3389/fcell.2025.1650884

56. Serpieri V, D'Abrusco F, Valente EM. The relevance of primary cilia in neurological disorders. The Lancet Neurology. 2025;24(9):763-775. doi:10.1016/S1474-4422(25)00226-1

57. Marley A, von Zastrow M. DISC1 regulates primary cilia that display specific dopamine receptors. PloS one. May 28 2010;5(5):e10902. doi:10.1371/journal.pone.0010902

58. Everett T, Ten Eyck TW, Wu CH, et al. Cilia loss on distinct neuron populations differentially alters cocaine-induced locomotion and reward. Journal of psychopharmacology. Feb 2024;38(2):200-212. doi:10.1177/02698811231219058

59. Berbari NF, Malarkey EB, Yazdi SM, et al. Hippocampal and cortical primary cilia are required for aversive memory in mice. PloS one. 2014;9(9):e106576. doi:10.1371/journal.pone.0106576

60. Stubbs T, Koemeter-Cox A, Bingman JI, et al. Disruption of Dopamine Receptor 1 Localization to Primary Cilia Impairs Signaling in Striatal Neurons. The Journal of neuroscience : the official journal of the Society for Neuroscience. Aug 31 2022;42(35):6692-6705. doi:10.1523/jneurosci.0497-22.2022

Chapter 5 Reference:

1. Berbari, N.F., et al., Bardet–Biedl syndrome proteins are required for the localization of G protein-coupled receptors to primary cilia. Proceedings of the National Academy of Sciences, 2008. 105(11): p. 4242-4246.

2. Domire, J.S., et al., Dopamine receptor 1 localizes to neuronal cilia in a dynamic process that requires the Bardet-Biedl syndrome proteins. Cellular and Molecular Life Sciences, 2011. 68: p. 2951-2960.

3. Avasthi, P., et al., A chemical screen identifies class a g-protein coupled receptors as regulators of cilia. ACS chemical biology, 2012. 7(5): p. 911-919.

4. Miyoshi, K., et al., Lack of dopaminergic inputs elongates the primary cilia of striatal neurons. PloS one, 2014. 9(5): p. e97918.

5. Baldi, P., et al., Large-scale analysis reveals spatiotemporal circadian patterns of cilia transcriptomes in the primate brain. Journal of neuroscience research, 2021. 99(10): p. 2610-2624.
6. Chen, K., et al., Circadian cilia transcriptome in mouse brain across physiological and pathological states. Molecular Brain, 2024. 17(1): p. 67.
7. Monfared, R.V., et al., Cilia in the brain display region-dependent oscillations of length and orientation. PLoS Biology, 2025. 23(7): p. e3003197.
8. Chen, X., et al., Ablation of type III adenylyl cyclase in mice causes reduced neuronal activity, altered sleep pattern, and depression-like phenotypes. Biological psychiatry, 2016. 80(11): p. 836-848.
9. Strobel, M.R., et al., Temporal ablation of the ciliary protein IFT88 alters normal brainwave patterns. Scientific Reports, 2025. 15(1): p. 347.
10. Floresco, S.B., The nucleus accumbens: an interface between cognition, emotion, and action. Annual review of psychology, 2015. 66(1): p. 25-52.
11. Murugan, M., et al., Combined social and spatial coding in a descending projection from the prefrontal cortex. Cell, 2017. 171(7): p. 1663-1677. e16.
12. Trezza, V., et al., Nucleus accumbens μ-opioid receptors mediate social reward. Journal of Neuroscience, 2011. 31(17): p. 6362-6370.
13. Nishitani, N., et al., Medial nucleus accumbens dopamine receptors modulate motivation for wheel running in male mice. Neuropsychopharmacology, 2025: p. 1-11.
14. Dölen, G., et al., Social reward requires coordinated activity of nucleus accumbens oxytocin and serotonin. Nature, 2013. 501(7466): p. 179-184.

15. Francis, T.C., et al., Nucleus accumbens medium spiny neuron subtypes mediate depression-related outcomes to social defeat stress. Biological psychiatry, 2015. 77(3): p. 212-222.
16. Luo, Y.-J., et al., Nucleus accumbens controls wakefulness by a subpopulation of neurons expressing dopamine D1 receptors. Nature communications, 2018. 9(1): p. 1576.
17. Qiu, M.-H., et al., The role of nucleus accumbens core/shell in sleep-wake regulation and their involvement in modafinil-induced arousal. 2012.
18. Ketchesin, K.D., et al., Diurnal Alterations in Gene Expression Across Striatal Subregions in Psychosis. Biol Psychiatry, 2023. 93(2): p. 137-148.
19. Roybal, K., et al., Mania-like behavior induced by disruption of CLOCK. Proceedings of the National Academy of Sciences, 2007. 104(15): p. 6406-6411.
20. Imbesi, M., et al., Dopamine receptor-mediated regulation of neuronal “clock” gene expression. Neuroscience, 2009. 158(2): p. 537-544.
21. Van Someren, E.J., et al., Bright light therapy: improved sensitivity to its effects on rest-activity rhythms in Alzheimer patients by application of nonparametric methods. Chronobiology international, 1999. 16(4): p. 505-518.
22. Stubbs, T., et al., Disruption of dopamine receptor 1 localization to primary cilia impairs signaling in striatal neurons. Journal of Neuroscience, 2022. 42(35): p. 6692-6705.
23. Donoghue, T., et al., Parameterizing neural power spectra into periodic and aperiodic components. Nature neuroscience, 2020. 23(12): p. 1655-1665.
24. Voytek, B., et al., Age-related changes in 1/f neural electrophysiological noise. Journal of neuroscience, 2015. 35(38): p. 13257-13265.

25. Chevallier, C., et al., The social motivation theory of autism. Trends in cognitive sciences, 2012. 16(4): p. 231-239.
26. Oishi, Y., et al., Slow-wave sleep is controlled by a subset of nucleus accumbens core neurons in mice. Nature communications, 2017. 8(1): p. 734.
27. Yorgason, J.T., D.M. Zeppenfeld, and J.T. Williams, Cholinergic interneurons underlie spontaneous dopamine release in nucleus accumbens. Journal of Neuroscience, 2017. 37(8): p. 2086-2096.
28. Soares-Cunha, C., et al., Nucleus accumbens medium spiny neurons subtypes signal both reward and aversion. Molecular psychiatry, 2020. 25(12): p. 3241-3255.